



**A STUDY ON CLIMATE CHANGE ADAPTATION AND RESILIENCE
STRATEGIES FOR OPTIMIZING BENEFITS OF THE MAHAWELI RIVER
BASIN IN SRI LANKA**

A Dissertation

Submitted to the National Graduate Institute for Policy Studies (GRIPS) and
International Centre for Water Hazard and Risk Management (ICHARM),
Public Works Research Institute (PWRI)

in Partial Fulfillment of the Requirements for the Degree of

Ph.D. in Disaster Management

by

Hemakanth Selvarajah

September 2021

Declaration

Except where specific reference has been made to the work of others, the work embodied in this thesis is the result of investigation carried out by the author. No part of this thesis has been submitted or is being concurrently submitted in candidature for and degree at any other institution.



(Hemakanth Selvarajah)

Abstract

Climate change, disasters and multiple non-climatic drivers reinforce the impacts globally and collectively affecting the social system, the quality of life, natural and built environment, and the food-water-energy nexus in which they are closely related to each other. Impacts due to climate change and subsequent disasters have to be strategically handled by connecting natural science and technology for policy making to implement adaptation and resilience strategies. Therefore, this research focuses on developing a common method to understand water-related disaster risks and proposing strategies for policy making in terms of disaster risk reduction and water resources management. To understand water-related disaster risks, this research developed an integrated approach for assessing climate change impacts by utilizing recent advancements in science and technology that integrate globally available data sources and a reliable hydrologic model. As a result, this research utilized the Data Integration and Analysis System of Japan (DIAS) for handling, manipulating, and downscaling big-data of GCMs and the Water Energy Budget-based Rainfall-Runoff-Inundation model (WEB-RRI) for reproducing various long-term hydrological variables more accurately. This approach was applied to the Mahaweli River Basin in Sri Lanka to understand climate change impacts on rainfall, inundation, floods and droughts. The results from four selected GCMs showed that MRB will yield sufficient water resources for future usage in various sectors. Further, meteorological and hydrological floods will also increase in the future climate. The study also found that MRB, especially its downstream region, is vulnerable to future droughts during the North East (NE) monsoon period and the Intermediate Monsoon-2 (IM-2) period. However, the overall trend of model responses showed uncertainty in future hydrological droughts and an increasing pattern in meteorological droughts.

The climate change impact assessment and analysis of the past reservoir operation confirmed that water availability, excess and shortage, which can influence the MRB system operation, will vary seasonally and spatially in the future. But these future changes depicts the information regarding average over a 20 years period only. Still, onset and withdrawal of these events are uncertain based on the available information. Therefore, it is necessary to use seasonal forecasting and short term weather prediction for flood and drought management. Hence, to utilize future water resources and manage flood and drought disasters to ensure food, water, and energy security, adaptation strategies were developed by utilizing seasonal forecasts and short-term weather prediction information. This strategy development was conducted by coupling JMA's seasonal forecast data and the downscaled versions of NCEP-GFS deterministic forecast data by WRF with the WEB-RRI model to simulate forecasted discharge at a selected location (Kotmale reservoir). Then, the simulated discharge was used to perform reservoir operation by RTC-tool 2, a real-time reservoir optimization tool. It is shown that by utilizing seasonal forecasts, optimization tools and reservoir operation rules, we can achieve flood and drought risk reduction by saving enough water for an upcoming agriculture season and enhance energy generation by pre-releasing a future flood through a power turbine. Moreover, the results of the short-term operation showed that the expected flood inflow can be utilized for power generation by pre-releasing the forecasted inflow and keeping the reservoir elevation at a low level to receive a future flood, thus preventing the reservoir from spilling.

Keywords: Disaster risk reduction, Climate change impact assessment, General Circulation Models, Water Energy Budget Rainfall Runoff Inundation Model, Decision making, Reservoir optimization, Seasonal forecast, Weather forecast.

Acknowledgments

I would like to express my sincere thanks to the Japan International Cooperation Agency (JICA) under the Government of Japan for giving me this once-in-a-lifetime opportunity by providing the scholarship to conduct this Ph.D. study.

I take this opportunity to sincerely thank Professor Toshio Koike from the bottom of my heart for his excellent and professional guidance throughout this research work as my supervisor. During the last three years, his encouragement, leadership, ever willingness, and kindness have kept me moving forward to explore multi-disciplines in the field of disaster management. He transferred his insight and expert knowledge to me as much as he could, and the everlasting smile on his face in welcoming me regardless of his situation will be remembered forever. I thank you, sir, for accepting me as one of your students. I am really proud and honored to be supervised by you.

Next, I would like to express my sincere gratitude to Professor Abdul Wahid Mohamed Rasmy, my co-supervisor of this research, for his continuous support in overcoming my difficult times during these three years. I admire his patriotism and passion for transferring his knowledge to others. His support in developing a hydrological model with learning programming languages and software has sharpened my research approach immensely. In addition to his support for my research work, he supported my daily life in Japan throughout these three years. I would always remember the hospitality provided by him, his wife, Mrs. Shifana Rasmy, and his kids, Rina, Sharaf, and Raid.

Further, I would like to express my gratitude to the other co-supervisor of my research, Professor Kenzo Hiroki, for providing profound policy related insights into my

studies. He has guided me with his experience and expert knowledge in water and disaster, whenever it was necessary.

My gratitude goes to the academic staff at International Centre for Water Hazard and Risk Management (ICHARM) and Public Works Research Institute, Tsukuba, Japan, for providing me substantial help in attaining knowledge related to science and technology to manage disasters. I would like to thank Professor Shinji Egashira, Professor Ushiyama, Dr. Imamura, Dr. Tamakawa, Dr. Shibo, and Dr. Aida for their valuable support. I would like to thank the evergreen assistants of ICHARM for their friendly arrangements of research related activities and for their friendship. Especially, I would like to thank Okawa san, Asami san, Yagi san, Sano san, Okubo san, and the energetic Mikiko san for looking after the logistics in and out of research life. Also, I would like to thank Okubo Masahiko for his English editing contribution throughout my studies. Further, I would like to thank my dear friends Hoang, Zhou, and Gul for being with me and for their valuable support in my research work.

I would like to thank all the staff members of the National Institute of Policy Studies (GRIPS), Japan, for their support in various aspects from the beginning till the end. Especially, I would like to appreciate the support of Awatha san, Oyama san, Sweeney san, and Yatabe san for helping me manage the courses and other administration related activities at GRIPS.

I wish to express my great gratitude to Dr. Sujeewa Lewangamage and Dr. G.H.A.C Silva for recommending me to the scholarship program.

I would like to thank Eng. S. Mohanarajah, former Director General of Irrigation, for his continuous support in bringing my professional as well as academic career into

good shape. Then, I would like to express my appreciation to the engineers, Laksiri Silva, Janaki Meegastanne, Inoka Wickramasinghe, Sugeeshwara Seenipellage, S. Krishnaroopan, Prasanna Thilakaratne, A.D.S. Gunawardene, I.D.S. Gunawardene, and many other engineers from the Irrigation Department for helping me in different means to successfully completing this study. Further, I would like to thank Mr. Sarath Chandrasiri Vithana, Dr. D.M.S. Dissanayake, Eng. G.K.T Samarathunga, Eng. Imesh Kariyawasam, and Eng. Sanjeewa Illangasinghe from the Mahaweli Authority of Srilanka, and Mr. Athula Karunanayake from the Department of Meteorology, Sri Lanka, for helping me in finding required ground data for the research purposes.

I wish to express my deepest regards to my parents, Rasaretnam Selvarajah and Inparani Selvarajah, for their dedication and support to bring me to this level. I am also thankful to my siblings, Howsalya, Rukshiya, Mirukshiya, Thulkanth, and Shobikanth, for their continuous trust in me.

Finally, I am indebted to my lovely wife, Shavitha, and my twin kids, Imaathra and Araathra, for believing in me and for standing by my side throughout this journey.

Table of Content

Abstract.....	ii
Acknowledgments	iv
Table of Content	vii
List of Figures.....	xi
List of Tables	xv
1 Introduction	1
1.1 Background	1
1.2 Research Objectives.....	4
1.3 Research Framework	5
1.4 Outline of Dissertation.....	7
2 Study Area	9
2.1 Introduction.....	9
2.2 Sri Lanka.....	11
2.2.1 Topography of Sri Lanka.....	11
2.2.2 Climate and hydrology of Sri Lanka	12
2.2.3 Population of Sri Lanka	13
2.2.4 Water resources of Sri Lanka	13
2.2.5 Agriculture led economy of Sri Lanka	15

2.2.6	Power and Energy in Sri Lanka.....	17
2.2.7	Climate change and natural disasters in Sri Lanka.....	18
2.3	Mahaweli River Basin and its development	20
2.3.1	Mahaweli River Basin system.....	22
2.3.2	Climate and topography of MRB	23
2.3.3	Management of Mahaweli River Basin.....	24
3	Development of an integrated approach for climate change impact assessment on hydro-meteorological characteristics of a river basin and its application in Mahaweli River Basin.	28
3.1	Introduction.....	28
3.2	Research Framework	34
3.3	Study area	35
3.4	Methodology.....	35
3.4.1	GCM selection and downscaling/bias correction	35
3.4.2	Hydrologic model.....	37
3.5	Data and model set-up	41
3.5.1	Data for GCM selection, past and future climate data	41
3.5.2	Data for bias correction of rainfall and hydrological modeling	44
3.5.3	Data for socio-economic damage assessment	47
3.5.4	Hydrological model set-up	48
3.5.5	Model performance metrics.....	49

3.5.6	Qualitative and quantitative decision index.....	49
3.6	Results and discussion	50
3.6.1	Meteorological assessment.....	50
3.6.2	WEB-RRI model calibration and validation	62
3.6.3	Hydrological assessment	64
3.6.4	Possible decision making based on the results	69
4	Development of climate change adaptation and resilience strategies for Kotmale reservoir operation.....	72
4.1	Introduction.....	72
4.2	Research framework	77
4.3	Study area	78
4.4	Methodology.....	78
4.4.1	Formulation of reservoir operation rules based on past observations	78
4.4.2	Hydrological model development	79
4.4.3	Dam module and optimization module	80
4.4.4	Performance Criterion Indexes (PCI) for evaluation and monitoring	82
4.4.5	Evaluation of optimization scheme in reservoir operation.....	84
4.4.6	Seasonal forecast discharge simulation and dam optimization scenarios	84
4.4.7	Short-term weather prediction discharge simulation and dam optimization scenarios	85
4.5	Data and model set-up	86

4.5.1	Data availability and limitations.....	86
4.5.2	Seasonal forecasting data.....	87
4.5.3	Short-term weather forecasting data.....	88
4.6	Results.....	88
4.6.1	Reservoir operation rules based on past observations.....	88
4.6.2	Seasonal operation optimization.....	97
4.6.3	Accumulating short-term operation by using short-term numerical weather prediction.....	105
5	Policy proposals.....	111
6	Conclusions.....	115
6.1	Climate change impact assessments.....	115
6.2	Climate change adaptation and resilience strategies.....	116
	References.....	120

List of Figures

Figure 1.1. Research framework	7
Figure 2.1. (a) Topography, and (b) Climatic Zones of Sri Lanka.....	11
Figure 2.2. (a) Sri Lanka River Basins, and (b) Sri Lankan River Basin Catchment area.	14
Figure 2.3. (a) Cropping Extents, and (b) Harvested Quantities.	15
Figure 2.4. Cropping extent percentage in 2019	16
Figure 2.5. (a) Year wise energy generation, and (b) Share of sources in power generation	18
Figure 2.6. Flood and Drought Disasters and Death toll in Sri Lanka	18
Figure 2.7(a) Topographical map of Sri Lanka with the demarcation of the Mahaweli River basin, (b) to-pography of Mahaweli River Basin, (c) land use with distribution of discharge measurement points, and (d) demarcation of climatic zones with rain gauge network.....	21
Figure 2.8. The schematic diagram of Mahaweli River Basin Multipurpose system (source: Mahaweli Authority of Sri Lanka)	22
Figure 2.9. Time series of Climatic seasons and Agriculture seasons	25
Figure 3.1. Research framework for climate change impact assessment.	34
Figure 3.2. GCM grid distribution over Sri Lanka (a) CanESM2, and (b) CNRM-CM5, and (c) GFDL-ESM2G, and (e) MPI-ESM-LR.....	44
Figure 3.3. Basin average temperature difference (future-past): (a) bar plot for monthly changes and (b) box and whisker plot for annual changes.	50

Figure 3.4. (a) Trend analysis of far past (1976-1996) vs near past (1997-2017) observed rainfall and trend analysis of past vs. future GCM rainfall of (b) CanESM2, (c) CNRM-CM5, (d) GFDL-ESM2G, (e) MPI-ESM-LR, and (f) Ensemble Mean.	51
Figure 3.5. (a) The comparison of basin average annual rainfall (mm/year) between past and future climate and percentage changes (%) for each selected GCM and (b) basin averaged seasonal rainfall differences (Future – Past) for selected GCMs and the ensemble mean	53
Figure 3.6. The comparison of annual average rainfall differences (future-past) in mm/year for the selected models and the ensemble mean.....	54
Figure 3.7. The comparison of seasonal average rainfall differences (future-past) for the selected models and the ensemble mean.	54
Figure 3.8. The comparisons of past and future climate seasonal average of variables influencing rainfall: a) geopotential height, b) specific humidity, and c) wind speed. ..	56
Figure 3.9. Anomalies of CWD and CDD of observed far-past (1976-1996) and near-past (1997-2017) rainfall and the past and future rainfall of the selected models.	58
Figure 3.10. Past average seasonal MCDD vs. future average seasonal MCDD plot (a) Can-ESM2, (b) CNRM-CM5, (c) GFDL-ESM2G, and (d) MPI-ESM-LR.	59
Figure 3.11. Comparison between observed discharge and simulated discharge: (a) model calibration for 1981-1982 under the natural river flow and (b) model validation for 2005 to 2015 with dam operations.	63
Figure 3.12. (a) Annual average discharge at Mannampitiya gauging station of the selected models and (b) seasonal average discharge difference at Mannampitiya gauging station of the selected models.....	65

Figure 3.13. First 20 peak flow and the last 20 low flow of daily average discharge values of the past and future 20 years of the selected GCMs.	66
Figure 3.14. (a) Past all-time inundation depth and (b) inundation depth deference between future and past of the selected GCMs.	67
Figure 3.15. Past vs. future all-time seasonal maximum inundation during the NE monsoon of the selected GCMs.....	68
Figure 3.16. Socio-economic damage assessment.....	68
Figure 4.1. Research framework.	77
Figure 4.2. Seasonal forecast data availability.	87
Figure 4.3. Mahaweli cultivation calendar	89
Figure 4.4. Seasonal rainfall at Kotmale, Polgolla, Victoria, Randenigala, and Rantambe gauging stations: (a) Climatic seasons, and (b) Agricultural seasons	90
Figure 4.5. Cumulative rainfall received at reservoir sites starting from October	91
Figure 4.6. Seasonal inflow to reservoirs and diversions (a) Climatic seasonal inflow, and (b) Agriculture seasonal inflow	91
Figure 4.7. Annual reservoir gross storage variation starting from October	92
Figure 4.8. Seasonal average spillage of Kotmale, Victoria, Randenigala, and Rantambe reservoirs; (a) Climatic seasons, and (b) Agricultural seasons.....	93
Figure 4.9. Cultivation extents from 2000 to 2020 during Yala and Maha seasons	94
Figure 4.10. Annual power generation starting from October	96
Figure 4.11. Cumulative basin average rainfall of April/May/June 2020.....	98
Figure 4.12. Cumulative sub basin average rainfall of April/May/June 2020 and the basin demarcation	99
Figure 4.13. Spatial distribution of monthly rainfall	100

Figure 4.14. Reservoir operation under Scenario 1	102
Figure 4.15. Reservoir operation under Scenario 2	103
Figure 4.16. Performance criterion indexes of ensemble mean under selected scenarios.	104
Figure 4.17. Basin average ensemble weather forecasted and observed rainfall	106
Figure 4.18. Kotmale reservoir operation.....	108
Figure 4.19. Optimized reservoir operation under selected operation rule	110
Figure 4.20. Reservoir optimization for selected operation rule	110

List of Tables

Table 3-1. Model selection summary for annual, SW monsoon, and NE monsoon period average.....	43
Table 3-2. Daily rain gauges in the Mahaweli River basin with names, climatic zones, locations and annual average rainfall in mm.	45
Table 3-3. Basin scale seasonal meteorological drought analysis.....	60
Table 3-4. Zonal scale seasonal meteorological drought analysis.....	61
Table 3-5. Model calibrated parameters for the MRB.....	63
Table 3-6. Basin scale annual assessment summary	69
Table 3-7. Basin and zonal scale seasonal meteorological drought summary	69
Table 3-8. Seasonal discharge at Peradeniya discharge location summary	69
Table 4-1. Data availability and limitations	86
Table 4-2. Design specifications of hydropower reservoirs	95
Table 4-3. Reservoir operation rule for Kotmale, Victoria, and Randenigala reservoirs	97
Table 4-4. PCIs for ensembles and ensemble mean of scenario 1	102
Table 4-5. PCIs for ensembles and ensemble mean of scenario 2	103

1 Introduction

1.1 Background

Energy, food and water always create a nexus among the water users and oftentimes, it forms the tradeoff between trilemma. Further, this trilemma is gradually increasing the complexity of making fundamental decisions under the increasing demand for food and energy with increasing natural disasters and decreasing water availability in the global context. Climate change enhanced by global warming progresses faster than ever before (Toby et al., 2020). Global warming is sensed most directly through water, as the phenomenon is inseparably connected to the water cycle, thus imposing threats on sustainable development, biodiversity and ecosystems (Teng et al., 2012; UN Water, 2019).

In the recent past, climate-related hazards such as floods, storms, heatwaves, and droughts have caused the majority of disasters globally (CREED, 2015; UN Water, 2019). Flood events are prominent in terms of numbers every year while long-lasting droughts affect millions of people concerning hunger, poverty and persistence of the underdevelopment (CREED, 2015). Furthermore, multiple non-climatic drivers are intensifying the impacts due to climate change and collectively affecting societies by putting pressure on power generation, agriculture sectors and transportation (Jiménez Cisneros et al., 2014). Climate change will affect not only the environment but also the global economy in the future (Toby et al., 2020). As a result, in 2015, three main global agendas were agreed by global leaders. First, the Sendai Framework for Disaster Risk Reduction was agreed (SFDRR), aiming at strengthening the resilience of societies to disasters (UN, 2015b). Second, the 2030 Agenda for Sustainable Development (SDG)

was adopted to eradicate poverty and hunger and bring about prosperity on a healthy and peaceful planet by tackling climate change (UN-Secretary-General, 2019). Third, the Paris Agreement was concluded to address climate change using an inclusiveness and participatory approach (UN, 2015a) as a response to adopt and mitigate the impacts of climate change.

SFDRR expects a substantial reduction of disaster risk and losses in lives, livelihoods, health, and the economic, physical, social, cultural, and environmental assets of persons, businesses, communities, and countries by 2030. In these circumstances, four priorities are identified for action of SFDRR, i.e., (i) understanding disaster risk; (ii) strengthening disaster risk governance to manage disaster risk; (iii) investing in disaster reduction for resilience; and (iv) enhancing disaster preparedness for effective response, and to “Build Back Better” in recovery, rehabilitation, and reconstruction, in order to manage disaster risks, implement mitigation measures, and strengthen adaptation mechanisms. Among these four priorities for action, the understanding of disaster risk plays a major role in Disaster Risk Reduction (DRR) (UN, 2015b). To implement SFDRR in policies and practices to reach sustainable development, disaster risk in all its dimensions of hazard characteristics, vulnerability, capacity, exposure of persons and assets, and the environment are need to be identified and understood. Although DRR has not always been a major theme in international development policy, the need for mainstream DRRs has been emphasized through the Sendai Framework in 2015 and integrated into the 2030 Agenda (Kellett & Caravani, 2013).

The SDGs consist of 17 goals and 169 targets. These targets and goals can be classified into five major categories: (a) Natural Environment (Goal 13: Climate Action,

Goal 14: Life Below Water, and Goal 15: Life on land); (b) Built Environment (Goal 9: Industry, innovation and infrastructure, Goal 11: Sustainable cities and communities, and Goal 12 Responsible consumption and production); (c) quality of life (Goal 1: No poverty, Goal 3: Good Health and Well-being, Goal 4: Quality Education, and Goal 8: Decent Work and Economic Growth); (d) Water-food-energy (Goal 2: Zero hunger, Goal 6: Clean water and sanitation, and Goal 7: Affordable and clean energy); and (e) Social system (Goal 5: Gender equality, Goal 10: Reduced inequalities, and Goal 16: Peace, justice, and strong institutions) (UN, 2019).

The PA aims to significantly reduce global greenhouse gas emissions to control the global temperature increase in this century to 2 °C above preindustrial levels while pursuing the means to limit the increase to 1.5 °C. The agreement includes obligations on all major emission countries to reduce climate pollution and strengthen those commitments over time. This agreement provides a way for developed nations to assist developing countries in their efforts to climate mitigation and adaptation. It creates a framework for transparent monitoring, reporting and ratcheting up countries' individual and collective climate goals (UN, 2015a).

Regarding recent activities of international organizations, the United Nations Development Program (UNDP) leads the main activities for each of the SDGs with the aim of achieving "sustainable development taking into account disaster risk" (UNDP, 2016). Whenever the DRR is to be performed, the SFDRR plays a key role in the action. In addition to the explanation of expected outcome of the SFDRR, there are four priority for actions which defined in the agreement such as 1) understanding the disaster risk, 2) strengthening the governance to managing disaster risk, 3) investing in disaster risk

reduction for resilience, and 4) improving disaster preparedness for response with building back better (UN, 2015b). Among the above four priority for actions, by understanding the disaster risk, the first action, the other three actions can be achieved.

In order to implement the SFDRR and achieving SDG targets, it is necessary to identify and understand disaster risk. But, significantly, most of the developing countries lack a proper framework to address these issues due to the gaps in science and technology. Therefore developing a common, sustainable, cost-effective and action-oriented research framework by mainstreaming science and technology in implementing SFDRR is a timely need to provide scientific information about DRR to policy makers for decision making.

Hence, this research was focussed on developing a common method to understand the water-related disaster risk and proposing strategies for policymaking in terms of DRR and WRM. This study focused on the impacts of climate change and disaster on the water and then food and energy to implement adaptation and resilience strategies through making changes in reservoir operation. Especially, as floods and droughts are prominent among water-related disasters, developing a common method to understand the water related disaster risk and proposing strategies for policy making in terms of disaster risk reduction and water resources management on a basin scale would enhance the effectiveness of DRR.

1.2 Research Objectives

Impacts due to climate change and subsequent disasters have to be strategically handled by connecting natural science and technology, engineering and social science for policy making to implement adaptation and resilience strategies. Therefore, developed a common method to understand water related disaster risk and proposing strategies for

policy making in terms of disaster risk reduction and water resources management by accomplishing the following objectives.

- Developing a methodology for understanding water related disaster risk through;
 - ✓ Identification of water related disasters which affect future water resources management through climate change impact assessment
- Developing an integrated approach for climate change adaptation and resilience strategies in optimizing benefits for river basins at the face of food-water-energy nexus

1.3 Research Framework

Several studies were identified through a literature review that attempted to develop a comprehensive research framework for water resources management through DRR. A hydro-agro-economic approach was developed based on basin decomposition for river basins where irrigation is the dominant water use to maximize the benefit of water used for irrigation, hydropower, and ecological water use by exploring various policy choices (Cai, McKinney, & Lasdon, 2003). This approach was socio-economic, and disaster management and climate change were not included. A compromise programming approach was developed and used for an Irrigation System to ensure efficient water regulation and plan regulation of reliable water, improving rice and tea production, domestic water supply, and environmental flow (Zarghaami, 2006). This approach also found to be socio-economic, and climate change was not addressed. Another socio-economic approach with a statistically-based analysis on the Tradeoff Frontier approach was used to show the compromise between rice cultivation and energy generation in the Mahaweli River Basin to visualize system-level tradeoffs among the Water-Energy-Food

nexus, especially when water scarcity is driving the nexus (Perrone & Hornberger, 2016). This approach also did not include disaster management and climate change.

Further, a decision support tool for water infrastructure investment planning within the Water-Energy-Food-Climate Nexus was developed to show Investment opportunities such as new hydropower plants, new or resized reservoirs, development of irrigated agriculture, and investments into the power grid in a transboundary basin in Africa (Payet-Burin, Kromann, Pereira-Cardenal, Strzepek, & Bauer-Gottwein, 2019). This approach has used historical streamflow data, driven from previous studies, to evaluate the socio-economic benefits and losses due to the proposed changes in the river basin. Still, the future climate scenarios were included in this study by referring to several past studies. Also, disaster management was not included in this study. Therefore, if a river basin lacks such climate change studies, this method could not be used for application in any river basins.

Therefore to integrate natural science, engineering and technology and social science to enable dynamic policy-making, a comprehensive adaptation strategy is developed in this study. The overall research framework and methodology of this study is shown in Figure 1.1. First, science and technology was utilized to develop a hydrological model by utilizing ground data, satellite data and climate model data to assess the impact in the future by comparing past and future conditions. Second, by considering disaster risk resilience and reduction, climate change adaptation and sustainable development, dam operations, water diversion and irrigation management of the past was assessed to check whether to change the operation mechanism and found that an optimized operation mechanism is needed. Accordingly, the operation strategies were

investigated according to the requirements. Hence, decisions were proposed for implementation for a resilient, sustainable society and environment. Therefore, we could achieve water security, energy security, food security, and flood management by implementing this approach.

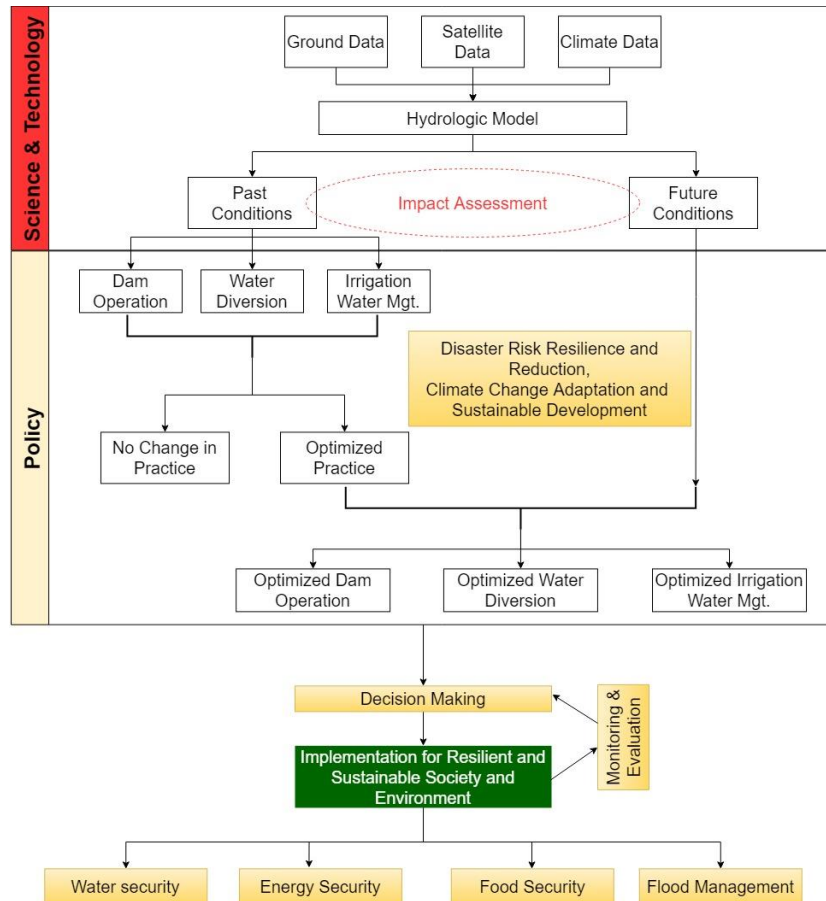


Figure 1.1. Research framework

1.4 Outline of Dissertation

The motivation, objective and research framework of this research were explained in this chapter. The study area information related to Sri Lanka and the Mahaweli River Basin are given in Chapter 2. Development of an integrated approach for climate change impact assessment on hydro-meteorological characteristics of a river basin and its

application to the Mahaweli River Basin is explained in Chapter 3. In Chapter 4, the development of climate change adaptation and resilience strategies for the Kotmale reservoir operation is discussed. The policy recommendations to the stakeholders in the MRB is provided in the Chapter 5 based on the scientific evidences driven from this research. The final chapter provides the concluding remarks of this study.

2 Study Area

2.1 Introduction

Sri Lanka, which relies heavily on natural resources such as water and land, is targetting sustainable development by mainstreaming its commitments to the SDGs, SFDRR, and PA. The government's Sustainable Sri Lanka 2030 Vision and Strategic Path (SS-SP:2030) set ambitious targets in a variety of sectors, including water, food and energy (PEC, 2019). The optimization of water use in response to increases in disasters induced by climate change in the recent past is highly prioritized in SS-SP: 2030. The key recommendations, which are related to this research topic, are scrutinized and listed as below:

- Adaptation to climate change impacts must have priority, especially to protect the poor and vulnerable.
- Implement urgent short, medium and long-term measures to reduce vulnerability to disasters (e.g., droughts, floods) and adapt to climate change.
- Enhance the capacity and ability to provide better seasonal rainfall forecasts and early warnings on extreme weather events leveraging modern technology and develop institutional arrangements to speedily respond to such early warnings.

Sri Lanka is located in the tropical region, and evidence shows that the occurrence of flood and drought events are on an increasing trend in the recent past (UN Water, 2019). According to IPCC, the 21st century has been projected, and contrast behavior in rainfall patterns among wet and dry regions and among wet and dry seasons will increase (IPCC, 2013a). Further, it says that there will be likely (66-100% probability) changes in the monsoon system, as such increased covered area, weaken winds and intensified

precipitation. Also, the monsoon onset dates will be advanced or will not have much change. As far as predicted changes in intensity and frequency are concerned, the present situation of drought and flood may intensify in the future. IPCC clearly indicates that countries in the tropical region such as Sri Lanka, which receive much of the rainfall from the monsoonal and inter-monsoonal rainfall, might get affected due to this varied nature of such future rainfall pattern.

Moreover, the Global Climate Risk Index, developed by Germanwatch, has ranked Sri Lanka in second place regarding the losses due to weather related disasters in 2017 (David Eckstein, 2019). Further, it says that this index could be served as a warning for preexisting vulnerability, which may increase with expected extreme events due to climate change. Loss of lives and damage to infrastructure will subsequently result in a burden on the economy of the country and will increase the vulnerability of the country to hazards. Therefore, it is timely to assess the impact of climate change on the water system of Sri Lanka to plan adaptation strategies against future challenges due to the increased disasters.

The Mahaweli river basin (MRB) has been selected as the pilot area for this study as it holds the status of the largest river basin in Sri Lanka and plays a major role in promoting the nation's economy by supplying 20% of the total power at its best through hydropower (CEB-SL, 2017) and by producing 25% of national production on average per annum (MASL-SL, 2018).

To understand the characteristics of the country and the study area (Mahaweli River Basin), this chapter is organized to describe the fundamental features related to this study.

2.2 Sri Lanka

2.2.1 Topography of Sri Lanka

Sri Lanka is a developing country which is lying within the tropical region (between $5^{\circ}55'E - 9^{\circ}51'E$, $79^{\circ}41'N - 81^{\circ}53'N$). The total land area is $65,610 \text{ km}^2$, out of which $2,905 \text{ km}^2$ is filled with inland waters (Department of Census and Statistics, 2021). Figure 2.1 shows a topographic map of the country, and as shown in the figure, around 60% of the land area is located within a broad first peneplain, whose elevation ranges between $0\sim 100 \text{ m}$ above Mean Sea Level (MSL). Another peneplain rises to 500 m above MSL and covers around 30% of the land area. Still another peneplain (covering 10% of land area), towards the south, rises steeply to form a mountain range that reaches an elevation of $2,524 \text{ m}$ above MSL.

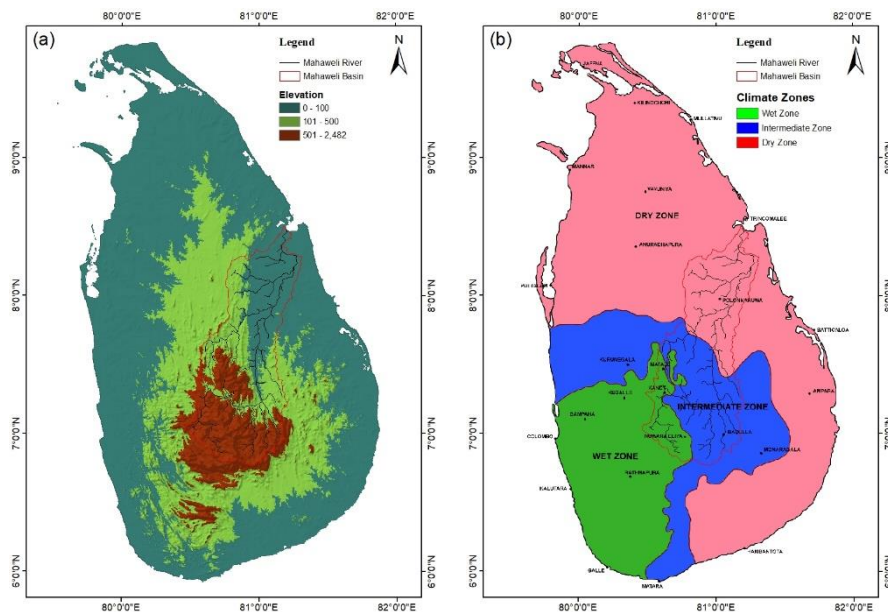


Figure 2.1. (a) Topography, and (b) Climatic Zones of Sri Lanka

2.2.2 Climate and hydrology of Sri Lanka

The hydrologic cycle of this tropical region island is impacted mainly due to the seasonally varying monsoon systems. The windward southern, western and central hill regions receive high rainfall during the South-West (SW) monsoon season, May to September, with annual rainfall ranging from 1000 to 4000 mm, while other regions on the leeward side experience less than 500 mm rainfall during the five months. On the other hand, during the North-East (NE) monsoon season, December to February, the eastern and southeastern parts record a significant rainfall ranging from 500 to 1200 mm, while other parts record less rainfall. In addition to the above two main monsoons, another two more inter monsoon systems called Inter Monsoon-1 (IM-1) and Inter Monsoon-2 (IM-2) are influencing the weather system of the country. IM-1 is the warmest season, March to April, in Sri Lanka, and the whole country receives localized thunderstorms especially in the afternoon period. The South Western slopes and hilly regions get more rainfall of around 250 mm, while the rest of the country receives rainfall varying between 100 to 250 mm. On the other hand, IM-2 brings thunderstorms in the afternoon from October to November, influenced by depression and cyclones in the Bay of Bengal. The whole island experiences strong winds and a balanced distribution of rainfall. The South Western slopes receive higher rainfall ranging between 700 to 1200 mm while other regions receive more than 400 mm annually, which leads to occasional flooding and landslides (DOM-SL, 2020).

A spatially varying pattern of rainfall is observed, and it is influenced by the complex nature of the central highland's topography, as shown in Figure 2.1 (a). Therefore, the Department of Agriculture has demarcated the island into three main agro climatic zones based on the spatial and temporal variability of annual rainfall, as shown

in Figure 2.1 (b): wet zone (more than 2500 mm), intermediate zone (1750-2500 mm) and dry zone (less than 1750 mm) (DOA-SL, 2020).

On the other hand, the mean annual temperature is about 27°C in the lowlands near the coastlines and 15°C in the central hilly region. The temperature decreases with a lapse rate of 6.6°C per 1000 m of elevation (FAO, 2011).

2.2.3 Population of Sri Lanka

In 2019, the total population was estimated to be around 22 million (The World Bank, 2021). For administration, the island is divided into 9 provinces, which are subdivided into 25 districts. The districts are further subdivided into 331 Divisional Secretary's Divisions (DS Divisions), which comprising the smallest administrative elements of the system called Grama Niladhari Divisions (GN Divisions; 14,022 in total). Much of the country's population is concentrated in the wet zone (southwest coastal regions and central regions), while the dry zone remains sparsely populated, especially in the north and east provinces (FAO, 2011).

2.2.4 Water resources of Sri Lanka

A total of 103 seasonal and perennial rivers, starting from the central part of the country, flow radially across various topographies and climatic zones before reaching the Indian Ocean around the island. The river network of Sri Lanka is shown in Figure 2.2 (a), and the catchment area statistics of the rivers is given in Figure 2.2 (b). The majority of the rivers, 75 in total, have a catchment area less than 500 sq.km. Among them, 41 rivers drain less than 100 sq.km area.

There are 7 major rivers draining more than 2000 sq.km. The largest river basin is the Mahaweli River Basin (MRB), which drains 10,366 sq.km and covers 16% of the

land area of the country. Other than this, there are four other river basins with a catchment area of over 2500 sq.km. Out of these four, three are located within the dry zone (Deruru Oya, Kala Oya, and Malwathu Oya) and connected with the MRB through trans-basin channels. The fourth river, the Kalu River, is located within the wet zone, and floods in this river create a major threat for the western region of Sri Lanka, including the Colombo, Kaluthara, and Ratnapura districts.

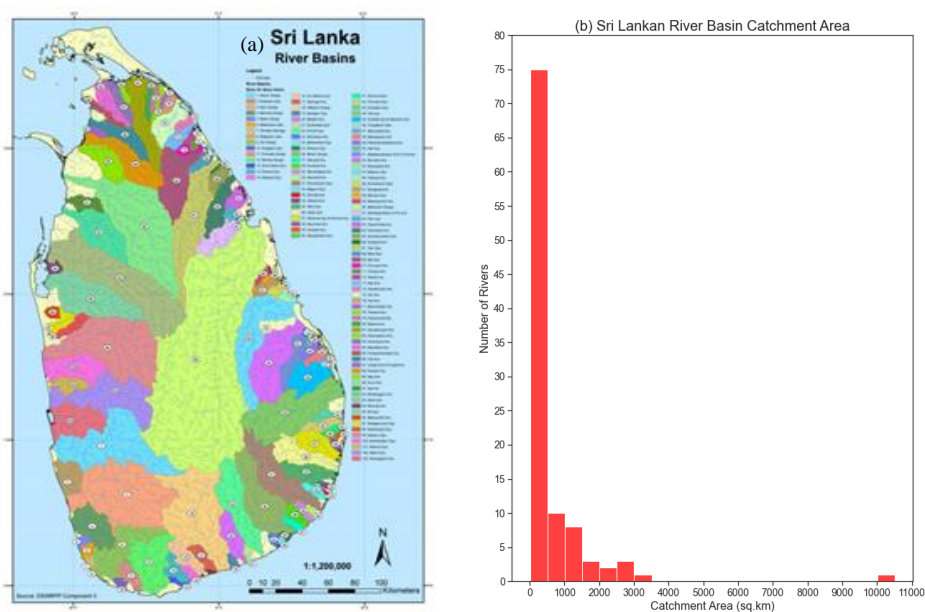


Figure 2.2. (a) Sri Lanka River Basins, and (b) Sri Lankan River Basin Catchment area.

Though the Kalu, Kelani, Gin, and Nilwala river basins in the southern part of the country cover only 13% of the land area, almost 30% of the population live in this portion of the nation. The dry-zone districts comprise 75% of the country (Amarasinghe, 2010).

According to an estimation in 1996, the total runoff is found to be 52,000 MCM/year on average, while the total dam capacity was 5940 MCM (Amarasinghe, 2010). Various categories of dams are constructed according to the materials they used, earthen, rock fill and concrete. The longest dam is called Parakrama Samudraya, which

is a 13.5 km long earthen dam with a storage capacity of 130 MCM. The tallest earthen dam is Senanayaka Samudraya, which is 34 m high and can contain 950 MCM of inflow. On the other hand, the tallest concrete dam with a height of 106m and a capacity of 730MCM is called the Victoria dam (Amarasinghe, 2010) and it is located in the Mahaweli River.

2.2.5 Agriculture led economy of Sri Lanka

Agriculture is the leading sector of the Sri Lankan economy. In response to seasonal rainfall, Sri Lanka has two agricultural seasons: Maha and Yala. In the current system, rice is the main crop variety and cultivating rice is the most important economic activity for the rural population of Sri Lanka. The total paddy cultivated area in 2019 was 1,116,933 hectares with a total yield of 4.5 million metric tons, as shown in Figure 2.3 (a) & (b) (DCS-SL, 2020a, 2020b).

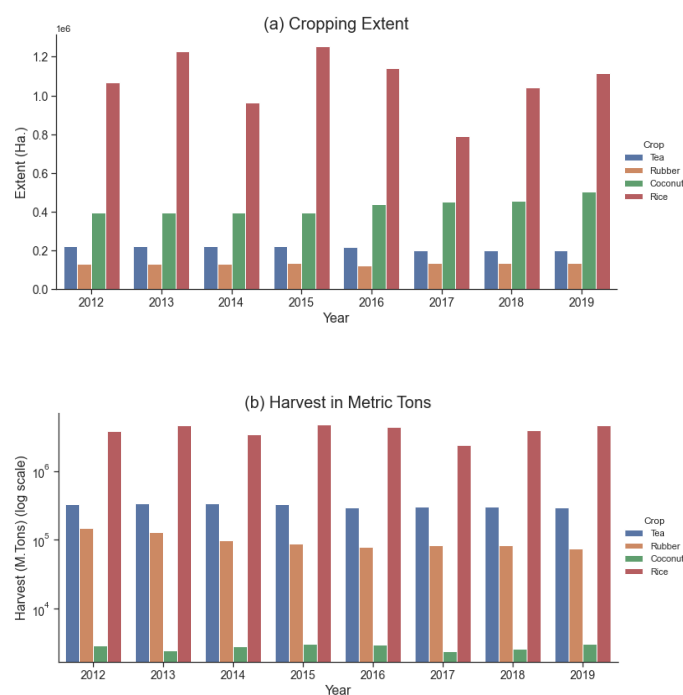


Figure 2.3. (a) Cropping Extents, and (b) Harvested Quantities.

The staple food of the Sri Lankan population is rice, and the country is self-sufficient in rice unless the cultivation is affected by natural disasters, and occasionally by wild animals and pests. In addition to rice, various other commercial crops are cultivated for local consumption as well as for export purposes. Other leading crop varieties are tea, rubber, and coconut. As shown in Figure 2.3 (a), the coconut accounts for the second highest cultivated extent with 503,452 hectares, followed by tea with 200,269 hectares and rubber with 137,608 hectares of cultivation extent in 2019 (DCS-SL, 2020a). Except for the above crop varieties, other crops such as maize, pepper, cinnamon, manioc, ground nuts, and chilies are cultivated in 6,000 to 10,000-hectare land areas in 2019. The crop cultivation extent composition in the year 2019 is given in Figure 2.4.

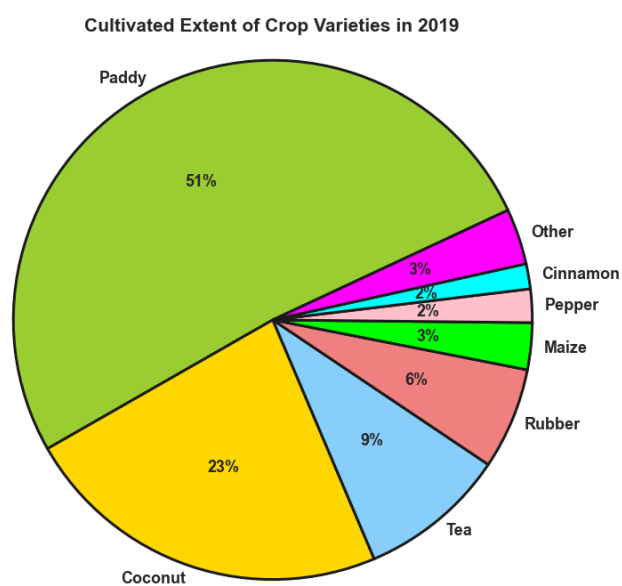


Figure 2.4. Cropping extent percentage in 2019

2.2.6 Power and Energy in Sri Lanka

According to the 2018 statistics published in the annual report of the Ceylon Electricity Board, the forms of power generation in Sri Lanka are hydropower (41.5%), oil (23.6%), coal (30.99%), wind (2.12%), and solar and biomass (1.78%) (CEB, 2018). According to this statistics, due to a higher rainfall received in the year 2018, the share of hydropower generation (6,382 GWh) went up to 41.5% compared to the previous years. The catastrophic year's (2017) hydropower generation found to be 27.22%. Further, it says that, by 2018, according to the government's policy to provide electricity to all, a 99.6% electrification level was achieved in Sri Lanka. Reflecting this achievement, the maximum demand reached up to 2,610.1 MW in 2018, while the total installed capacity was 4046 MW (hydropower: 1,793 MW, thermal: 2,037 MW, and solar, biomass, and wind power: 216 MW). As shown in Figure 2.5 (a) and (b), the share of energy generation among the past years varies according to the water availability in the hydropower reservoirs.

By the end of 2018, the total installed hydropower was 1793 MW. Sixteen (16) major hydropower reservoirs with an installed capacity of 1,280.75 MW and 206 mini hydropower plants with 512.2 MW were in operation by 2018 (CEB, 2018). Mahaweli Complex (in Mahaweli River), Laxapana Complex (in Kelani River), and Samanala Complex (Walawe River) are the leading major hydropower generating dam clusters with installed capacities of 815.2 MW, 370.5 MW, and 87 MW, respectively.

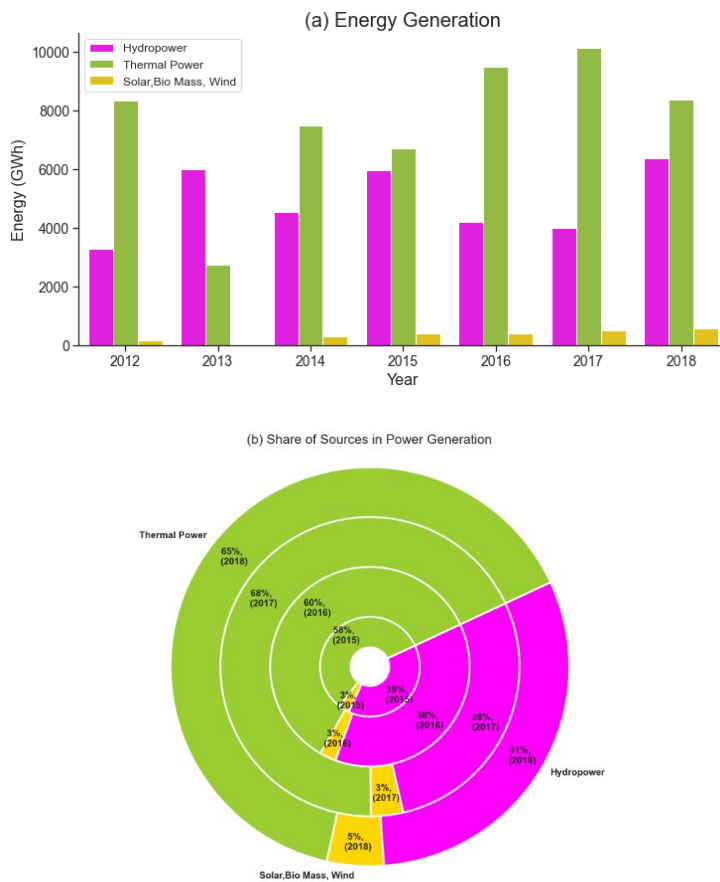


Figure 2.5. (a) Year wise energy generation, and (b) Share of sources in power generation

2.2.7 Climate change and natural disasters in Sri Lanka

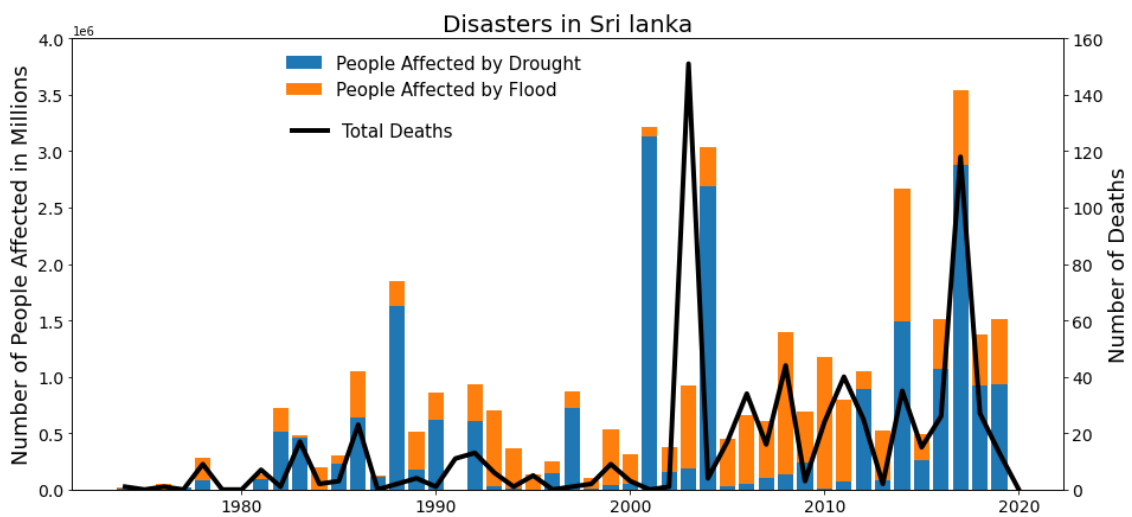


Figure 2.6. Flood and Drought Disasters and Death toll in Sri Lanka

Due to the climatic, topographic and hydrologic complexity, the Sri Lankan river basins are highly vulnerable to extreme weather events such as floods, droughts and landslides, and evidence shows that the occurrence of flood and drought events are on an increasing trend in the recent past, as shown in Figure 2.6 (UN Water, 2019). Loss of lives and damage to infrastructure will subsequently result in a burden on the economy of the country and will increase the vulnerability of the country to hazards. IPCC clearly indicates that countries in the tropical region, such as Sri Lanka, which receive much of the rainfall from the monsoonal and inter-monsoonal rainfall, might get affected due to the nature of future rainfall patterns (IPCC, 2013a).

2.2.7.1 Food Security

The rice sector in Sri Lanka has been challenged by the increasing impact of climate change: stagnation of yield growth, high production and labor costs, low private sector investment, and poor mechanization and use of technology among farmers. In recent years, Sri Lanka has been adversely affected by extreme weather conditions. As a result of the floods and droughts that occurred in various parts of Sri Lanka in 2017, as shown in Figure 2.3 (b), there was a deficit of 44% of the country's rice requirement, and this shortage had to be met by importing about 700,000 tons of rice (World-Grain, 2019). “Improving the resilience and sustainability of Sri Lanka’s national rice economy through environmentally sustainable approaches is of utmost importance to address the complex challenges of population growth, agricultural production, and climate change in Sri Lanka,” said Matthew Morell, Director General of the International Rice Research Institute. He further said that: “We are honored to have Sri Lanka’s continued trust and we remain committed to support their efforts to restore rice self-sufficiency and attain food security” (World-Grain, 2019).

2.3 Mahaweli River Basin and its development

The Mahaweli River is the largest river and the only perennial river in the country. The length of the river is 335 km, and it integrates the rainfall falling on all the three agro-climatic zones located within its catchment area of 10,300 sq.km (Figure 2.7). In the mid-20th century, the population in Sri Lanka (former Ceylon) had risen sharply. It was noted that more than three-quarters of the settlements were located in the wet zone (density more than 1,200 people per square mile) (MASL, 2020), which created an imbalance in the distribution of the population over the landmass; i.e., over 75% of the population were living within 30% of the total land. This situation urged the government to develop agricultural production in the dry zone. Therefore, the government decided to reclaim the dry zone for irrigated agriculture and shifted the population to the dry zone. As a result, the Mahaweli Development Plan was developed to utilize MRB's and the adjacent river basin's water resources to achieve the followings:

- Increase local agricultural production to satisfy the need of the population growth
- Decrease imports of agricultural goods
- Improve the economic conditions
- Develop the agriculture industry
- Reduce unemployment
- Improve food security through local production
- Contribution to the power sector

This development has taken place in different phases, and MRB has been interconnected with the other 4 major rivers to form a complex water management system consisting of multipurpose cascade reservoirs supplying water for irrigated agriculture and hydropower generation. It forms a major cluster of river basins covering 40% of the nation's land area, and water is being supplied from the Mahaweli River to the other four. Hence, the water resources of the other four river basins, namely Kala Oya, Malwathu Oya, Yan Oya and Maduru Oya, mainly or partly dependent on MRB.

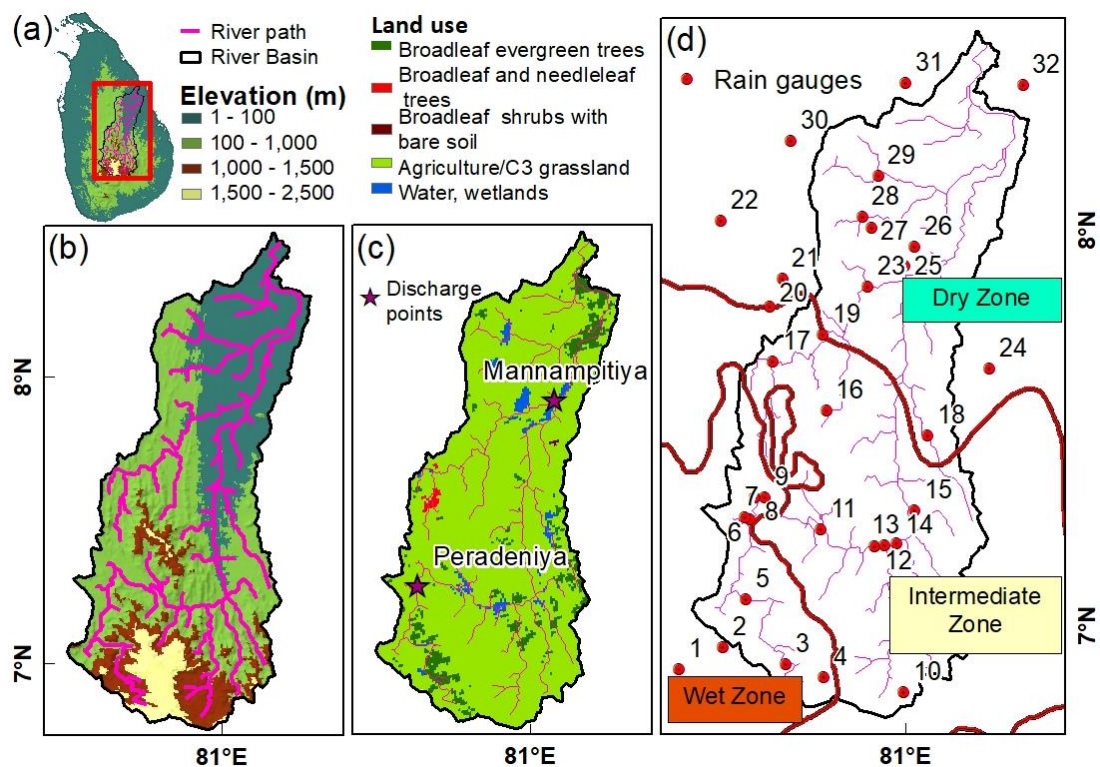


Figure 2.7(a) Topographical map of Sri Lanka with the demarcation of the Mahaweli River basin, (b) to-pography of Mahaweli River Basin, (c) land use with distribution of discharge measurement points, and (d) demarcation of climatic zones with rain gauge network

2.3.1 Mahaweli River Basin system

As explained earlier, MRB's water resources are shared with four other river basins mainly for paddy cultivation. The five basins create a complex irrigation network, which feeds nearly 100,000 hectares in a normal year. The system has been divided into several sub systems and named as shown in this Figure 2.8.

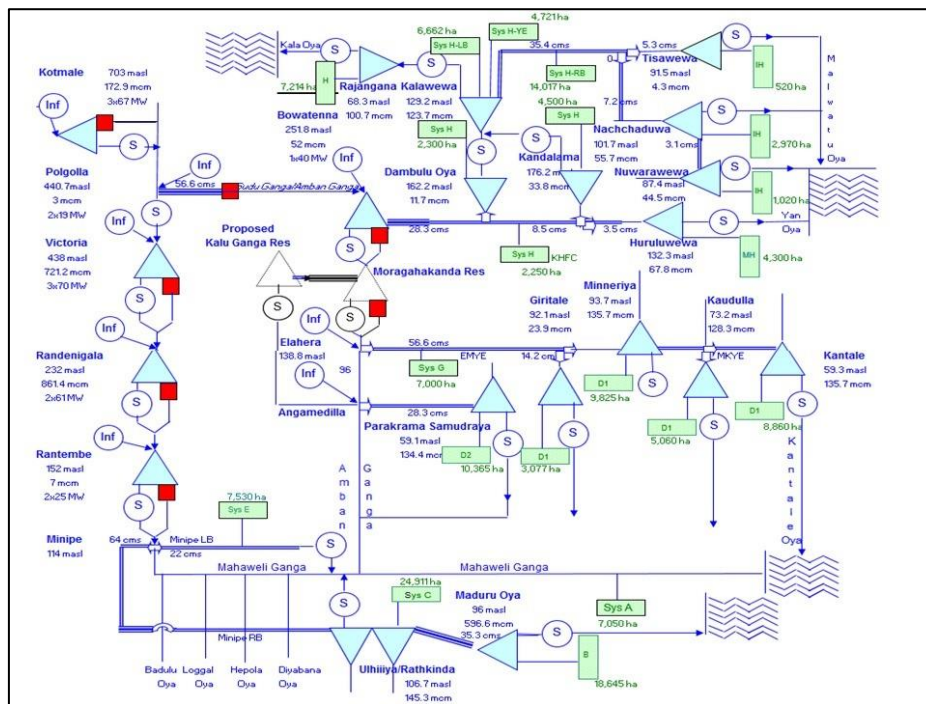


Figure 2.8. The schematic diagram of Mahaweli River Basin Multipurpose system (source: Mahaweli Authority of Sri Lanka)

MRB is a complex water management system consisting of more than 24 multipurpose reservoirs supplying water for irrigated agriculture, drinking water supply and generating hydropower. The hydro power is generated at 8 power stations while issuing water for irrigation, 8 power stations (total installed capacity of 839 MW). There are 4 major diversion points (Polgolla, Bowatenna, Elehara and Minipe) to divert water from the main stream to the irrigation schemes and downstream reservoirs. A total of 27 major irrigation schemes are receiving water from this basin with a total command area

of around 160,000 hectares (arable land area). The schematic diagram of the MRB multipurpose system is shown in Figure 2.8 (MASL-SL, 2018). In this figure, the reservoirs are shown by blue triangles, which are connected by the single blue lines representing the rivers; the red square shapes represent the hydropower plants, and the green rectangles represent the irrigation schemes in different names. Further, the circles with the letter 'S' represent supply channels, the circles with 'Inf' represent the inflow from its own catchments, the term 'masl' means the elevation in meters above mean sea level, the term 'mcm' is to represent the full supply capacity of a reservoir in terms of million cubic meters, and the term 'MW' explains the installed capacity of the power generators. In addition to that, the double and multiple thick lines represent manmade inter- and trans-basin tunnels in the system. Especially, the water yield in this river basin is diverted at the four main diversion weirs: the Polgolla, Minipe, Bowatenna, and Mavillaru diversions.

2.3.2 Climate and topography of MRB

Mahaweli is the only river in Sri Lanka, which intersects all these three climatic zones, as shown in Figure 2.7 (d) and topographic categories (Figure 2.7 (b)); thus, the rapid change of stream flow can be observed. The upper basin is located within the wet and intermediate climatic zones, while the dry low-lying agricultural plains are located within the dry zone. Within a year, different parts of MRB experience varied climatic conditions at a time horizon; i.e., when the upstream end of MRB experiences a rainy season, the downstream end experiences a dry season. The NE monsoon (December to February) brings more rainfall to the downstream region of MRB (~ 500-1200 mm). During the SW monsoon (May to September), the upstream region in the central hill receives high rainfall amounts (> 3000 mm), while the downstream region in the dry zone

experiences less than 500 mm rainfall. The IM-1 period (March to April) is famous for its warm weather, and the hilly region of MRB gets more rainfall of around 250 mm, while the rainfall over the rest of the basins varies between 100 to 250 mm. On the other hand, IM-2 stays over the country from October to November, bringing thunderstorms in the afternoon as a result of the influence of depressions and cyclones in the Bay of Bengal, and brings a balanced distribution of rainfall over 700 mm.

Due to the topographic, climatic and hydrologic complexity, this river basin is highly vulnerable to water related disasters such as floods and droughts. According to the Mahaweli Authority of Sri Lanka (MASL), the occurrence of heavy flood events have increased due to the increased intensity of rainfall by a large amount of downpour within a short period of time, and MRB experiences longer dry spells, particularly in the dry zone during cultivation periods.

2.3.3 Management of Mahaweli River Basin

The reservoirs and the irrigation systems are managed by different organizations according to the purpose of the reservoir in the multi-purpose system. The main three organizations, which are involved in managing the system, are the Mahaweli Authority of Sri Lanka, the Irrigation Department, and the Ceylon Electricity Board. In terms of agriculture, the MASL and ID-SL are the key entities for the management.

The Water Management Panel (WMP) comprises all the stakeholders under MRB and is the main body for policy making regarding water management. The Water Management Secretariat (WMS) provides technical support to the WMP regarding operational policy making and coordination among the stakeholders.

Reflecting the seasonal rainfall, the cultivation is carried out in the basin in two agricultural seasons: Maha (November to February) and Yala (May to August) seasons. Between these two main agricultural seasons, there are two off-seasons such as off season-1 between Maha and Yala (March and April) and off season-2 between Yala and Maha (September and October). The time series diagram of the climatic seasons and the agriculture seasons are given in Figure 2.9.

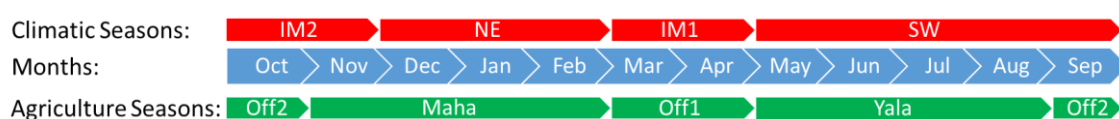


Figure 2.9. Time series of Climatic seasons and Agriculture seasons

The WMS is responsible for the preparation of the Seasonal Operation Plan (SOP). This plan is issued just before the beginning of each agriculture season (Maha and Yala). SOP is prepared through a consultative process, and all the stakeholders are required to submit their initial operation objectives for the season to WMS before the beginning of the season. In preparation of the SOP, the system is analyzed on a monthly basis for its irrigation and hydropower potential (MASL, 2020), and the documents are circulated among the stakeholders with the following contents:

- Planning assumptions
- Cultivation calendar
- Anticipated irrigation water balances
- Irrigation diversion schedules
- Anticipated reservoir trajectories
- Estimates of energy generation

2.3.3.1 Decision making process by WMS

The decision making process varies according to the main agriculture seasons, and the strategy of the WMS for decision making for each agriculture season is given below (MASL, 2015a, 2015b).

- The cultivation extent is decided based on the reservoir storage capacity at the beginning of the cultivation season
- Reliability of irrigation deliveries to irrigation systems – 80%
- Diversion policy at Polgolla – a long-term average diversion of 875 million cubic meters (mcm) per annum.
- Reservoir operation rules
- Reliability of power & energy demand – 100%
- Rationing policies – limited to the firm energy requirement of the reservoir in case of droughts
- Hydrology of the past 30 years

This plan is prepared on a monthly basis for 6 months, and hydrological uncertainties play a major role in determining the effectiveness of this SOP. A dry hydrologic condition over the past 30 years is used to estimate reliable irrigation water supply to maintain a high degree of reliability in supporting the planned crop. As a result, the potential water availability during a wet season is not properly estimated at the planning stage of the season. Therefore, understanding the seasonal variability of hydro-metrological variables

in advance through a reliable seasonal forecasting system can make room for more economic benefits for the river basin.

3 Development of an integrated approach for climate change impact assessment on hydro-meteorological characteristics of a river basin and its application in Mahaweli River Basin.

3.1 Introduction

Though climate change affects all areas of the world, some vulnerable nations, including least developed countries and small island developing states, will be affected most (Masson-Delmotte et al., 2018). Evidence shows that the globe is changing faster in terms of climate than ever before, and there will be a crisis not only on the environment but also on the global economy in the future (Toby et al., 2020). Therefore, strengthening disaster resilience is the key for achieving sustainable development. In these circumstances, climate change impact assessment is essential for each country in achieving their international obligations to address climate change, implement mitigating measures, and strengthen adaptation mechanisms.

Floods and droughts share a significant portion among the water-related disasters. Thus, climate change impact assessment at the basin scale provides a basis for understanding their influences on our environment and economy (Koike et al., 2014). Such assessments involve handling the cumbersome amount of data generated by several GCMs, which run under various future emission scenarios, and their applications in hydrological models. GCMs are the best tool currently available to estimate climate change; however, their outputs contain uncertainties and thus cannot be used directly for impact assessment studies (Freer et al., 2013; Nyunt, Koike, & Yamamoto, 2016; Rasmy, Koike, Lawford, & Hara, 2015). Therefore, decision-makers are only able to make decisions under uncertainties of GCMs. Such uncertainties are due to, for example, coarse

spatial and temporal resolution, the formulation of physical processes and parameterizations, the formulation of scenarios, the initial and boundary conditions of ensembles, the inconsistency of grid resolution between GCMs and basin-scale hydrologic models, and the structure and formulation of hydrological models (Bender, 2008; Mendez, Maathuis, Hein-Griggs, & Alvarado-Gamboa, 2020; Nyunt et al., 2016; Woldemeskel, Sharma, Sivakumar, & Mehrotra, 2014). Therefore, to address climate change impact under uncertainties of GCMs on basin-scale hydrology (i.e., floods, droughts, and water availability), assessment certainly requires: a) identifying appropriate GCMs for the study domain by eliminating GCMs that are poor at simulating past climatology; b) reducing biases in the selected GCMs using downscaling methods and bias correction algorithms; and c) choosing a physically-based distributed hydrologic (i.e., seamless) model that is capable of consistently simulating long-term, various hydrological responses for past and future climate through a literature review of various model developments.

Several past studies have attempted to understand the climate changes on a basin scale (hydro-meteorological characteristics) by overcoming the above scientific challenges (Gebrechorkos et al., 2020; Gosain et al., 2006; Koike et al., 2014; Nyunt et al., 2016; Pandey, Gosain et al., 2017; Rasmy et al., 2015). But none of the previous studies presented a comprehensive approach to assessing the climate change starting from model selection to the hydrological impact assessment including the inundation assessment. Therefore this study integrates all the components and assessment approaches to produce a comprehensive and cost-effective method that can be used in any of the river basins worldwide.

A study by Gosain et al. (2006) quantified the impact of climate change on the water resources of Indian river systems by coupling a specific GCM output to a hydrological model to generate hydrological responses except.

Reliable precipitation outputs from GCMs are essential to address the impact of climate change. To reduce uncertainty in GCM outputs, the performances of GCMs over a particular region can be evaluated by comparing their key meteorological elements (precipitation, air temperature, outgoing longwave radiation, sea surface temperature, sea level pressure, zonal wind and meridional wind) with historical reference data for a group of GCM outputs (Koike et al., 2014; Nyunt et al., 2016). This model evaluation is to verify whether selected GCMs can reasonably simulate the important mechanism of regional climate and to reduce the computational load of calculations and thus increase confidence levels on selected models and their representations at a local scale. The Data Integration and Analysis System of Japan (DIAS) has archived the World Climate Research Program's coupled-model inter-comparison project phase 5 (CMIP5) data on climate projections (Taylor, Stouffer, & Meehl, 2012) to facilitate GCMs' evaluation and selection processes effectively. Additionally, DIAS has developed a user-friendly CMIP5 data analysis tool (CMIP5-DIAS) to minimize the complexity in format, handle a massive amount of data, and provide easy access to data for all users from several disciplines (Kawasaki et al., 2017). This tool has been designed to compare historical reference data or reanalysis data (Koike et al., 2014) with a group of climate model outputs spatially, e.g., 2-D statistical analysis, to enable an effortless selection of appropriate models for a targeted region without downloading and processing big-data sets.

Generally, the reduction of biases in selected GCMs involves the applications of downscaling methods and/or bias correction algorithms. Downscaling (e.g., dynamic and statistical) approaches enable data transformation from coarse resolutions of GCMs to finer resolutions (Koike et al., 2014; Nyunt et al., 2016; Rasmy et al., 2015; L. E. I. Zhang et al., 2020). Though dynamic downscaling is a physically based approach using high-resolution numerical weather forecast models to produce finer-scale information from information based on coarse-grid GCMs by maintaining essential spatial correlation and physical relationships (Maurer & Hidalgo, 2008; Tang et al., 2016), it requires more computational power for multi-decadal simulations of an ensemble of GCMs with various emission scenarios, and thus is not feasible for individual countries or river basins (Maurer & Hidalgo, 2008; Nyunt et al., 2016). In this regard, the statistical downscaling approach has advantages over the dynamic approach as it involves downscaling variables using historical observations by preserving physically reasonable spatial and temporal relationships over a large spatially heterogeneous landmass (Maurer & Hidalgo, 2008). There are several statistical downscaling approaches introduced in literature, such as the constructed analogues method, linear interpolation, spatial disaggregation, and bias-correction and spatial disaggregation (Wood, Leung, Sridhar, & Lettenmaier, 2004). Similarly, CMIP5-DIAS has implemented a statistical-downscaling and bias-correction approach based on the study by Nyunt et al. (2016) and thus is taken into consideration in this study.

The estimation of the surface water budget consists of numerous processes which interact among them (e.g., rainfall, snowfall, canopy and ground interception, evapotranspiration, infiltration, and surface and subsurface flow). Therefore, climate change impact assessment of floods and droughts requires reliable physically-based

hydrologic models for a comprehensive understanding of floods and droughts as these two phenomena occur within a river basin sequentially. Hydrologic models should be able to simulate all significant components of hydrology for a long term, which are needed to reliably simulate past and future climate variables such as peak flows, flood inundation extents, and low flows seamlessly. The models are required to accommodate dynamic atmospheric long-term forcing data from historical or reanalysis products and GCM outputs, the basin-scale integration of globally available static data to represent topography, land use, and soil types with dynamic data to represent vegetation phenology. Moreover, the basin-scale integration of global data should be achieved. This is possible only with physically-based distributed hydrologic models (DHM) with horizontal discretisation. Therefore, the spatial distribution of the parameters of physical relevance (e.g., soil, land use, and vegetation dynamics) is represented and physical processes of interactions that allows change of parameter values based on physical processes for calibration and validation.

In the past, several physically-based distributed models were developed and used either separately or in an integrated manner, based on the complexity of the environmental challenge, by coupling suitable models to fulfil the requirements and utilize the individual strengths of the models. For example, two models (the MIKE SHE model and the FEFLOW model) were coupled to address a complex water-resources problem (Yamagata et al., 2012). The Water Energy Budget-based Distributed Hydrologic Model (WEB-DHM), which is capable of representing soil-atmosphere interaction, evapotranspiration and soil moisture fluctuation with the assimilation of remotely sensed input for representing vegetation phenology, was used in long-term climate studies (Jaranilla-Sanchez, Wang, & Koike, 2011; Wang et al., 2009a). Though WEB-DHM has

shown reasonable accuracy in reproducing water and energy budget estimations in the form of discharge and surface soil moisture on the basin scale (Jaranilla-Sanchez et al., 2011), it cannot be used for flood-related risk analysis and impact assessment under changing climate in a watershed (Rasmy, Sayama, & Koike, 2019) because of its limitations in simulating flood-inundation processes due to its model structure (i.e., flow-interval concept) and flow routing formulation (i.e., kinematic wave model). The Water Energy Budget-Based Rainfall-Runoff-Inundation (WEB-RRI) model has been developed to address this particular issue by incorporating water and energy budget processes, land-vegetation-atmosphere interactions, multi-layer soil moisture dynamics, and 2D lateral water flows to improve interception, evapotranspiration (ET), infiltration, runoff, and inundation processes, and then to improve the accuracy of low flow estimation, flood onset timing, peak flood discharge, and inundation characteristics. Notably, it is compatible with various input variables produced from multiple data sources such as satellites, reanalyses, in-situ, and GCM projections for long-term seamless simulation of past and future events (Rasmy et al., 2019). Therefore, assessing climate change impact using the WEB-RRI model can provide reliable and additional information on the basin-scale water cycle in contrast with earlier hydrological models.

Accordingly, this chapter presents an integrated new approach for assessing climate change impacts on the hydro-meteorological characteristics of river basins. The new approach provides evidence-based information to support policymakers for better decision making under the uncertainties of GCMs by identifying more appropriate climate models which can express the past climate of the study area and clarifying uncertainties among the range of outputs from selected GCMs. This method integrates the merits of CMIP5 data analysis and downscaling tools developed in DIAS and the

WEB-RRI model that is capable of reproducing various long-term hydrological variables for producing basin-scale evidence on climate change impact.

3.2 Research Framework

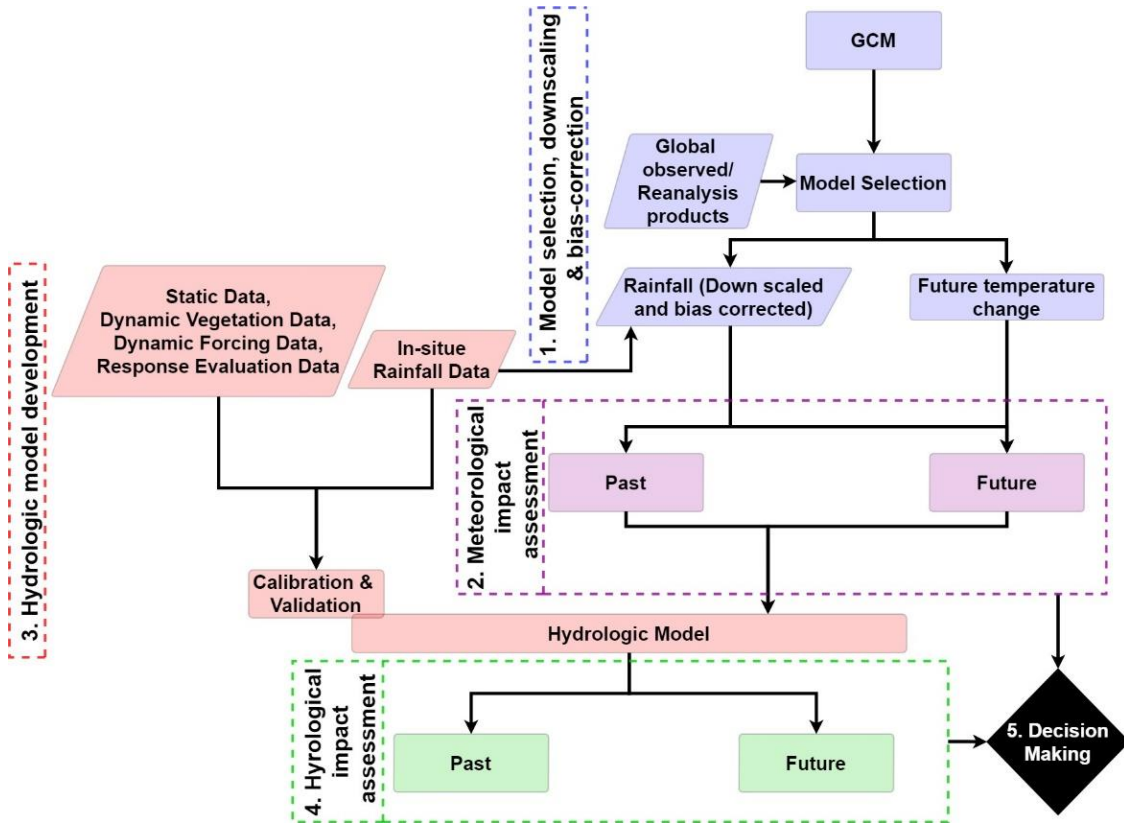


Figure 3.1. Research framework for climate change impact assessment.

This chapter focuses on developing a research framework using the present cutting-edge science and technology to assess the impact of climate change on river basins by identifying climate change signals and clarifying uncertainties. Figure 3.1 shows the overall research framework and methodology of this chapter. The research framework includes five main components: 1) GCMs selection and downscaling/bias correction of rainfall; 2) climate change impact assessments on meteorology; 3) DHM development to simulate the basin hydrological responses; 4) climate change impact assessments on

hydrology; and 5) facilitation of decision-making procedures. The details on the major components are described in Section 4: Methodology.

3.3 Study area

From this research's standpoint, it is crucial to select a study area that experiences wet and dry extremes due to various topographic and climatic conditions, is sensitive to climate change, and ensures the accessibility of locally-available, long-term, high-quality, and well-distributed rainfall and discharge data. The MRB which satisfies the above conditions was studied in this chapter.

3.4 Methodology

As stated in Section 3.2, this section describes the methodology of major components of the research framework implemented in this chapter.

3.4.1 GCM selection and downscaling/bias correction

3.4.1.1 GCM selection

According to past studies, GCMs have higher levels of uncertainties in reproducing past climatology or important rainfall mechanisms, and their performances vary significantly in a particular climatic region (Suzuki-Parker et al., 2018). The selection of suitable GCMs, which can represent the regional climate of the study area, is crucial for multi-model analysis. Since GCMs' resolutions are very coarse compared to basin-scale resolutions, choosing rainfall only from GCMs to check their performance is not appropriate because rainfall from GCMs may not reliably represent the regional mechanisms that influence rainfall. Hence, this study selected and compared GCM-simulated key meteorological variables such as temperature, humidity, radiation, wind speed, and precipitation with global reanalysis and observation data for the interested

regional and local domains. The domain scale of each variable is selected based on its representation of synoptic-scale phenomena that influence the rainfall mechanism over the study area. Spatial correlation (Scorr) and root mean square error (RMSE) were used for the quantitative comparison analysis of GCM outputs.

The monthly performance indices (i.e., Scorr and RMSE) were estimated for each selected variable of GCMs against observation or reanalysis data, and then seasonal and annual average performance indices were calculated (Nyunt et al., 2016). A Scorr index of 1 was given when the Scorr value of a GCM was greater than the Scorr value of the ensemble average of all GCMs, and otherwise, the Scorr index was set to 0. Similarly, if the individual RMSE value of a GCM was less than the ensemble average, an RMSE index of 1 or otherwise 0 was assigned. Further, an index for each meteorological variable (meteorological variable indexes) was calculated and given the value 1 if the sum of the Scorr index and the RMSE index was greater than 1, the value -1 if the sum of the Scorr index and the RMSE index was less than 1, or the value 0 if neither condition applied. Moreover, the total index was calculated by summing up all the corresponding meteorological variable indexes of each model. Finally, summing up the annual and seasonal total indexes of each model, the grand total was calculated.

3.4.1.2 Statistical bias correction and downscaling of precipitation

This study mainly targets the climate change impact on regional monsoon and its impact on local river basin. We analysed the GCM uncertainty by selecting the model which can reproduce the basic current climate and the bias correction is done by using the available highly dense rain gauge network data in the targeted basin to obtain high spatial resolution climate model outputs.

To downscale and bias-correct the selected GCMs precipitation outputs, CMIP5-DIAS employed a three-step statistical bias correction function (Kawasaki et al., 2017). At each rain gauge location, the time-series of GCM data were extracted and then divided into extreme-rainfall, normal-rainfall, and no-rainfall based on thresholds. The Generalized Pareto Distribution was used for extreme-rainfall correction, the gamma distribution was used for normal-rainfall correction, and the statistical ranking order was used for no-rain days correction (Nyunt et al., 2016). The bias-corrected rainfall data at each gauge location were resampled to hydrological model grids using the Thiessen polygon method and at 1-hour temporal resolution using a uniform distribution approach.

3.4.1.3 Temperature correction

The RCP8.5 radiative forcing scenario has been selected to assess the climate change under the business as usual condition in this study. The RCPs are the radiative forcing pathways which define an emission trajectory and concentration by the year 2100 (Stefanidis, Panagopoulos, & Mimikou, 2018; van Vuuren et al., 2011). For temperature correction, climatological differences of monthly temperature between the 20th-century historical reproduction data and the RCP8.5 future scenario data were quantified. The climatological differences in temperature were added to the past reanalysis temperature data to produce future temperature data for future hydrological simulations.

3.4.2 Hydrologic model

WEB-RRI, a physically-based distributed hydrological model, was used in this study to evaluate the water and energy flux components of MRB and then climate change impact on the river basin. Formulations of physical processes in WEB-RRI include the vertical transfer of moisture and energy fluxes, soil-vegetation-atmosphere interactions,

soil structure, soil moisture dynamics, lateral movements of water flow, and interaction between vertical and horizontal water flows. The overall structure of this model has four components: a) Simple Biosphere Model 2 module for the vertical energy and water flux transfer between land and atmosphere (Rasmy et al., 2019; Sellers, Los, et al., 1996; Sellers, Randall, et al., 1996); b) module for vertical soil water exchange based on Richard's equation and Darcy's equations for groundwater recharge (Rasmy et al., 2019; Wang et al., 2009a); c) 2-D diffusive wave lateral flow module for surface flow and groundwater flow (Rasmy et al., 2019; Sayama, Ozawa, Kawakami, Nabesaka, & Fukami, 2012); and d) the 1-D diffusive wave river flow module (Brunner, Simmons, Cook, & Therrien, 2010; Rasmy et al., 2019; Sayama et al., 2012). This model estimates evapotranspiration, soil moisture variation, low flow, flood onset timing, peak flood discharge, and inundation characteristics as response by taking numerous meteorological input (Rasmy et al., 2019). The governing equations of the above modules are given below;

(a) Simple Biosphere Model 2 module

The mass balance equation for the plant canopy interception is given by:

$$\frac{\partial M_{cw}}{\partial t} = P - D_d - D_c - \frac{E_{ci}}{\rho_w} \quad (1)$$

The mass balance equation for the ground interception in Simple Biosphere Model 2 is given by:

$$\frac{\partial M_{gw}}{\partial t} = D_d + D_c - \frac{E_{gi}}{\rho_w} \quad (2)$$

where subscripts cw and gw denote canopy and ground water storage, respectively. M , P , D_d , and D_c are the intercepted water (m), precipitation (m), canopy through fall rate (m/s), and canopy drainage rate (m/s), respectively. E_{ci} and E_{gi} are the evaporation rates of intercepted water from canopy and ground. ρ_w is the density of water (kg/m^3) and t is time in seconds. The maximum amount of canopy interception per unit area is defined by the Leaf Area Index (LAI) times 0.0001 m (Sellers, Randall, et al., 1996).

(b) The unsaturated zone vertical flow is given by the following water balance equations:

Surface layer soil moisture W_1 is given by:

$$\frac{\partial W_1}{\partial t} = \frac{1}{\theta_s D_1} \left(Q_1 - Q_{12} - \frac{E_g}{\rho_w} + \delta_1 \right) \quad (3)$$

Root zone soil moisture W_{ri} is given by:

$$\frac{\partial W_{ri}}{\partial t} = \frac{1}{\theta_s D_i} \left(Q_{i-1,i} - Q_{i,i+1} - \frac{E_{ct,i}}{\rho_w} + \delta_{ri} \right) \quad (4)$$

Deep layer soil moisture W_{di} is given by:

$$\frac{\partial W_{di}}{\partial t} = \frac{1}{\theta_s D_i} (Q_{i-1,i} - Q_i + \delta_{di}) \quad (5)$$

where Q_1 is the infiltration of water into the first soil layer (m/s), $Q_{i-1,i}$ is the water flow from the $i - 1^{th}$ layer to the i^{th} layer, E_g is the ground surface evaporation rate from surface soil layer, $E_{ct,i}$ is the vegetation canopy transpiration rate through the stomata ($\text{kg/m}^2/\text{s}$) in the i^{th} layer of the root zone, D_i is the depth of the i^{th} soil layer (m), θ_s is

the saturated volumetric water content (m^3/m^3), ρ_w is the density of water (kg/m^3), and δ is the flow added or subtracted due to the horizontal and vertical movement of ground water flow (Wang et al., 2009b).

(c) 2-D diffusive wave lateral flow module

The equations for flow calculations in x- and y- directions are as follows:

$$q_x = -\frac{1}{n} h^{5/3} \sqrt{\left| \frac{\partial H}{\partial x} \right|} \text{sgn} \left[\frac{\partial H}{\partial x} \right] \quad (6)$$

$$q_y = -\frac{1}{n} h^{5/3} \sqrt{\left| \frac{\partial H}{\partial y} \right|} \text{sgn} \left[\frac{\partial H}{\partial y} \right] \quad (7)$$

The mass balance equation is spatially discretized for calculating changes in water level at each grid as follows:

$$\frac{dh^{i,j}}{dt} = \frac{q_x^{i-1,j} - q_x^{i,j}}{\Delta x} + \frac{q_y^{i,j-1} - q_y^{i,j}}{\Delta y} + h_e^{i,j} \quad (8)$$

where q_x and q_y are the unit width discharges in x- and y-directions, n is Manning's roughness parameter, h is the height of water from the surface, H is the height of water from the datum, sgn is the signum function. $q_x^{i,j}$ and $q_y^{i,j}$ are the discharges in x- and y-directions from a grid cell at a location (i,j) , and $h_e^{i,j}$ is the effective overland storage of water (m) due to rainfall after accounting all the sinks (interception, ET, and infiltration) and sources (e.g. upward movement of ground water flow) at a grid cell location (i,j) (Sayama et al., 2012).

(d) 1-D diffusive wave river flow module

1D diffusive wave equation, which is the same equation as Eq. 7 and q_y was set it to zero to get a one-dimensional flow equation (Rasmy et al., 2019; Sayama et al., 2012; Wang et al., 2009b).

Model calibration and validation were performed for the period when the basin was under natural flow conditions before the construction of any dams in the upper reach of the discharge measurement location. Two test scenarios were analysed in this research; the baseline scenario and the future scenario. In the baseline scenario, past hydrological simulations were carried out for 20 years (1981 to 2000), based on the CMIP5 20th century historical reproduction test scenario forcing data. In the future scenario, simulations were done for 2026 to 2045, based on RCP8.5 scenario model output variables.

3.5 Data and model set-up

3.5.1 Data for GCM selection, past and future climate data

GCMs represent the physics of the atmosphere and ocean for simulating the response of global climate as a result of increasing greenhouse gas emission (IPCC, 2013b). CMIP5-DIAS archives a total of 44 GCM model outputs of various experiments, including climate projections of the four scenarios of RCP2.6, RCP4.5, RCP6.0 and RCP8.5, as well as historical reference data from institutions around the world. Global observations and re-analysis products from 1981 to 2000 were utilized to select the reasonable number of GCMs based on their regional- and local-scale performance using different types of databases. For precipitation, the Global Precipitation Climatology Project dataset was used for evaluating GCMs' monthly climatology of precipitation (Adler et al., 2003). The Outgoing Longwave Radiation at the top of the atmosphere was obtained from the

National Oceanic and Atmospheric Administration (Liebmann & Smith, 1996). Sea Surface Temperature data were collected from the Hadley Centre (Rayner et al., 2003). The rest of the variables were obtained from the Japanese 55-year Reanalysis (JRA-55) (Kobayashi et al., 2015).

Asian monsoons and other climate drivers such as Indian Ocean Dipole and the El Niño Southern Oscillation influence the climate patterns of countries in the Indian Ocean region (Sahu, Yamashika, & Takara, 2010). To include the effect of climatic drivers at local and regional scales, the performance evaluation of GCMs was carried out in two spatial domains over Sri Lanka. The domains were 1) regional domain (45°E- 140°W, 35°S - 35°N) for SST, SLP, zonal wind, and meridional wind, and 2) local domain (73°E- 89°E, 1°N - 15°N) for other selected variables (e.g., PR, T_{air} , and OLR). Moreover, to represent temporal and seasonal variations, the SW and NE monsoon periods were considered along with monthly climatology. During the final evaluation, close attention was given to GCMs that could appropriately reproduce precipitation.

According to the scoring method described in Section 3.4.1.1, the models with a high grand total were selected for further analysis. As shown in Table 3-1, four models with a grand total over 12 were selected, while poor-performance models were removed in terms of precipitation (the MPI-ESM-MR during the SW monsoon and the ACCESS1.0 during the NE monsoon). Models that did not have the complete set of data for future rainfall (CanCM4, GFDL-CM2.1, and MPI-ESM-P) were also removed.

Table 3-1. Model selection summary for annual, SW monsoon, and NE monsoon period average.

Model Name	Institute	Country	Annual		SW monsoon		NE monsoon		Grand Total *	Remarks
			Precipitation	Total Index	Precipitation	Total Index	Precipitation	Total Index		
ACCESS1.0	CSIRO-BOM	Australia	0	4	1	6	0	3	13	PPR
ACCESS1.3	CSIRO-BOM	Australia	-1	-3	-1	-3	-1	3	-3	
BCC-CSM1.1	BCC	China	-1	-1	-1	2	0	1	2	
BCC-CSM1.1(m)	BCC	China	0	-2	0	-3	0	1	-4	
BNU-ESM	BNU	China	1	3	1	1	1	1	5	
CanCM4	CCCMA	Canada	1	5	1	5	1	4	14	FF
CanESM2	CCCMA	Canada	1	6	1	5	0	2	13	Selected
CCSM4	NCAR	USA	1	3	1	4	-1	0	7	
CESM1(BGC)	NCAR	USA	1	3	1	5	0	1	9	
CESM1(CAM5)	NCAR	USA	1	5	1	6	-1	0	11	
CESM1(FASTCHEM)	NCAR	USA	1	-1	1	3	-1	0	2	
CESM1(WACCM)	NCAR	USA	1	6	1	0	-1	3	9	
CMCC-CESM	CMCC	Italy	-1	3	-1	5	1	2	10	
CMCC-CM5	CMCC	Italy	-1	3	-1	4	0	3	10	
CNRM-CM5	NCMR	France	1	6	1	5	1	4	15	Selected
CNRM-CM5-2	NCMR	France	0	4	0	3	1	3	10	
CSIRO-Mk3.6.0	CSIRO-QCCCE	Australia	-1	-1	-1	-1	0	1	-1	
FGOALS-g2	LASG-CES	China	0	-1	0	-1	1	0	-2	
FIO-ESM	FIO	China	1	2	1	3	-1	-1	4	
GFDL-CM2.1	NOAA-GFDL	USA	1	4	1	7	1	5	16	FF
GFDL-CM3	NOAA-GFDL	USA	1	4	1	6	-1	0	10	
GFDL-ESM2G	NOAA-GFDL	USA	1	5	1	6	1	2	13	Selected
GFDL-ESM2M	NOAA-GFDL	USA	1	1	1	2	1	3	6	
GISS-E2-H	NASA-GISS	USA	-1	-2	-1	-2	0	2	-2	
GISS-E2-H-CC	NASA-GISS	USA	-1	0	-1	-2	0	3	1	
GISS-E2-R	NASA-GISS	USA	-1	0	-1	-1	0	5	4	
GISS-E2-R-CC	NASA-GISS	USA	-1	2	-1	-1	0	3	4	
HadCM3	MOHC	UK	-1	0	0	2	0	1	1	
HadGEM2-ES	MOHC	UK	-1	0	0	2	1	5	7	
INM-CM4	INM	Russia	0	-2	1	1	0	-1	-2	
IPSL-CM5A-LR	IPSL	France	0	-2	0	-3	-1	-4	-9	
IPSL-CM5A-MR	IPSL	France	0	-1	0	0	0	-2	-3	
IPSL-CM5B-LR	IPSL	France	-1	-4	-1	-4	-1	0	-8	
MIROC-ESM	UT	Japan	0	-3	-1	-4	0	0	-7	
MIROC-ESM-CHEM	UT	Japan	0	-2	-1	-3	0	-1	-6	
MIROC4h	UT	Japan	0	2	-1	0	1	4	6	
MIROC5	UT	Japan	1	5	1	5	0	2	12	
MPI-ESM-LR	MPI-N	Germany	1	7	1	7	1	5	19	Selected
MPI-ESM-MR	MPI-N	Germany	1	6	0	1	3	5	19	PPR
MPI-ESM-P	MPI-N	Germany	1	7	1	7	1	6	20	FF
MRI-CGCM3	MRI	Japan	-1	-2	-1	-4	0	3	-3	
MRI-ESM1	MRI	Japan	-1	-4	0	-5	-1	0	-9	
NorESM1-M	NCC	Norway	1	-1	1	2	-1	-3	-2	
NorESM1-ME	NCC	Norway	1	0	1	2	0	-1	0	

Grand Total* = Annual Total Index + SW Total Index + NE Total Index

FF = Failed to simulate Future rainfall

PPR = Poor Precipitation Representation in past

The selected models and their latitudinal and longitudinal grid size are CanESM2 (2.7906°, 2.8125°), CNRM-CM5 (1.4008°, 1.40625°), GFDL-ESM2G (2.0225°, 2.0°), and MPI-ESM-LR (1.8653°, 1.875°). The grid locations of the selected models over Sri Lanka are given in Figure 3.2.

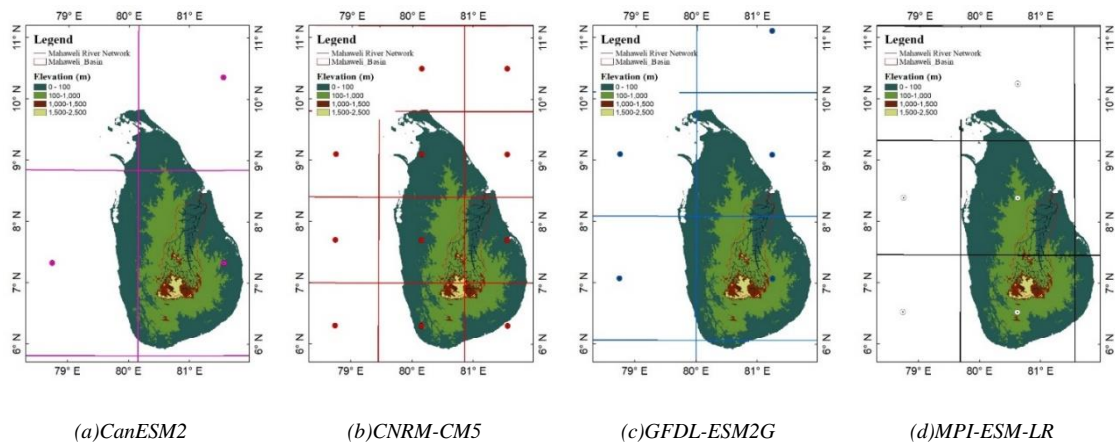


Figure 3.2. GCM grid distribution over Sri Lanka (a) CanESM2, and (b) CNRM-CM5, and (c) GFDL-ESM2G, and (e) MPI-ESM-LR.

3.5.2 Data for bias correction of rainfall and hydrological modeling

a) Long-term rainfall data: Daily rainfall data recorded at 32 rain gauge stations (Figure 2.7 (d)) by respective organizations (Mahaweli Authority of Sri Lanka, Irrigation Department, and Department of Meteorology) were obtained for the period from 1980 to 2018. Table 3-2 lists rain gauges and their respective climatic zones with the locations and annual average rainfall.

b) Elevation and hydrographic data: HydroSHEDS (Hydrological data and maps based on Shuttle Elevation Derivatives at multiple Scales) is a mapping product which provides seamless hydrographic data in multiple spatial resolutions. This is a collection of geo-referenced vector and raster data sets which were derived based on high-resolution digital elevation data of NASA's Shuttle Radar Topography Mission (SRTM) (Lehner, Verdin, & Jarvis, 2008). HydroSHEDS provide various topographic maps which are compatible with WEB-RRI model for hydrological analysis (Rasmy et al., 2019). This study used the 15 arc-second (~500 m at the equator) void-filled digital elevation model, as in Figure 2.7 (b), from which drainage direction data and flow accumulation data were acquired for the model setup.

Table 3-2. Daily rain gauges in the Mahaweli River basin with names, climatic zones, locations and annual average rainfall in mm.

No.	Station Name	Climatic Zone	Latitude (N)	Longitude (E)	Annual Average Rainfall (mm)
1	Maliboda	Wet	6.89	80.43	4582
2	Watawala	Wet	6.95	80.54	5141
3	Calidonia	Wet	6.90	80.70	3759
4	Ambewela	Wet	6.87	80.80	2071
5	Kotmale	Wet	7.06	80.60	3237
6	Peradeniya_ID	Wet	7.27	80.61	1823
7	Peradeniya_Bot_Gar.	Wet	7.27	80.60	1919
8	Katugastota	Wet	7.32	80.62	1780
9	Polgolla	Wet	7.32	80.65	1808
10	Bandarawela	Intermediate	6.83	81.00	1519
11	Victoria	Intermediate	7.24	80.79	1466
12	Randenigala	Intermediate	7.20	80.92	1687
13	Rantembe	Intermediate	7.20	80.95	1726
14	Minipe LB	Intermediate	7.21	80.98	1645
15	Mapakadawewa	Intermediate	7.29	81.03	1800
16	Illukumbura	Intermediate	7.54	80.80	2528
17	Bowatenna	Intermediate	7.67	80.67	1649
18	Ulhitiya	Dry	7.48	81.06	1899
19	Elehara	Dry	7.73	80.79	1812
20	Dambuluoya	Dry	7.81	80.66	1794
21	Kandalama	Dry	7.88	80.69	1388
22	Kalawewa RB	Dry	8.02	80.54	1339
23	Angamedilla	Dry	7.86	80.91	1591
24	Maduru oya	Dry	7.65	81.22	1723
25	Parakramasamudraya	Dry	7.91	81.00	1572
26	Palugasdamana	Dry	7.96	81.03	1426
27	Girithale	Dry	8.00	80.92	1364
28	Minneriya	Dry	8.03	80.89	1258
29	Kaudulla_Wewa	Dry	8.14	80.93	1425
30	Huruluwewa	Dry	8.22	80.71	1263
31	Kantalai	Dry	8.37	81.00	1465
32	Allai_Tank	Dry	8.37	81.30	1315

c) Soil and land-use data: the Food and Agriculture Organization's 9 km-spatial-resolution soil-type distribution data were used to represent spatially heterogeneous soil parameters such as saturated hydraulic conductivity for the surface soil layer, the root zone, and the groundwater layer, saturated soil moisture content, residual soil moisture

content, and Van Genuchten alpha and n. In addition, USGS's 1 km-spatial-resolution land-use data were used for classifying land-use and vegetation types, as in Figure 2.7 (c). Soil-type data and land-use data at various spatial resolutions were resampled to model a grid resolution (~500 m horizontally) by using a linear interpolation method.

d) Dynamic vegetation data: The WEB-RRI model also requires the Fraction of Photo-synthetically Active Radiation (FPAR) and the Leaf Area Index (LAI) for the estimation of terrestrial energy, water, and carbon budget processes (Rasmy, Sayama, & Koike, 2019). Moderate Resolution Imaging Spectroradiometer (MODIS) global products (MOD15A2) of the Terra satellite provide information on LAI and FPAR based on 08-day temporal resolution composites at 1 km spatial resolution. These data were downloaded from the NASA Earth Observation Data and Information System (Breeick, 2020) and projected and resembled to the WEB-RRI model grid by NASA's Modis Reprojection Tool (MRT).

e) Hydrological model forcing data: Atmospheric forcing data for the WEB-RRI model (except rainfall data) were obtained from the Japanese 55-year Reanalysis project (JRA-55) of the Japan Meteorological Agency (JMA) (Kobayashi, et al., 2015). JRA-55 produces data at 0.125° spatial and 3-hour temporal resolutions for variables such as air temperature, specific humidity, zonal wind, meridional wind, cloud cover, downward shortwave radiation, downward longwave radiation, and surface pressure. Therefore, the spatial and temporal resampling was done to acquire data at WEB-RRI model resolution (~500 m horizontal and 1 h temporal resolutions) by using a linear interpolation method.

f) Discharge data: For the purpose of calibration and validation of the WEB-RRI model, daily discharge data recorded in the Peradeniya discharge location (7.27E,

80.61N) by the Irrigation Department were collected for the period from 1980 to 2018 (Figure 2.7 (c)).

The WEB-RRI all-time Past and Future inundation files for each GCMs were obtained and the shapefile of the inundation area more than 1m depth of inundations have been regenerated. This regenerated shapefiles were overlaid on top of the following dataset in the Google Earth Engine (GEE) to estimate the inundated population and inundated cropland and urban area respectively.

3.5.3 Data for socio-economic damage assessment

In recent years, an increased number of inundation modelling studies have taken place on flood events and the assessments of flood-related impacts where sufficient ground data are available at catchment scales (Afifi et al., 2019; Kiczko & Mirosław-Świątek, 2018; Papaioannou et al., 2019; Zhu et al., 2019); however, the application of flood inundation modelling is useful in the catchments, which have insufficient flood-related data (Papaioannou et al., 2019). Accordingly, in the absence of MRB's flood-related and socio-economic data, we used the model simulated flood inundation area and the global dataset on population and land use in this study. Therefore, we obtained the WEB-RRI all-time Past and Future inundation files for each GCMs, and regenerated the shapefile of the inundation area more than 1m depth of inundations. These regenerated shapefiles were overlaid on top of the following dataset in the Google Earth Engine (GEE) to estimate the inundated population and inundated cropland and urban area.

a) Population data: The dataset for reference epoch for 2015 of Global Human Settlement Layer data on population grids, 250 m resolution, which is archived in the GEE data catalogue (European-Commission, 2015), were used as the reference data to

assess the affected population in the past and future. Due to the unavailability of future population growth in the basin area, the past observed population data was used for the future damage estimation.

b) Cropland and urban area data: The 2013 dataset of MODIS Land Cover Type Yearly Global 500 m resolution data archived in GEE was used to assess the past and future affected cropland and urban area (Friedl & Sulla-Menashe, 2019). A similar assumption employed to the population data was used for the future damage assessment due to the unavailability of the cropland and urban area coverage.

3.5.4 Hydrological model set-up

To calibrate the model, we need energy budget data and water budget data. The energy budget data is obtained from reanalysis, and the water budget data is obtained from observed rainfall and discharge, and the evaporation is calculated by energy budget in the model.

The data required for the WEB-RRI model set-up (Section 3.5.2) were projected into a common projection system of ~500 m spatial and 1-hour temporal resolutions. Several assumptions were taken into consideration in this study to address various limitations in data and model integration. Future static data on topography, soil type and land use were assumed to be the same as the past data. In addition, since the MODIS data for LAI and FPAR are only available from the year 2000 to the present, the data for previous years (1980 to 1999) were assumed to be the same as the data of the year 2000.

3.5.5 Model performance metrics

Performance metrics, Nash-Sutcliffe Efficiency Coefficient (NSE) (Nash & Sutcliffe, 1970), Mean Bias Error (MBE), and Root Mean Square Error (RMSE), were used for the evaluation of model performance and other assessment purposes.

$$Nash = \frac{\sum(O_i - \bar{O})^2 - \sum(O_i - S_i)^2}{\sum(O_i - \bar{O})^2} \quad (9)$$

$$MBE = \frac{\sum(S_i - O_i)}{N} \quad (10)$$

$$RMSE = \sqrt{\frac{\sum(S_i - O_i)^2}{N}} \quad (11)$$

where O is observed discharge, S is model simulated discharge, and N is the number of data points used for the calculation

3.5.6 Qualitative and quantitative decision index

Based on quantitative information from GCMs, with the range of uncertainty, qualitative assessments were carried out to provide a range of the confidence level for future decision making, which is similar to the method used in IPCC-AR4 (i.e., very-low to very-high), to discuss the findings of this research. The qualitative levels of confidence used in this study were as follows: very likely (if all four models agree), likely (if three of them agree), and uncertain (if two models agree and two disagree).

The range of the confidence level was derived either from %Change or actual future-minus-past values ranging from the lowest to highest model outputs. The change rate (%Change) was defined as the percentage difference between future and past

characteristic variables per unit past characteristic variable. In the following analysis, the range was decided in either positive direction or negative direction, including the zero values given wherever the level of confidence was certain.

3.6 Results and discussion

In this research, two sets of GCM outputs (i.e., past and future climates) were analysed. The past climate analysis was carried out for 20 years during the historical model simulation period (1981 to 2000), and the future climate analysis was done for the 20-year period from 2026 to 2045 for the RCP8.5 scenario (i.e., business as usual). This section also focuses on producing scientific evidence for decision making by identifying climate change signals, clarifying the range of GCM uncertainty, and classifying the levels of confidence and their ranges for hydro-meteorological variables. The spatial and temporal variations of rainfall, temperature, discharge, and inundation extent were investigated for both climates.

3.6.1 Meteorological assessment

3.6.1.1 Basin-scale temperature changes

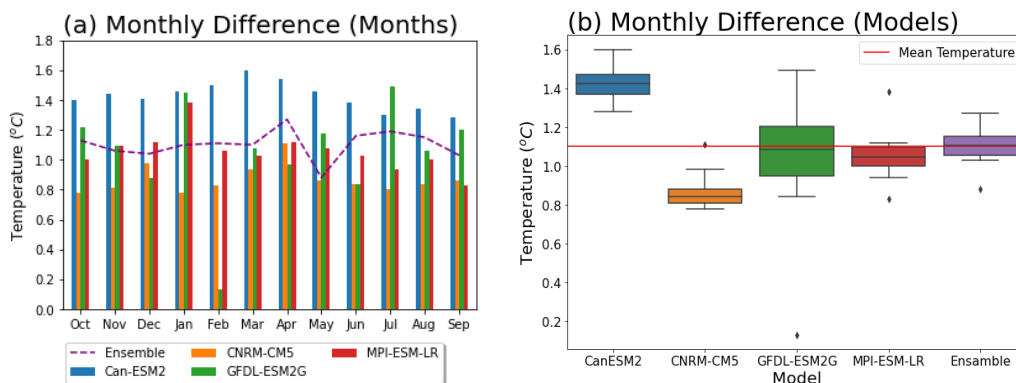


Figure 3.3. Basin average temperature difference (future-past): (a) bar plot for monthly changes and (b) box and whisker plot for annual changes.

Monthly climatology of future and past basin averaged temperature of selected GCMs was calculated to investigate the global warming impact, and their differences (i.e.,

future minus past) were plotted in Figure 3.3 (a) and (b). Each model shows an increase in temperature in the future climate. CanESM2 (1.3-1.6 °C), GFDL-ESM2G (0.8-1.5 °C), and MPI-ESM-LR (0.9- 1.1 °C) show higher increases, whereas CNRM-CM5 show a lower increase of 0.8-1.0 °C. On average, an increase of about 1.1 °C was projected over the targeted future 20-years. Future temperature data were prepared for hydrological model simulations by adding the climatological differences of GCM simulated temperature to the reanalysed temperature dataset to account for evapotranspiration changes.

3.6.1.2 Monotonic trend of rainfall

The basin is divided into three zone based on the climatic regimes (wet, intermediate, and dry), and the zonal averages were calculated for observed data and GCM model outputs. The monotonic rainfall trends projected by GCMs and observed by ground data were investigated for each climatic zones and for the whole basin (Figure 3.4).

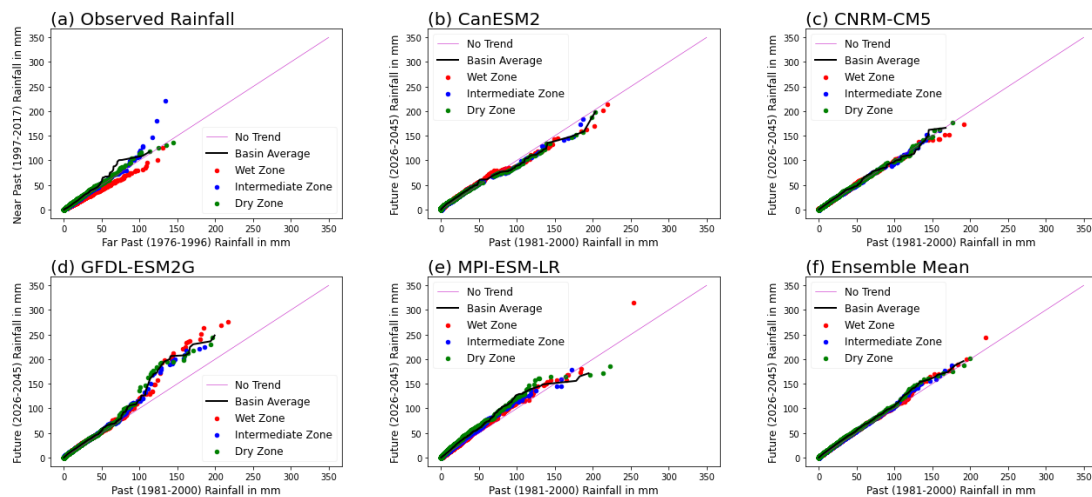


Figure 3.4. (a) Trend analysis of far past (1976-1996) vs near past (1997-2017) observed rainfall and trend analysis of past vs. future GCM rainfall of (b) CanESM2, (c) CNRM-CM5, (d) GFDL-ESM2G, (e) MPI-ESM-LR, and (f) Ensemble Mean.

As shown in the Figure 3.4 (a), wet zone average rainfall and most extreme rainfall of dry zone show decreasing trend in near past while the most extreme rainfall of intermediate zone show an increasing trend. On basin scale, the extreme rainfall of observed rainfall show an increasing trend in near past. As shown in Figure 3.4 (b-e), based on the basin average rainfall plot, GFDL-ESM2G and MPI-ESM-LR illustrate a future increase in rainfall, while CanESM2 shows a decreasing trend in future rainfall. Also, the future basin average rainfall simulated by CNRM-CM5 shows nearly no change. Hence, the GCMs show that this analysis cannot obtain a certain future trend in rainfall and a firm conclusion. Though the GCMs show an uncertain future trend, the observed basin averaged rainfall shows an increasing trend in near-past rainfall.

Since the monotonic trend show only the changes in low and extreme values, the annual and seasonal climatological changes should be investigated to understand the future trend in rainfall.

3.6.1.3 Changes in annual climatology of rainfall

The annual average rainfall changes between past and future among the selected GCMs were analysed at the basin scale, and the results are presented in Figure 3.5 (a). As shown in the figure, all models show an increasing trend in basin average rainfall; hence, it is very likely that the future climate will experience more rainfall compared to the past climate. The rainfall is projected to increase by about 19% (~370 mm/year) in the future. In addition, CanESM2, GFDL-ESM2G, and MPI-ESM-LR show higher rainfall increase rates (23%, 20%, and 24%, respectively) due to higher warming rates, whereas CNRM-CM5 show a lower increase rate (10%) due to a lower warming rate (Figure 3.3). This projection can be supported by the Clausius-Clapeyron equation saying that more

moisture will be held at a warmer atmosphere; therefore, the warmer climate predicted heavier rainfall increase in the future. A similar study conducted in India, another Asian monsoon Regional country, by Chaturvedi *et al.*, (2012) (Chaturvedi, Joshi, Jayaraman, Bala, & Ravindranath, 2012; Christensen et al., 2013) has confirmed a future increase in all-India mean precipitation, under the business as usual scenario, due to increased warming effect.

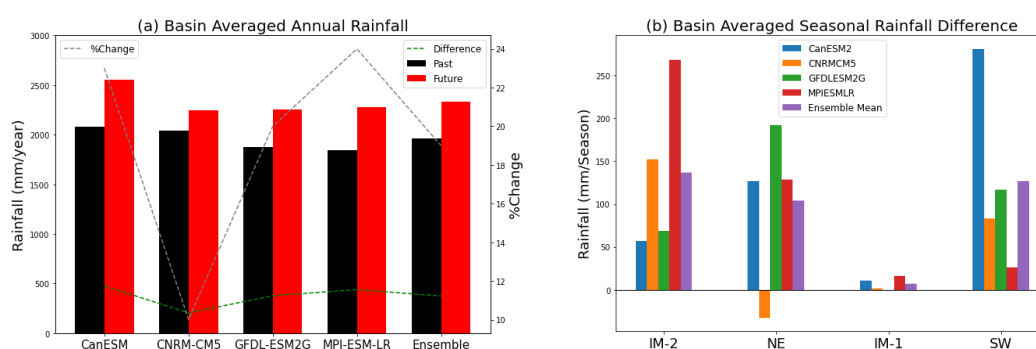


Figure 3.5. (a) The comparison of basin average annual rainfall (mm/year) between past and future climate and percentage changes (%) for each selected GCM and (b) basin averaged seasonal rainfall differences (Future – Past) for selected GCMs and the ensemble mean

As stated earlier, rainfall in Sri Lanka is influenced mainly by seasonally-varying monsoon systems and their interactions with the island’s topography, and thus the elevated regions receive more rainfall. Figure 3.6 (a) to (e) compares the spatial distribution of changes in annual average rainfall for the GCMs and their ensemble mean. All four models indicate that the southern hilly region of MRB will very likely receive more rainfall in the upstream area under the future warmer climate.

In addition, it is also important to note that the spatial changes of rainfall projected by CNRM-CM5 will take place at a much lower rate compared to those projected by the other models, as it projected a lower warming rate (Figure 3.3 (b)).

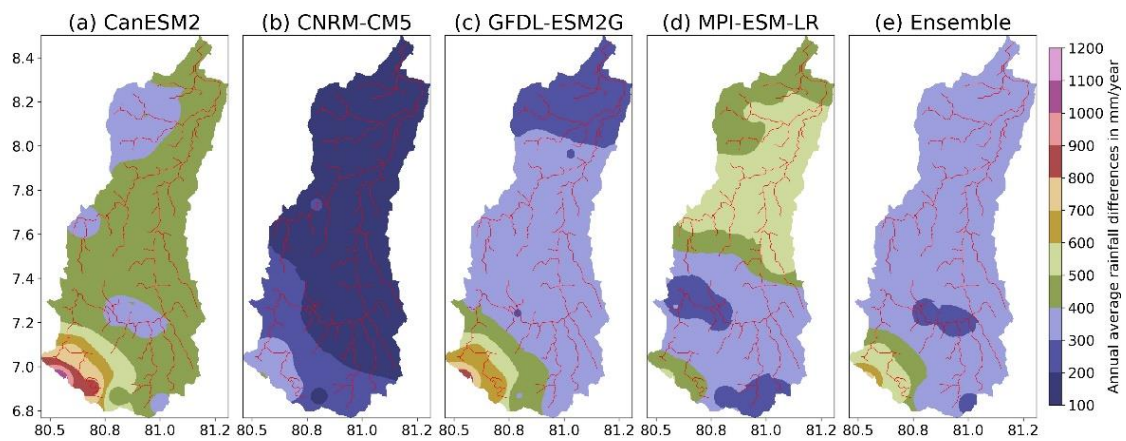


Figure 3.6. The comparison of annual average rainfall differences (future-past) in mm/year for the selected models and the ensemble mean.

3.6.1.4 Changes in seasonal climatology of rainfall

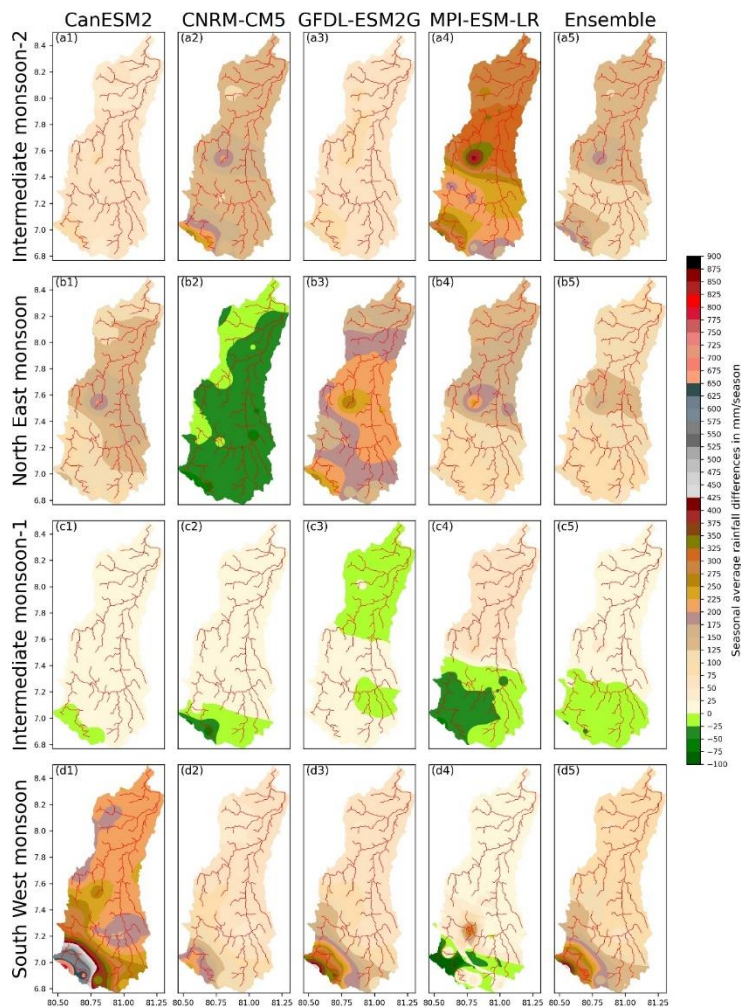


Figure 3.7. The comparison of seasonal average rainfall differences (future-past) for the selected models and the ensemble mean.

To understand the seasonal changes in rainfall, the spatial distribution of seasonal climatology differences was calculated and is shown in Figure 3.7. The basin average seasonal rainfall changes are shown in Figure 3.5 (b). Rainfall changes during two major seasons (i.e., NE, and SW monsoons) will be discussed first. As shown in Figure 3.7 (b1 to b5), during the NE monsoon, three models except CNRM-CM5 project an increase in rainfall, and the basin average changes are ~ 100-200 mm more or less uniformly throughout the basin.

The exceptional reduction in the rainfall projected by CNRM-CM5 will be discussed in the next paragraph. During the SW monsoon (Figure 3.5 (b)), all the model-projected rainfall increases (~ 25-300 mm) in the future climate with CanESM2 showing the largest increase and MPI-ESM-LR showing the smallest increase in the basin average rainfall. As for the spatial distributions during this season (Figure 3.7 (d1 to d5)), all models other than MPI-ESM-LR show a higher rainfall increase in the hilly region compared to the downstream region. Therefore, it is likely that both NE and SW monsoon seasons will bring a considerable amount of rainfall in the warmed future climate. The investigation on the other two seasons (i.e., IM-2 and IM-1) showed that during the IM-2 season, it is very likely that rainfall will increase as all the models projected a rainfall increase in the warming climate throughout the basin (Figure 3.7 (a1 to a5)). Among the other models, MPI-ESM-LR predicted the largest rainfall increase in the uppermost and middle regions of the basin during the IM-2 season. On the other hand, the IM-1 season, which brings less rainfall to the basin, will cause no change or a slight increase in basin averaged rainfall (Figure 3.5 (b)); however, the distribution map (Figure 3.7 (c1 to c5)) reveals no clear clues on the location of the changes. In general, from the beginning of May (i.e., the onset of the SW monsoon) through the IM-2 season (October and

November) until the withdrawal of the NE monsoon (i.e., February), the seasonal rainfall will increase in the future climate.

To investigate exceptional reductions in the rainfall projected by CNRM-CM5 during the NE monsoon and by MPI-ESM-LR during the SW monsoon, weather variables which influence the rainfall mechanism over the island, such as geopotential height, specific humidity, and wind speed, were analysed at the 850 hPa level. The basin averaged values of each variable for the NE and SW monsoon seasons are given in Figure 3.8.

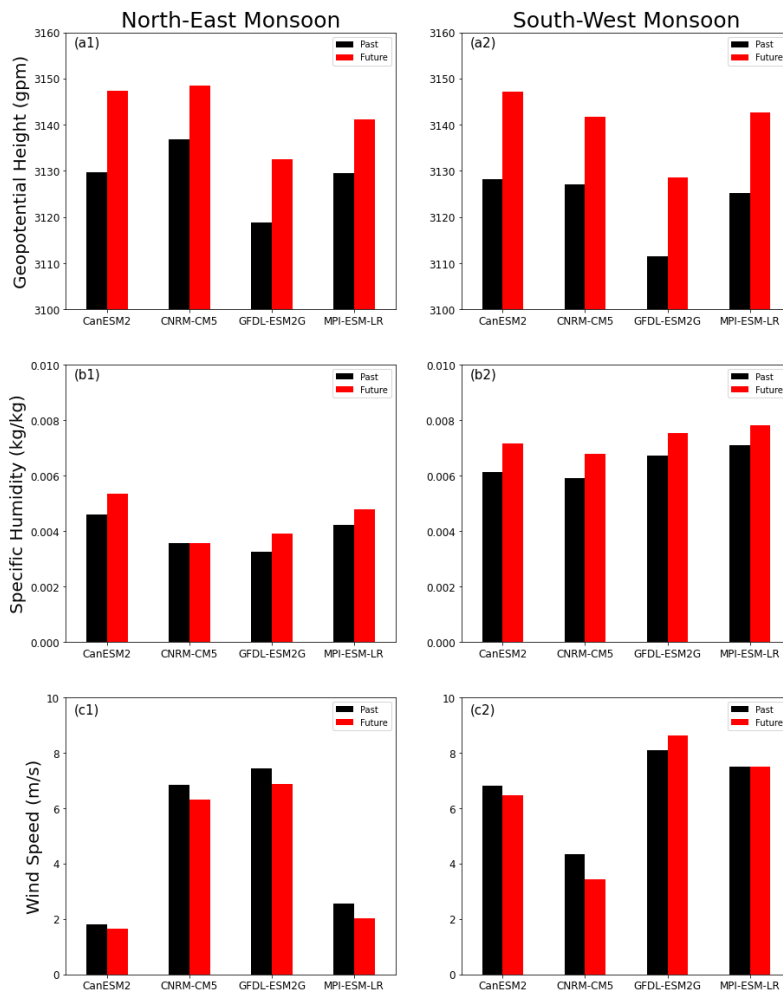


Figure 3.8. The comparisons of past and future climate seasonal average of variables influencing rainfall: a) geopotential height, b) specific humidity, and c) wind speed.

As shown in Figure 3.8 ((a1) and (a2)), the geopotential height will increase in the future climate due to increases in temperature in all the models for both seasons. In the case of the reduction in the rainfall projected by CNRM-CM5 during the NE monsoon, the wind speeds projected by all the models show a reduction in its strength (Figure 3.8 (c1)), which indicates that the weakened wind may not be a reason. However, as shown in Figure 3.8 (b1), all the models show an increase in the specific humidity except CNRM-CM5, which shows a marginal reduction in this variable. Therefore, the reduction in the rainfall projected in the future climate by CNRM-CM5 could be due to a marginal reduction in the specific humidity during the NE monsoon. In the case of the rainfall reduction by MPI-ESM-LR during the SW monsoon, no difference is observed in either geopotential height (Figure 3.8 (a2)) or specific humidity (Figure 3.8 (b2)) from MPI-ESM-LR. Though there is almost no change in wind speed (Figure 3.8 (c2)) during the SW monsoon, this will not be a reason as other models show mixed responses though still showing an increase in rainfall. The reason why MPI-ESM-LR shows less rainfall during the SW monsoon could be related to model physics and parametrizations and their interaction with misrepresentation of topographical features, which needs further investigation.

3.6.1.5 Extreme event data analysis: Meteorological rainfall extremes and droughts

Rainfall extremes were investigated based on the anomalies of climate indices of consecutive wet/dry days for the past and future basin average rainfall outputs of GCMs. The consecutive wet days (CWD) index is defined as the consecutive number of days during a year with daily rainfall higher than 0.05 mm/day, while the consecutive dry days (CDD) index is defined as the consecutive number of days during a year with daily rainfall

less than 0.05 mm/day. Zhang et al., (2012) (Y. Zhang et al., 2012) also introduced a similar definition. The anomaly is defined as the departure for a year from the climatological averages of CWD and CCD. The positive anomaly values were rank-ordered and plotted against the ranks in Figure 3.9.

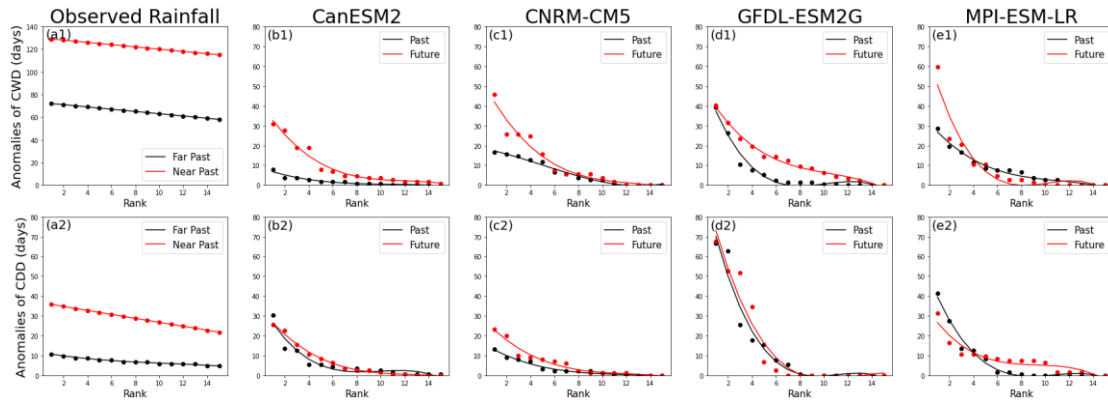


Figure 3.9. Anomalies of CWD and CDD of observed far-past (1976-1996) and near-past (1997-2017) rainfall and the past and future rainfall of the selected models.

Figure 3.9 (a1)-(e1) shows the anomalies of CWD for observed rainfall (near past: 1997-2017, far past: 1976-1996) and the projected rainfall by the four selected GCMs. Figure 3.9 (a1) shows a clear increase in anomalies of CWD observed during the near-past period compared to the far-past period. As depicted in Figure 3.9 (b1)-(e1), CanESM2, CNRM-CM5 and GFDL-ESM2G show a clear increment in CWD in the future, whereas MPI-ESM-LR shows an increment in most extreme anomalies but a reduction for the other cases of CWD. Therefore, it is likely that future annual wet days will increase under the warming climate.

Similarly, the anomalies of annual CDDs for observation and each GCM are shown in Figure 3.9 (a2)-(e2). A clear increment in anomalies of CDD is also observed for the near-past period compared to the far-past period (Figure 3.9 (a2)). As shown in Figure 3.9 (b2)-(e2), CanESM2, CNRM-CM5, and GFDL-ESM2G show a clear increment in

CDD in the future, while MPI-ESM-LR shows a reduction in most extreme anomalies but an increase in the other cases of CDD. Therefore, it is likely that future annual dry days will increase under the warming climate.

3.6.1.5.1 Seasonal behaviour of drought

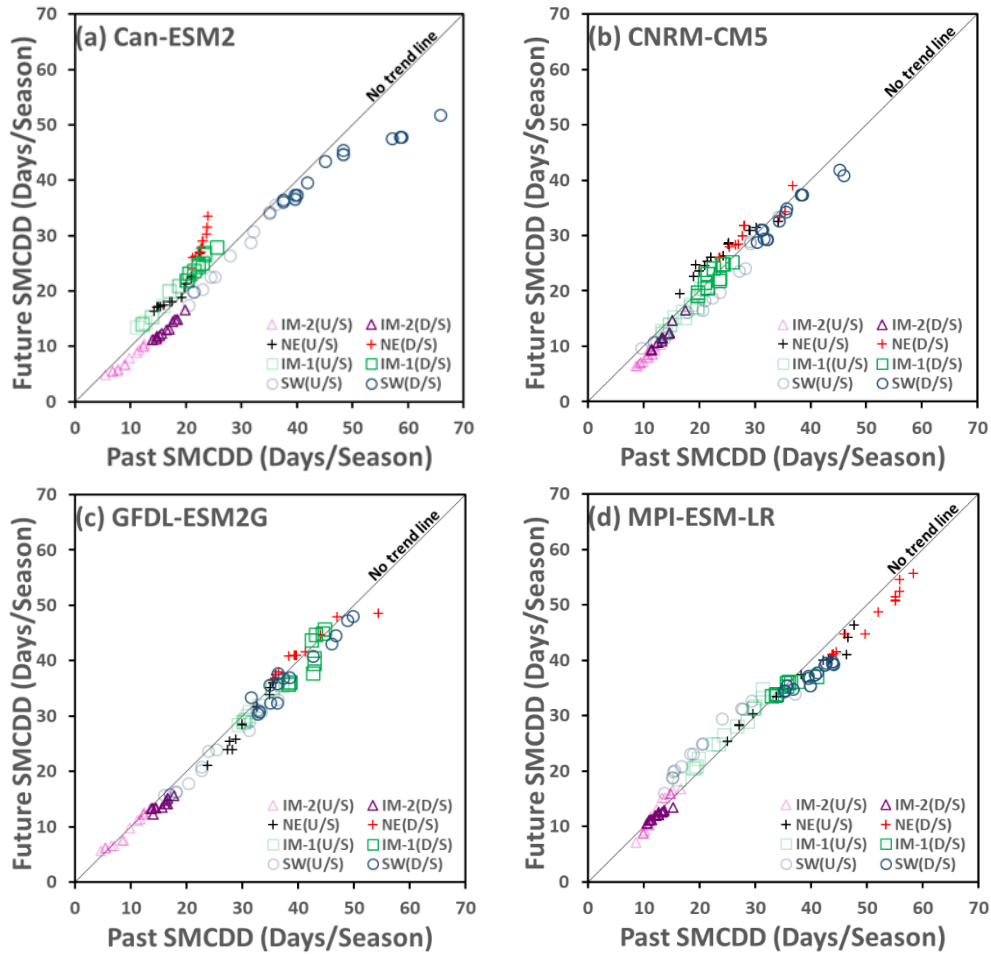


Figure 3.10. Past average seasonal MCDD vs. future average seasonal MCDD plot (a) Can-ESM2, (b) CNRM-CM5, (c) GFDL-ESM2G, and (d) MPI-ESM-LR.

Further, to identify the seasonal behaviour of droughts in the four climate seasons, assessment was carried out in three different spatial scales: the basin scale, upstream zonal scale (U/S: includes wet and intermediate climatic zones) and downstream zonal scale (D/S: includes dry climatic zones). Though CDD is defined as an annual value conventionally (Nakano, Kanada, Kato, & Kurihara, 2011), to identify a spatial variation

in each season, seasonal CDD was analysed in this section. The seasonal maximum CDD (SMCDD) was defined as the maximum seasonal value of CDD between the first and last days of each season. Past average SMCDD vs future average SMCDD of the 32 rain gauge locations are plotted in Figure 3.10 and analysed as given in Table 3-3 and Table 3-4.

In this case, four assessment criteria were used to identify the trend of future SMCDD based on the percentage of number of rain gauge stations within the considered spatial scale (basin scale, or upstream zonal scale, or downstream zonal scale) as follows: Decrease (0% to 24%), General decrease with a notable exception (25% to 49%), General increase with a notable exception (50% to 74%), and Increase (75% to 100%). To obtain final decision, General decrease- and General increase- with notable exceptions were considered as decrease and increase, respectively.

Table 3-3. Basin scale seasonal meteorological drought analysis.

Season	Spatial Scale	Model	% of number of stations within the spatial scale above No trend line in Figure 3.10	Trend of future SMCDD	Decision
IM-2	Basin	CanESM2	0	Decrease	Very likely decrease
		CNRM-CM5	0	Decrease	
		GFDL-ESM2G	19	Decrease	
		MPI-ESM-LR	34	General decrease with a notable exception	
NE	Basin	CanESM2	97	Increase	Likely increase
		CNRM-CM5	81	Increase	
		GFDL-ESM2G	69	General increase with a notable exception	
		MPI-ESM-LR	16	Decrease	
IM-1	Basin	CanESM2	100	Increase	Uncertain
		CNRM-CM5	31	General decrease with a notable exception	
		GFDL-ESM2G	12	Decrease	
		MPI-ESM-LR	84	Increase	
SW	Basin	CanESM2	0	Decrease	Very likely decrease
		CNRM-CM5	3	Decrease	
		GFDL-ESM2G	9	Decrease	
		MPI-ESM-LR	44	General decrease with a notable exception	

As shown in Table 3-3, all the models show a decreasing trend in future SMCDD during the IM-2 and SW monsoon seasons; thus it is very likely that future meteorological droughts will decrease during these seasons. Similarly, an increase in future

meteorological drought is likely during the NE monsoon since three models show an increasing trend and one model shows a decreasing trend. In comparison, GCMs projected an uncertain trend in future meteorological drought during the IM-1 season since two models show an increasing trend and two models show a decreasing trend.

Table 3-4. Zonal scale seasonal meteorological drought analysis.

Season	Spatial Scale	Model	% of number of stations within the spatial scale above No trend line in Figure 3.10	Trend of future SMCDD	Decision
IM-2	U/S zone	CanESM2	0	Decrease	Likely decrease
		CNRM-CM5	0	Decrease	
		GFDL-ESM2G	35	General decrease with a notable exception	
		MPI-ESM-LR	53	General increase with a notable exception	
D/S Zone	D/S Zone	CanESM2	0	Decrease	Very likely decrease
		CNRM-CM5	0	Decrease	
		GFDL-ESM2G	0	Decrease	
		MPI-ESM-LR	13	General decrease with a notable exception	
NE	U/S zone	CanESM2	94	Increase	Uncertain
		CNRM-CM5	88	Increase	
		GFDL-ESM2G	47	General decrease with a notable exception	
		MPI-ESM-LR	29	General decrease with a notable exception	
D/S Zone	D/S Zone	CanESM2	100	Increase	Likely increase
		CNRM-CM5	73	General increase with a notable exception	
		GFDL-ESM2G	93	Increase	
		MPI-ESM-LR	0	Decrease	
IM-1	U/S zone	CanESM2	100	Increase	Uncertain
		CNRM-CM5	6	Decrease	
		GFDL-ESM2G	0	Decrease	
		MPI-ESM-LR	100	Increase	
D/S Zone	D/S Zone	CanESM2	100	Increase	Likely increase
		CNRM-CM5	60	General increase with a notable exception	
		GFDL-ESM2G	27	General decrease with a notable exception	
		MPI-ESM-LR	67	General increase with a notable exception	
SW	U/S zone	CanESM2	0	Decrease	Likely decrease
		CNRM-CM5	6	Decrease	
		GFDL-ESM2G	0	Decrease	
		MPI-ESM-LR	82	Increase	
D/S Zone	D/S Zone	CanESM2	0	Decrease	Very likely decrease
		CNRM-CM5	0	Decrease	
		GFDL-ESM2G	20	Decrease	
		MPI-ESM-LR	0	Decrease	

Table 3-4 shows the zonal scale seasonal meteorological drought analysis. The results are discussed for each selected zones as follows;

a) Upstream zone seasonal meteorological drought: three models project a future decrease of SMCDD in IM-2 and SW monsoon seasons thus the future meteorological drought during IM-2 and SW seasons is likely to decrease. On the other hand, future

meteorological drought during NE and IM-1 monsoon seasons is uncertain as half of the models show increase while other half show decrease of SMCDD.

b) Downstream zone seasonal meteorological drought: the future meteorological drought during IM-2 and SW seasons is very likely to decrease since all the models show an increasing trend in future SMCDD. During NE and IM-1 monsoon season the meteorological drought is likely to increase as three of the GCMs show an increasing trend of SMCDD.

According to the drought analysis, the NE monsoon season and the IM-1 season are alarming about future meteorological droughts. The results show a likely increase in future drought during the NE monsoon at the basin scale, especially in the downstream zone where major agricultural activities take place, while the future condition in the upstream zone is uncertain. Further, during the IM-2 season, the agricultural area in the downstream zone will be affected by a likely increase in future drought while the future drought condition is uncertain at the basin scale in the upstream zone.

3.6.2 WEB-RRI model calibration and validation

The WEB-RRI model was developed to model the hydrological responses of a basin to the past and future climate. The model was calibrated at the Peradeniya discharge location (Figure 2.7 (c)) using the observed discharge data from 1981 to 1982, which corresponds to the period prior to the Kotmale Dam construction and its operation since 1985. The calibrated model satisfactorily reproduced the base flow and the peak flood with NSE equal to 0.84, MBE equal to 0.91 m³/s, and RMSE equal to 24.48 m³/s (Figure 3.11 (a)). Subsequently, as shown in Table 3-5, the calibrated parameters were validated

at the same discharge location for the period from 2005 to 2015 with the dam effect (dam operation data is obtained from Mahaweli Authority).

Table 3-5. Model calibrated parameters for the MRB

Parameters	Unit	Value
Soil Parameters (basin average)		
Saturated water content (θ_s)	m^3/m^3	0.54
Residual soil water content (θ_r)	m^3/m^3	0.07
Saturated hydraulic conductivity for soil surface	mm/h	12.88
Van Genuchten parameter (α)	m^{-2}	0.03
Van Genuchten parameter (n)		1.43
Soil Depth (DS)	m	1.50
River Parameters		
Manning's roughness coefficient for river		0.06
Manning's roughness coefficient for slope		0.60
Width parameter (CW)		8.00
Width parameter (SW)		0.34
Depth parameter (Cd)		0.90
Depth parameter (Sd)		0.20

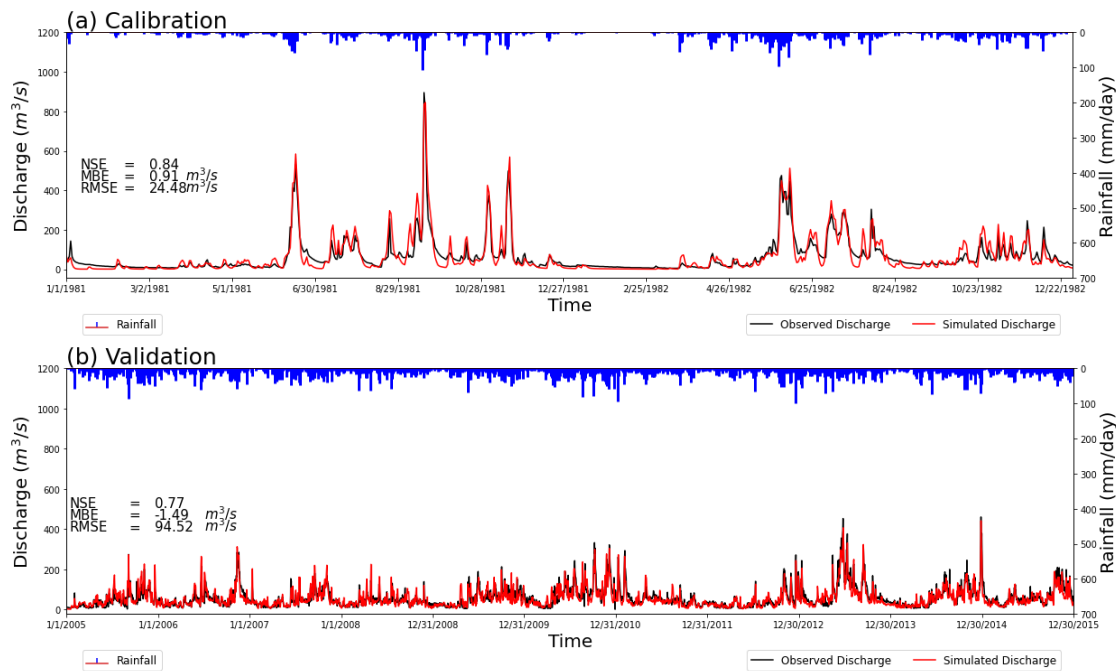


Figure 3.11. Comparison between observed discharge and simulated discharge: (a) model calibration for 1981-1982 under the natural river flow and (b) model validation for 2005 to 2015 with dam operations.

During the validation period, the model-simulated discharge at the Peradeniya location was compared to the observed discharge. During the validation period, the model performance indices were NSE equal to 0.77, MBE equal to $-1.49 m^3/s$, and RMSE equal

to 4.52 m³/s (Figure 3.11 (b)). Mainly, the low flow during the dry period, the flow just before the flood onset, the peak flood discharge, and the exact timing of these events were represented satisfactorily during both calibration and validation periods.

3.6.3 Hydrological assessment

The WEB-RRI model simulated the natural flow conditions of the basin without considering any dam effects, as long-term data on dam effects are not available for the past and future study periods. The seasonal averages of the simulated river discharges and hydrological extremes of flood and drought events were investigated at the downstream confluence point, the Mannampitiya discharge location (Figure 2.7 (c)). The all-time maximum inundation depth at each grid cell for both the climates was calculated and used to make spatially distributed inundation maps, which were then used for damage assessments.

3.6.3.1 Discharge analysis

The past and future annual average discharges and seasonal average discharge differences are shown in Figure 3.12 ((a) and (b)). Clear increasing signals are observed during the three seasons (i.e., IM2, NE, and SW monsoons), indicating that the basin will yield a higher amount of flow at the discharge location in the future. The approximate range of increments will be ~ 16.3 m³/s-149.0 m³/s for IM-2, ~3.4 m³/s -107.1 m³/s for the NE monsoon, and 7.0 m³/s ~35.3 m³/s for the SW monsoon in the future climate. During IM-1, except for MPI-ESM-LR, the other three models projected a decrease in flow rate (-10.8 m³/s ~23.8 m³/s). Therefore, it is very likely that the discharge will increase in the future during the NE, SW, and IM- 2 seasons, and it is also likely to project a reduction in discharge during the IM-1 season. Consequently, the estimated annual

average discharge is very likely to increase in the future climate, and the values may range from $\sim 11 \text{ m}^3/\text{s}$ to $57 \text{ m}^3/\text{s}$ as the percentage changes in the range between 4%-24%.

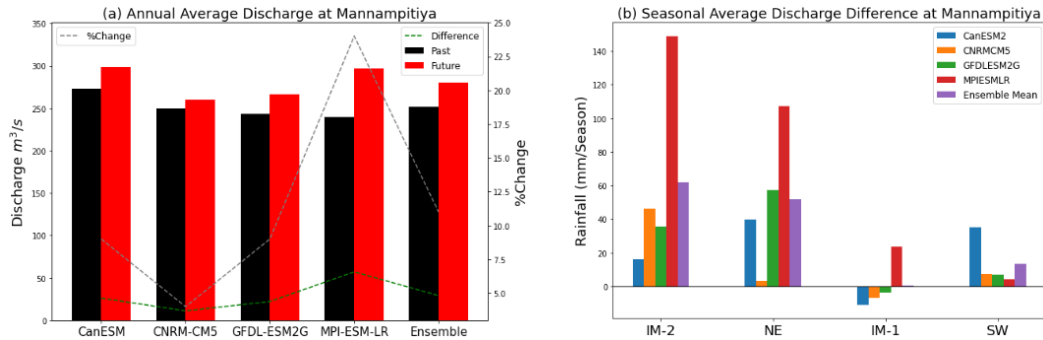


Figure 3.12. (a) Annual average discharge at Mannampitiya gauging station of the selected models and (b) seasonal average discharge difference at Mannampitiya gauging station of the selected models.

3.6.3.2 Extreme event data analysis: Hydrological floods and droughts

Hydrological extremes are investigated in this section. The daily average discharge simulated for the past and future climates were rank-ordered, and the first 20 peak discharges were analysed for extreme floods, and the last 20 low flows were analysed for droughts.

Figure 3.13 (a1)-(d1) shows the first 20 peak discharges estimated by the WEB-RRI model for the inputs from CanESM2, CNRM-CM5, GFDL-ESM2G, and MPI-ESM-LR, respectively. As shown in the figures, the projected future peak discharges are significantly higher in CanESM2 and MPI-ESM-LR and marginally higher in the other two models. Therefore, peak discharges are very likely to increase in the future; thus, hydrological floods are very likely to increase in the future climate in this basin. Similar findings were reported in the Assessment Report 5 of the IPCC, explaining that GCMs have projected the impacts associated with increased flooding with high confidence in the case of small islands (Hoegh-Guldberg et al., 2018).

Figure 3.13 (a2)-(d2) shows the last 20 low-flow events for the selected model for both climates. CanESM2 and MPI-ESM-LR project a similar pattern of nearly no change in the future low flow; however, CNRM-CM5 and GFDL-ESM2G project an increase in the future low flow. Therefore, the trend in future hydrological droughts is uncertain, and thus, a firm conclusion cannot be attained based on the GCM projections. Similar findings were reported in the Assessment Report 5 of the IPCC that the overall global scale sign of drought trends has been assessed with low confidence except for the high confidence projections of increased droughts in some regions of the world (Hoegh-Guldberg et al., 2018). This low confidence level of GCMs in projecting future droughts could be an arguable reason for the observed uncertainty in projected hydrological droughts.

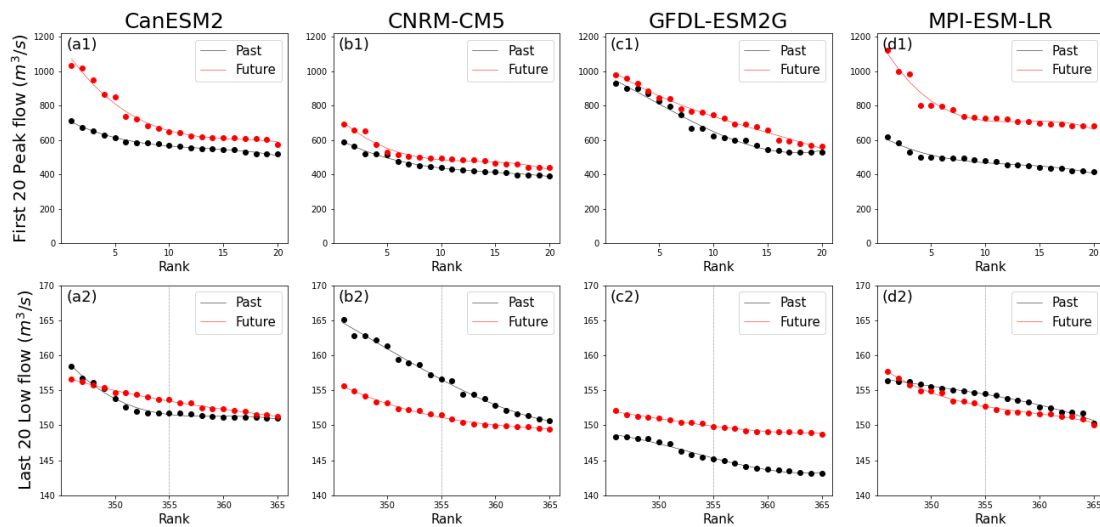


Figure 3.13. First 20 peak flow and the last 20 low flow of daily average discharge values of the past and future 20 years of the selected GCMs.

3.6.3.3 Inundation analysis

The difference between past and future climates in all-time maximum inundation depth at each grid cell was estimated from the WEB-RRI simulated inundation gridded data for each GCM individually and is plotted in Figure 3.14 ((b1) to (b4)), and the past all-time inundation depth gridded data is given in Figure 3.14 ((a1) to (a4)) for reference.

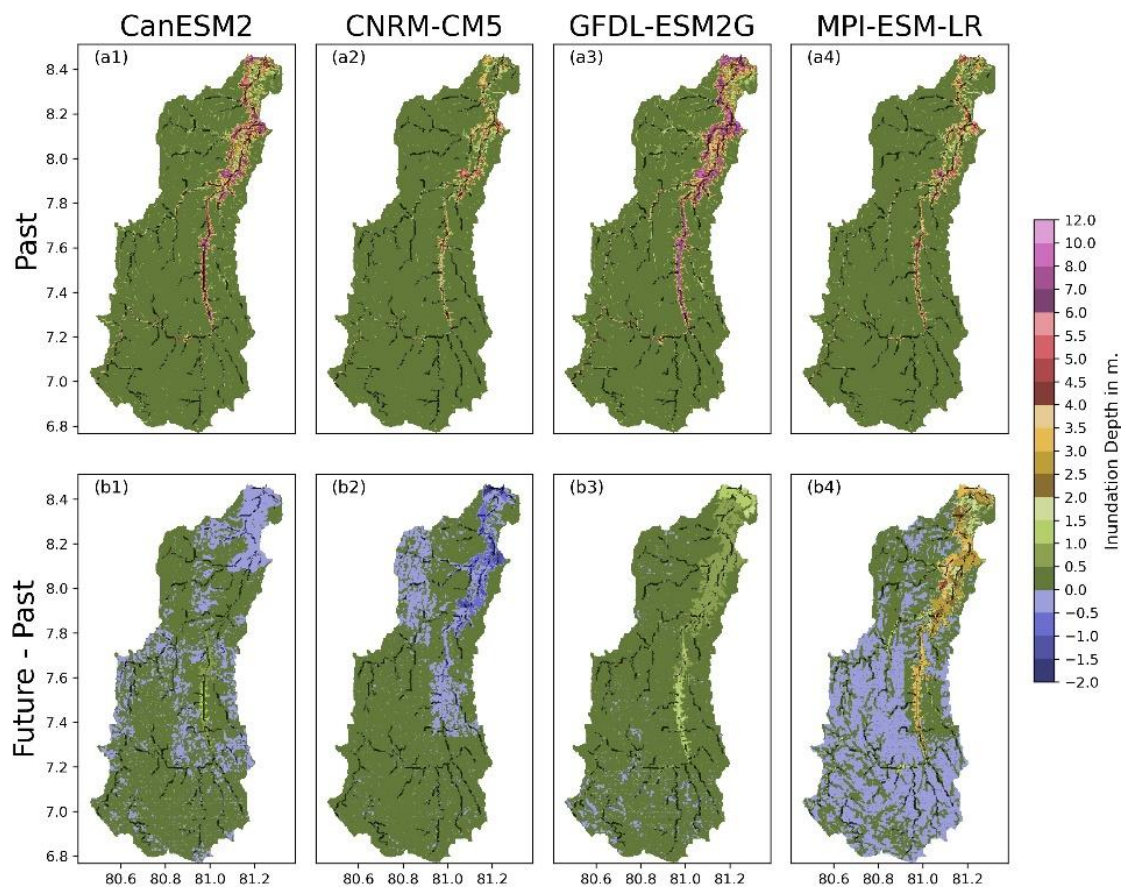


Figure 3.14. (a) Past all-time inundation depth and (b) inundation depth difference between future and past of the selected GCMs.

As shown in the above figure, except for the CNRM-CM5 model, the other three models project an increase in the inundation extent for all-time flood depth. Therefore, it is likely that the flood inundation area and risk will increase in the basin under the future climate. The contrasting behaviour of CNRM-CM5 can be attributed to the reduction in future rainfall due to a low warming rate and the reduction in rainfall during the NE monsoon, which brings a considerable amount of rainfall to the downstream area of the basin. To verify the simulation results further, the all-time seasonal (i.e., NE monsoon) maximum inundation depths simulated by the WEB-RRI model were estimated. Figure 3.15 shows the scatter plot of past versus future all-time seasonal maximum inundation depths during the NE monsoon for all the model grids. As shown in the figure, CNRM-

CM5 projects a decrease in all-time seasonal inundation depth in the future climate compared with those in the past climate during the NE Monsoon, whereas the other three models project clear increases in the future inundation depth. Therefore, this contrasting behaviour of a decreased inundation depth from CNRM-CM5 is due to uncertainties in rainfall projections during the NE monsoon season.

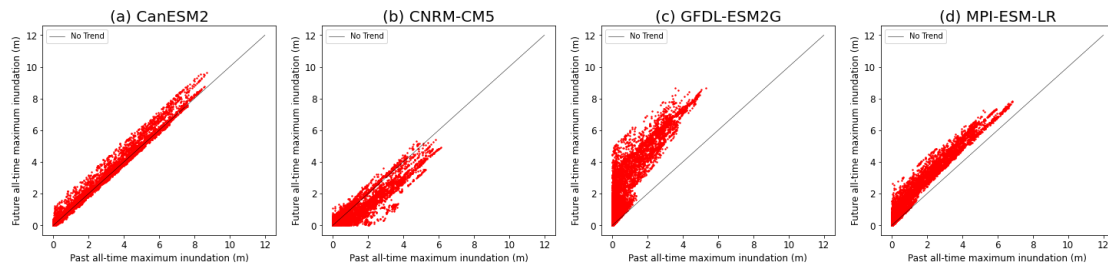


Figure 3.15. Past vs. future all-time seasonal maximum inundation during the NE monsoon of the selected GCMs.

3.6.3.4 Socio-economic damage analysis

To understand the impact of climate change on the socio-economic features, the population data and land cover data were set into layers in GEE. Additionally, the past and future simulated inundation over 1 m deep from WEB-RRI has been overlaid for each selected GCM, and the statistics of inundated population, cropland and urban area were extracted for analysis, as shown in Figure 3.16. The following results were obtained from the analyses: (a) it is very likely that flood damage to the population will increase; (b) it is likely that damage to the cropland will increase; and (c) inundation of urban area will likely will increase in the future.

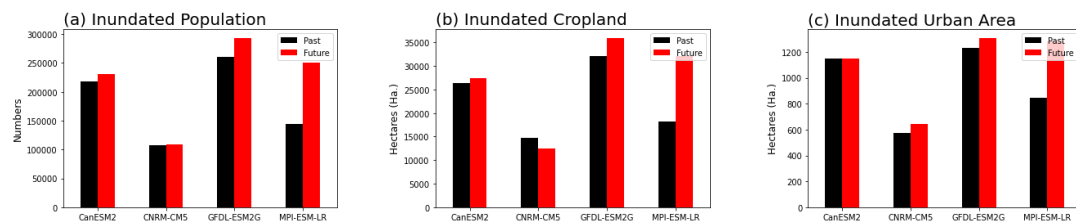


Figure 3.16. Socio-economic damage assessment.

3.6.4 Possible decision making based on the results

Increases in flood and drought events in river basins could impact the ecosystem and socio-economic structure of riparian settlements, and thus the country. Disaster risk reduction against floods and droughts can be handled by policymakers in numerous strategies such as soft and hard countermeasures. This study identifies the critical future climate changes on hydro-meteorological characteristics of MRB by applying this new approach. The qualitative level of confidence based on the temporal and spatial scale are summarised in Table 3-6 (basin scale annual assessments), Table 3-7 (basin and zonal scale seasonal meteorological assessments), and Table 3-8 (seasonal discharge).

Table 3-6. Basin scale annual assessment summary

	Meteorological Assessment			Hydrological Assessment		
	Future rainfall	Future flood	Future drought	Future Discharge	Future flood	Future drought
Level of confidence	Very likely increase	Likely increase	Likely increase	Very likely increase	Very likely increase	Uncertain

Table 3-7. Basin and zonal scale seasonal meteorological drought summary

Temporal scale	Spatial scale	Level of Confidence of Future meteorological drought
IM-2	Basin	Very likely decrease
	U/S zone	Likely decrease
	D/S zone	Likely decrease
NE	Basin	Likely increase
	U/S zone	Uncertain
	D/S zone	Likely increase
IM-1	Basin	Uncertain
	U/S zone	Uncertain
	D/S zone	Likely increase
SW	Basin	Very likely decrease
	U/S zone	Likely decrease
	D/S zone	Very likely decrease

Table 3-8. Seasonal discharge at Peradeniya discharge location summary

Temporal scale	Level of Confidence of Future discharge
IM-2	Very likely increase
NE	Very likely increase
IM-1	Likely decrease
SW	Very likely increase

For example, as shown in Table 3-6, the future rainfall is very likely to increase, future meteorological- flood and drought are likely to increase in the basin-scale annually. On the other hand, future discharge and hydrological flood are very likely to increase while the future hydrological drought is uncertain. The qualitative level of confidence of hydro-meteorological characteristics derived in this study can be utilized by policymakers to make decisions for future disaster risk reduction. Information on an increasing level of confidence of rainfall, meteorological- and hydrological- flood and discharge is an indication of 1) future negative changes in terms of disasters and 2) future positive changes in terms of water resources. Policymakers could react in two directions by implementing soft or hard countermeasures: one is to mitigate disasters, and the other is to utilize water resources, or opportunities brought in by disasters for the betterment of societies and the environment. On the other hand, the increasing level of confidence in the meteorological drought shows a possible water shortage in the future climate. Drought monitoring and mitigation should be strategically considered by policymakers to handle this situation in future for reducing future risk. Further, under an uncertain level of confidence, decision-makers can decide to either implement new countermeasures or continue the current disaster management practices.

Making decisions based on the range at the level of confidence is another crucial factor in the decision-making process. The range provides a spectrum of GCM outputs under uncertainty; thus, decisions are to be made under this uncertainty. The gap between the low end and the high end in the range varies according to selected hydro-meteorological characteristics, and the selection of appropriate model output corresponding to the value in the range depends on type of countermeasures to be implemented for disaster risk reduction. For example, the future-discharge increase range

lies between $11 \text{ m}^3/\text{s}$ ~ $57 \text{ m}^3/\text{s}$ with a very likely increasing level of confidence. In such situation, it is desirable to use low-end models for future infrastructure designs i.e., hard countermeasures, while high-end models could be selected for managing disasters through soft countermeasures. Further, the statistical bias-correction does not represent the spatial and temporal connectivity as this method uses the three-step rank-order statistical approach. Therefore, first, it is best to utilize the statistical downscaling method to identify the spectrum of suitable models with less computational effort. And then, apply the dynamical downscaling method to obtain quantitative outputs which could represent the spatial and temporal connectivity for infrastructure development at the local scale.

4 Development of climate change adaptation and resilience strategies for Kotmale reservoir operation

4.1 Introduction

The climate change impact assessment and analysis (chapter 3) showed that the future water availability, excess and shortage, which can influence the MRB system operation, will vary seasonally and spatially in the future. But these future changes depicts the information regarding average over a 20 years period only. Still, onset and withdrawal of these events are uncertain based on the currently available information from GCMs. As the quantity of future water resources increase has not been quantified in this research, adaptation strategy development by making changes to the reservoir operation by utilizing seasonal forecasting and short-term weather prediction information is focused in this chapter.

The forecast informed reservoir operation is selected as an alternate solution for increasing reservoir capacity, which is a costly hard countermeasure, by considering the temporal and spatial variation of reservoir storage and rainfall pattern. For example, a major water resource increase has been identified during this SW monsoon, but the SW monsoon rainfall mainly falls within the upstream region while the downstream region undergoes a dry period. Therefore the water received in the upstream region can be managed using the available reservoir storage capacity downstream. The MRB will receive high rainfall during the SW monsoon in the upstream region, where the upstream reservoirs will be spilling. Meanwhile, the downstream reservoirs will be at a low level due to the excess water usage for Yala seasonal agriculture and the dry weather conditions downstream during the SW monsoon. Hence it is necessary to distribute the water

received upstream spatially as well as temporally to the downstream. Therefore, it reduces the necessity of storage increase by adding a new reservoir or resizing the reservoir.

A specific adaptation strategy is developed for disaster risk reduction and water resources management by dam operation. Particularly the usefulness of forecast informed reservoir operation in a specific decision-making process is discussed in this chapter. Previous studies on seasonal streamflow forecasting have suggested various methods to improve the accuracy of seasonal flow forecasts (Crochemore, Ramos, & Pappenberger, 2016; Lucatero, Madsen, Refsgaard, Kidmose, & Jensen, 2018). However, not much attention has been paid to forecast informed reservoir operation for disaster risk reduction and water resources management (Kompore, Yoshikawa, & Kanae, 2020). On the other hand, Mateo et al., (2014) established a operation strategy by combining physically based hydrological models to explicitly simulate the impacts of reservoir operation on flooding, but forecast informed reservoir operation was not included in that study. Further, a very recent study has proposed use of seasonal streamflow predictive data to support adaptive reservoir operation while accounting for reservoir operation for disaster risk reduction and water resources management (Kompore et al., 2020). Still the short-term weather forecasting was not addressed in their study. Therefore the seasonal forecast, and short-term numerical weather prediction data for ensemble forecast informed reservoir operation for formulating adaptation strategies against climate change is addressed in this chapter.

Implementation of a successful seasonal operation, based on seasonal forecast information, can benefit in bringing food security, energy security, water security and disaster management of a region through an efficient water resources management.

Cultivation extent, the crop variety to be cultivated, and avoiding cultivation within the flood plain can be decided base on the water availability of the upcoming 2 to 3 months period during a cultivation season. Further, curtailment of power generation, planning optimum hydropower generation and power plant maintenance scheduling can be performed based on seasonal forecasted information. Disaster management centers can plan for early actions in case of an identified future risk of flood and drought. In addition to this, the reservoir operation can be optimized during the off seasons (i.e. the period between two cultivation seasons where there is no or very few cultivation activities are taken place).

In addition to the seasonal planning, to minimize flood damage by sudden abrupt changes in the weather (heavy precipitation events) and optimize water usage, short-term numerical weather prediction up to next couple of days for reservoir operation is beneficial. Therefore, water managers can jointly manage the floods and droughts with increased benefits.

In terms of seasonal planning, the stakeholders widely use the past climate information to anticipate the potential water resources in the upcoming couple of months which is highly ineffective in rapidly changing weather conditions under climate change (Viel, Beaulant, Soubeyroux, & Céron, 2016). The practice of applying the past observed data is being continued due to the lack of future seasonal forecast rainfall information in many countries (Kompore et al., 2020). Due to this fact, the water managers are left with no clues regarding the future rainfall and unexpected extreme events, and it widely misleads them to inefficient seasonal planning. Further due to the reason that the forecasting accuracy is usually better by using the ensemble mean than by using a single

forecasting method (Seko, Kunii, Yokota, Tsuyuki, & Miyoshi, 2015; Ushiyama, Sayama, & Iwmi, 2017) and decision making under uncertainty can be facilitated within the spectrum of ensembles, use of ensemble predictions are desirable in such sensitive decision making in water sectors. Therefore a reliable ensemble seasonal forecast is needed for effective seasonal planning.

Further, the forecast information regarding meteorological variables (i.e. precipitation, air temperature, outgoing longwave radiation, sea surface temperature, sea level pressure, and wind) are provided by the Meteorological Agencies and those information are need to be converted into streamflow predictions to enable water managers to make decision based on water resources availability for the near future. In order to obtain streamflow predictions, forecast information needs to be coupled with basin-scale hydrologic models with dam modules regardless of spatial and temporal resolutions. Further, a hydrological model which can be coupled with various input variables produced from multiple data sources such as satellites, reanalysis, in-situ, and general circulation models to seamlessly simulate the monitoring operation is needed for this operation. Also, the hydrological model should be capable of reproducing the actual conditions of hydrological parameters at each time step and should be able stopped at any time step and restarted from the previous history. Therefore a seamless hydrological model with dam module which can be restarted by using the past memory is needed for streamflow generations.

Reservoir rule curves are used in reservoir operation for decision making in any reservoir in terms of water usage within the Water-Energy-Food nexus (Kangrang, Prasanchum, & Hormwichian, 2018). In order to mitigate flood and drought, majority of

the reservoirs around the world are operated using rule curves which derived from historical streamflow and reservoir storage data (Prasanchum & Kangrang, 2018). These rule curves are defined to maintain the reservoir water level within a range of control level in order either to prevent flooding or to reserve sufficient water to meet the needs for cultivation and prevent water shortages during the dry season (Kangrang et al., 2018; Komporn et al., 2020). Therefore it is vital to perform reservoir operations under predefined reservoir operation rules.

Therefore to develop adaptation strategies to tackle flood and drought disasters and perform efficient water resources management by using forecast information under these scientific challenges, we certainly require: a) reliable ensemble seasonal forecast data; b) to couple forecast outputs from numerical weather models with a physically-based distributed hydrological model which can produce basin-scale hydrological responses at each time step with the capability of restarting at any time step with historical record; c) to couple the hydrologic response with an effective reservoir module to generate reservoir releases; and d) an effective reservoir operation rule curve for decision making.

Accordingly, this chapter presents an integrated approach for developing resilience strategies to adopt future climate changes and disasters through the optimized dam operation of the Kotmale reservoir in the case of a) seasonal planning and b) short-term dam operation for flood control. This approach provides evidence for the policy makers in MRB for future adaptations under forecasting uncertainties. This chapter discusses coupling WRF model outputs (seasonal weather prediction and numerical weather forecasting) with the WEB-RRI model to simulate discharge information and making the maximum use of simulated discharge data by coupling them with real-time

reservoir optimization tools for increasing benefits from water resources and minimising flood and drought damage in an integrated manner.

4.2 Research framework

Figure 4.1 illustrates the overall research framework and methodology of this chapter. This framework comprises eight main components: 1) formulation of dam operation strategies; 2) hydrological model development; 3) seasonal flow forecasting; 4) short-term weather forecasting; 5) development of dam module; 6) dam optimization scheme; 7) monitoring and evaluation; and 8) decision making. The details on the major components are described in Section 4.4: Methodology.

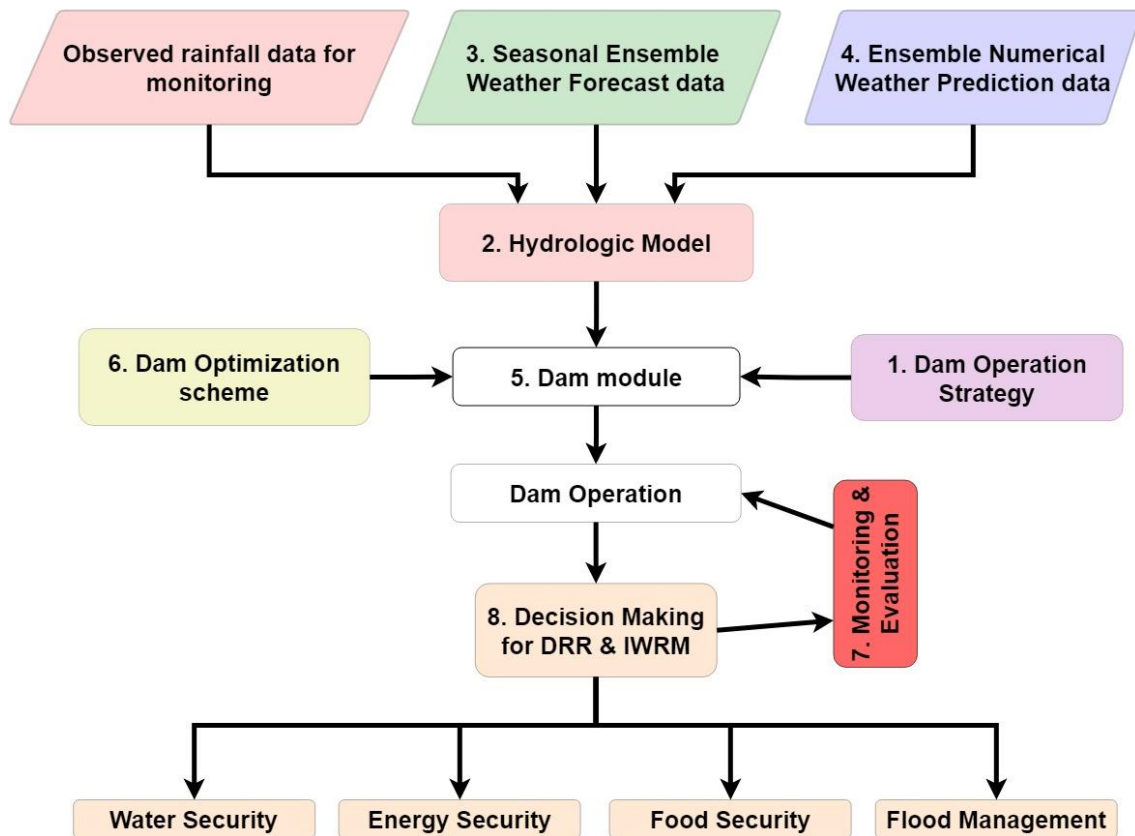


Figure 4.1. Research framework.

4.3 Study area

MRB system is a complex, cascade reservoir system and requires a well-coordinated operation to manage the system holistically. Therefore, within the scope of this study, from the upper reach dam (Kotmale reservoir), standardized operation rules were developed to make this complicated scientific challenge simple.

4.4 Methodology

As stated in Section 4.2, this section describes the methodology of the major components of the research framework implemented in this chapter. To understand the seasonal and weather pattern behaviours, analyses were conducted on rainfall, reservoir operations, and other data such as documents received from the Irrigation Department and websites. Further, as the selected river basin is a complex basin, the upstream reservoir (i.e. the Kotmale reservoir) has been selected for experimenting the application of seasonal forecast data and short-term numerical weather prediction data to reservoir operation.

4.4.1 Formulation of reservoir operation rules based on past observations

The past operation of this river basin will be fully understood by reviewing the past seasonal operation plans, observed dam operation data, observed diversion data, observed cultivation and yield data, observed power generation data, and a flood disaster management assessment study carried out by Indika et al. (2018).

SOPs issued by the WMS were collected from the Irrigation Department and analysed for the period from 2010 to 2020 to understand the system's past operations and behaviour. Further, to assess the past performance, the annual reports of MASL from 2012 to 2015 were scrutinized. Plans regarding cultivation calendars, planning

assumptions, diversion plans, and energy release were studied and compared with the performance from the annual reports, and the observation is summarized.

Further, observed data regarding rainfall and reservoir operation were studied to understand the seasonal behaviour of rainfall patterns and the inflow to the reservoirs. In addition to that, the observed diversion data and demand data analysis were carried out by a previous study has been incorporated into this analysis to formulate the reservoir operation rules for seasonal planning and flood disaster management.

4.4.2 Hydrological model development

The WEB-RRI model is used in this research to simulate the hydrological response by coupling the model with the forecasted weather parameters. The functions and formulation of the WEB-RRI model have been discussed in detail in the sub topic 3.4.2 of the previous chapter. The Water Energy Budget based Rainfall Runoff Inundation model (WEB-RRI) is compatible with various input variables produced from multiple data sources such as satellites, reanalysis, in-situ, and GCM projections for long-term seamless simulation of past and future events. Further, it can reproduce the actual conditions of hydrological parameters at each time step and can be stopped at any time step and restarted from the previous history to reduce the computational burden of a warming-up period in practical applications such as flood forecasting and seasonal prediction (Rasmy et al., 2019). Therefore, it can be used to produce seasonal and short-term hydrologic variables (discharge, inundation, root zone soil moisture, groundwater table, and evapotranspiration) by using forecasted data.

4.4.3 Dam module and optimization module

Dam module to simulate dam release according to the demand requirements is not available in WEB-RRI model. Therefore, an open source dam module which has an optimization solvers is used in this study. The dam module developed by Deltares, Netherlands called RTC Tool 2 was used in this research.

4.4.3.1 RTC-Tools 2

The simulated discharge from the WEB-RRI model has been coupled with a real-time control tool (RTC-Tools-2). RTC-Tools-2 is developed as a Python Application Programming Interface (API) developed for water resources management, operational flood management, and reservoir operation. This tool has been developed by integrating: a) Modelica models to represent physical reservoirs with their components such as spillways, tunnels, and sluice openings by declarative equations; b) a framework called CasADi to convert Modelica models into symbolic mathematical syntaxes which are accessible in the Python language; and c) a nonlinear optimization solver called IPOPT for optimization problem solving (Deltares, 2021).

4.4.3.2 Modelica models

OpenModelica is an object oriented modeling and simulation open-source tool which is used to represent the physical properties of the system components in the form of declarative equations (OpenModelica, 2021). The basic water balance equation of the reservoir has been assigned in the model with fixing the maximum tunnel discharge as a constraints. The maximum targeted storage boundary conditions are assigned based on the selected scenarios.

4.4.3.3 CasADi Python framework

OpenModelica compiles declarative equations written in the Modelica language. This compiler transforms Modelica models into a symbolic mathematical representation accessible in the Python package called CasADi. RTC-Tools 2.0 then discretizes these equations, couples time series of WEB-RRI simulated discharge, and interfaces resulting optimization problems with a non-linear programming solver called IPOPT (Deltares, 2021).

4.4.3.4 RTC-Tools 2 optimization scheme

This research prioritizes filling a reservoir to a targeted storage capacity at the end of a time horizon. Therefore, a large-scale nonlinear optimization scheme in IPOPT (Wächter, 2009) is used. IPOPT implements an interior-point line-search filter method. Also, it is vital to note that the algorithm is only trying to find a local minimizer of the problem; if the problem is nonconvex, many stationary points with different objective function values might exist, and it depends on the starting point and algorithmic choices which particular one the method converges to (Wächter, 2009). IPOPT is an open source software package and widely used in various sectors, such as engineering, scientific and medical applications, to address nonlinear programming cost functions in the form given below:

$$\min_{x \in \mathbb{R}^n} f(x) \quad (4-1)$$

$$\text{s.t.} \quad g^L \leq g(x) \leq g^U \quad (4-2)$$

$$x^L \leq x \leq x^U \quad (4-3)$$

where $x \in \mathbb{R}^n$: the optimization variables with lower and upper bounds,

$x^L \in (\mathbb{R} \cup \{-\infty\})^n$ and $x^U \in (\mathbb{R} \cup \{+\infty\})^n$, $f: \mathbb{R}^n \rightarrow \mathbb{R}$ is the objective function, and $g: \mathbb{R}^n \rightarrow \mathbb{R}^m$ are the constraints. Functions $f(x)$ and $g(x)$ can be a linear or nonlinear and convex or nonconvex, but it should be twice continuously differentiable. Constraint $g(x)$ has the lower bound $g^L \in (\mathbb{R} \cup \{-\infty\})^m$ and the upper bound $g^U \in (\mathbb{R} \cup \{+\infty\})^m$.

4.4.4 Performance Criterion Indexes (PCI) for evaluation and monitoring

To evaluate the performance of the optimization scheme, reliability, vulnerability, resilience (Hashimoto et al., 1982), and sustainability (Sandoval-Solis et al., 2011) indexes are used in this research.

- (a) Reliability: How frequent a water demand is met (time based reliability) and how close to the total amount demanded (volumetric reliability).

$$Deficit = \begin{cases} X_{Demand,t}^i - X_{Supplied,t}^i & \text{if } X_{Demand,t}^i > X_{Supplied,t}^i \\ 0 & \text{if } X_{Demand,t}^i = X_{Supplied,t}^i \end{cases} \quad (4-4)$$

$$Reliability(time)^i = \frac{(No. of times Deficit_t^i) = 0}{n} \quad (4-5)$$

$$Reliability(volume)^i = \frac{X_{Supplied,t}^i}{X_{Demand,t}^i} \quad (4-6)$$

Where $X_{Demand,t}^i$ is the water demand, $X_{Supplied,t}^i$ is the water supplied, and n is the total number of time steps.

- (b) Vulnerability: the severity of deficits (The average of water supply deficits, expressed as a percentage of the water demand).

$$Vulnerability^i = \frac{\left(\frac{\sum Deficit_t^i}{No. of times Deficit_t^i > 0 occurred} \right)}{Water Demand^i} \quad (4-7)$$

- (c) Resilience: The system's capacity to adapt to changing conditions. Resilience must be considered as a statistic that assesses the flexibility of water management policies to adapt to changing conditions. The definition of resilience is the probability that a system recovers from a period of failure, e.g., a deficit in water supply. For our specific case, resilience is the probability that a time-step of no-deficit follows a time-step of deficit in the water supply for the i^{th} water user. Resilience is a useful statistic to assess the recovery of the system once it has failed.

$$Vulnerability^i = \frac{(No. of times Deficit_t^i = 0 follows Deficit_t^i > 0)}{No. of times Deficit_t^i > 0 occurred} \quad (4-8)$$

- (d) Sustainability: An index that aggregates a set of performance criteria. It is the geometric average of a group of 'M' performance criteria for a given water user i:

$$SI^i = \left[\prod_{m=1}^M Performance\ Criteria_m^i \right]^{1/M} \quad (4-9)$$

$$SI^i = \left[Rel(time)^i * Rel(volume)^i * Res^i * (1 - Vuln^i)^i \right]^{1/4} \quad (4-10)$$

4.4.5 Evaluation of optimization scheme in reservoir operation

The reservoir optimization scheme used in this study has been evaluated during a selected time horizon (2nd March 2010 to 1st May 2010) with an assumption that the dam manager received observed inflow to the Kotmale reservoir as 100% accurate forecast information on 2nd March 2010. The optimization scheme used in this analysis is based on the condition that the optimizer is trying to fill the reservoir to reach the observed storage at the end of the time horizon. A single objective optimization is used, which minimizes the outflow and tries to fill the reservoir. The initial storage, final storage and power tunnel discharge of the time horizon were regarded as observed by the dam manager. The maximum discharge capacity of the power tunnel (113 m³/s) was considered for operation by assuming that all the power turbines were fully functioning.

4.4.6 Seasonal forecast discharge simulation and dam optimization scenarios

According to the cultivation calendriers of MRB (Figure 2.9), the months of March and April are considered to be an off-season between the Maha and Yala cultivation seasons. To evaluate the level of confidence in the seasonal forecast data for decision making, the past seasonal prediction rainfall data were compared with observed rainfall data from the Hydrological Management Information System (HMIS) online data of Sri Lanka, as the manual rain gauge observation data for the considered year (2020) was not available.

Further, for reservoir optimization within the off-season between the Maha and Yala seasons of 2020 was analyzed. The seasonal forecast ensembles (13 ensembles and ensemble mean) of 2nd March 2020 were utilized to implement the optimization of the dam operation to fill the reservoir to the desired elevation at the end of the time horizon

(2nd March 2020 ~ 1st May 2020). The end date of this time horizon was selected as the first date of the Yala season.

It is targeted to utilize the seasonal forecast information of the beginning of March 2020 to optimize the reservoir operation to perform the following actions:

- Fill the reservoir for the purpose of the maximum usage of the water for the “Yala” cultivation.
- By allowing a flood storage capacity at the beginning of the “Yala” cultivation to minimize downstream damage according to the reservoir operation rules described in the following sub-sections. By doing this, generating hydropower and subsequently filling the downstream reservoirs for agriculture and hydropower are expected.

4.4.7 Short-term weather prediction discharge simulation and dam optimization scenarios

The Kotmale reservoir operation rules was analyzed in this section. During the past three years, this reservoir recorded two spilling events: Event 01, which lasted for 7 days from 16th August 2018 to 22nd August 2018 and resulted in a total amount of 52.99 MCM spillage and Event 02, which lasted for 3 days from 9th August 2020 to 11th August and resulted in 6.93 MCM spillage. Considering the data availability and the significance of the spillage, Event 01 was selected for evaluation. To understand the level of confidence in the weather prediction data for decision making, the forecasted rainfall data were compared with observed rainfall data obtained from Hydrological Management Information System (HMIS) online data of Sri Lanka. Further, the ensemble forecasted rainfall data were coupled with the WEB-RRI model to generate forecasted discharge at





the Kotmale reservoir. Then, according to a reservoir operation strategy, the selected ensemble forecasted discharge information was coupled with a reservoir optimization tool to operate the reservoir.



4.5 Data and model set-up

4.5.1 Data availability and limitations

The seasonal forecast data from the Japan Meteorological Agency and short-term weather prediction data from the National Centre for Environmental Prediction were dynamically downscaled to the specified spatial resolutions as shown in the Table 4-1. Due to fact that unavailability of long term forecast data over the river basin, the bias correction and the reliability checking were limited in this study. Further, the HMIS online data was used for the monitoring operation by WEB-RRI model. Still, as shown in the table, the Irrigation Department has found that there are several inconsistencies among the automated rain gauges and manual rain gauges at locations where both gauges are available (Hettiarachchi, 2017). Moreover, daily reservoir operation data obtained from the Mahaweli Authority regarding storage, elevation, sluice and spill discharge were resampled to hourly data for evaluation purposes.

Table 4-1. Data availability and limitations

Data	Source	Resolution	Data availability					Limitations
			~ 2016	2017	2018	2019	2020	
1 Seasonal forecast	JMA → WRF	40 km → 15 km Every 5 day						Bias correction and evaluation of data reliability are limited
2 Weather prediction	NCEP → WRF	27 km → 4 km Daily						Bias correction and evaluation of data reliability are limited
3 Observed rainfall	HMIS	Hourly						Inconsistencies in HMIS rainfall
4 Reservoir data	MASL	Daily						Daily data is resampled to obtain hourly data

<p>JMA : Japan Meteorological Agency (JMA/MRI-CPS2) NCEP : National Centers for Environmental Prediction WRF : Weather Research and Forecasting model HMIS : Hydrological Management Information System MASL : Mahaweli Authority of Sri Lanka</p>	<p> - Seasonal operation period (March to May of 2020)</p> <p> - Short-term dam operation period (16th to 22nd of August 2018)</p>
--	--

4.5.2 Seasonal forecasting data

Nowadays, many seasonal forecast products are freely available from various institutes in the form of both graphical products and underlying digital data. One of the approaches in seasonal forecasting is done by means of large-scale General Circulation Models (GCM) (Alagiyawanna & Jayawardana, 2015; Palmer & Anderson, 1994; Vautard, Plaut, Wang, & Brunet, 1999). GCM-based seasonal forecasts cover large-scale domains, and that information has to be downscaled by using Weather Research and Forecasting (WRF) models to minimize practical limitations in basin-scale applications. The Japan Meteorological Agency (JMA) provides 13 ensemble members in five-day intervals to generate 65 ensemble integrations for a three-month seasonal ensemble prediction system (JMA, 2002). The data availability for the year 2020 is shown in Figure 4.2. The coarse resolution of the JMA/Meteorological Research Institute-Coupled Prediction System version2 (JMA/MRI-CPS2) has been dynamically downscaled by the WRF model v.3.7.1 to generate a 15 km resolution model domain.



Figure 4.2. Seasonal forecast data availability.

4.5.3 Short-term weather forecasting data

Flood forecasting is an effective tool to mitigate flood damage (Ushiyama, Sayama, Tatebe, Fujiokacc, & Fukami, 2014). Advanced flood forecasting centers have attempted coupling NWP with streamflow simulation and hydrological models in the past decade since the prediction capability of NWP have steadily increased as ensemble forecasting and data assimilation techniques have improved (Cloke & Pappenberger, 2009; Cuo, Pagano, & Wang, 2011; Ushiyama et al., 2014). ICHARM used lagged ensemble using the Global Forecast System (GFS) of the National Centers for Environmental Prediction (NCEP-GFS) since this type of ensemble is well suited for operational flood forecasting (Ushiyama et al., 2014). In this study, GFS rainfall forecasts (27 km spatial resolution) and their downscaled version by the Weather Research and Forecasting Model (WRF) of 4 km resolution, a regional weather prediction model, provided by ICHARM were used in the WEB-RRI model as input for flood forecasting. This weather prediction is updated every 24 hours over the Sri Lankan domain. Furthermore, the lagged ensemble is composed of forecasts from updated initial conditions; thus, it can be performed to coordinate daily operations, which updates forecasts.

4.6 Results

4.6.1 Reservoir operation rules based on past observations

4.6.1.1 Seasonal Operation Plan of WMS

SOP is issued just before the beginning of each agricultural season. According to the cultivation calendars issued in the past SOPs, 3 to 3.5-month paddy variety and other field crops are cultivated in the irrigation schemes, as shown in Figure 4.3. Cultivation

extents and dates are decided mainly based on the water availability in the reservoirs at the beginning of the season. In the normal year, the Yala season starts on 20th April and ends on 10th August, and the Maha season starts on 25th October and ends on 25th February. In a dry year, the Yala season starts on 10th May and ends on 10th August, while Maha starts on 20th November and ends on 4th March. During dry years, the cultivation is forgone or done with reduced cultivation, cultivating less water-consuming field crops instead of rice. The data shows that the cultivation of paddy has been reduced in the recent past, and other less water-consuming crops have been cultivated in increased amounts mainly in system H (the system which mainly depends on Mahaweli water).

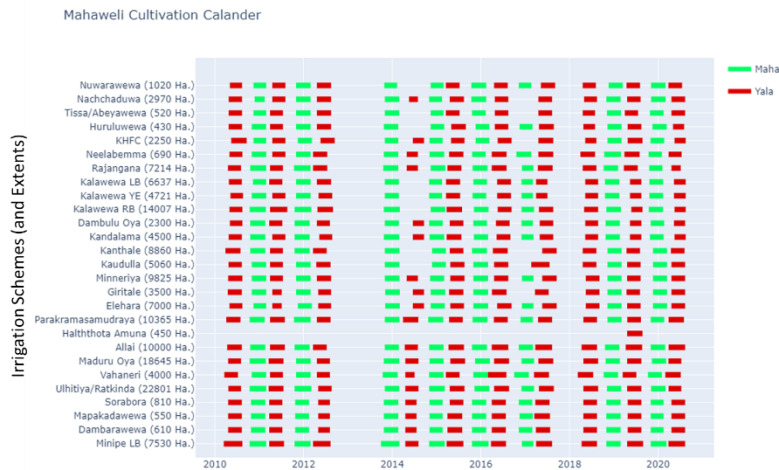


Figure 4.3. Mahaweli cultivation calendar

4.6.1.2 Observed rainfall

Past observed rainfall data from MASL from 2000 to 2018 were analyzed to understand the seasonal (climatic and agricultural) and spatial variation (starting from the upstream-end reservoir, Kotmale, to the downstream reservoir, Rantambe). Figure 4.4 (a & b) shows the box-and-whisker plot of climatic seasonal rainfall and agricultural

seasonal rainfall at specified rain gauge stations in MRB. The median values of each station corresponding to each season are given in white letters on top of the box plots.

According to Figure 4.4 (a), the Kotmale reservoir (upstream of MRB) receives the highest accumulated seasonal rainfall during the SW monsoon season. In terms of median values, the upstream area of MRB receives more than five times as much rainfall as its downstream area (Victoria, Randenigala, and Rantambe). During the NE monsoon, the downstream area receives more rainfall compared to the upstream area. Kotmale receives a 292 mm rainfall while Rantambe receives 1030 mm during the season in terms of median values. The IM-1 season seems very dry despite a fair amount of rainfall during the season. Reflecting rainfall during the SW monsoon season, as shown in Figure 4.4 (b), the Yala agricultural season receives less rainfall in the downstream area of MRB. This behavior justifies the usage of irrigation water for agriculture during this season, as most arable land is located in the downstream area. On the other hand, the Maha cultivation is carried out during the latter part of the IM-2 season, and in the NE monsoon season, the downstream area receives high amounts of rainfall which could be effectively used for rain-fed cultivation with supplementary irrigation whenever rainfall shortage occurs.

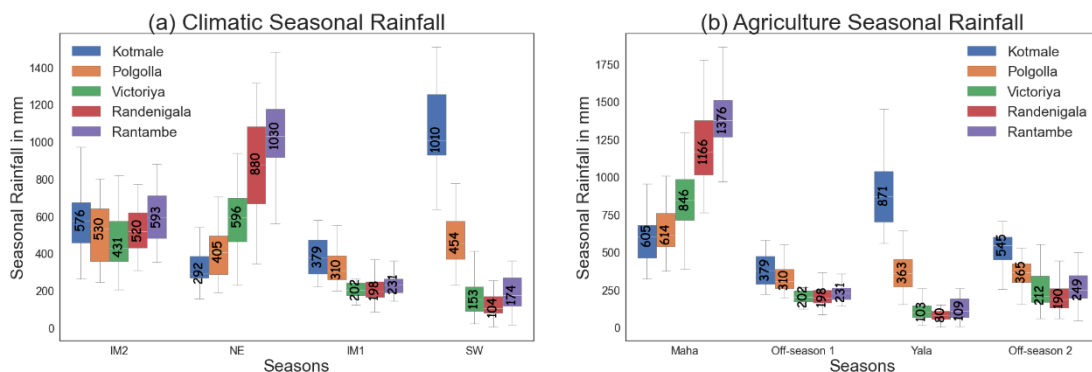


Figure 4.4. Seasonal rainfall at Kotmale, Polgolla, Victoriya, Randenigala, and Rantambe gauging stations: (a) Climatic seasons, and (b) Agricultural seasons

The cumulative rainfall observed in the selected years at the Kotmale, Victoria, and Randenigala reservoir sites is plotted, starting from October in Figure 4.5. As shown in the figure, both a sudden increase in rainfall due to an abrupt weather change and a gradual rainfall increase due to normal conditions can be observed. Events that bring a large amount of rainfall can be commonly observed during the NE monsoon period, especially in the downstream reservoirs (Victoria and Randenigala).

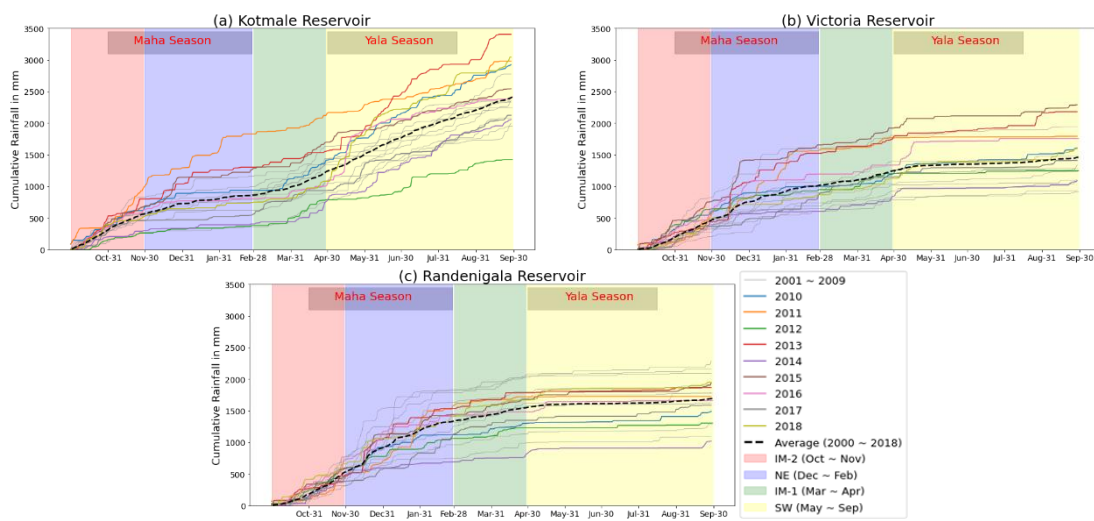


Figure 4.5. Cumulative rainfall received at reservoir sites starting from October

4.6.1.3 Observed inflow to reservoirs

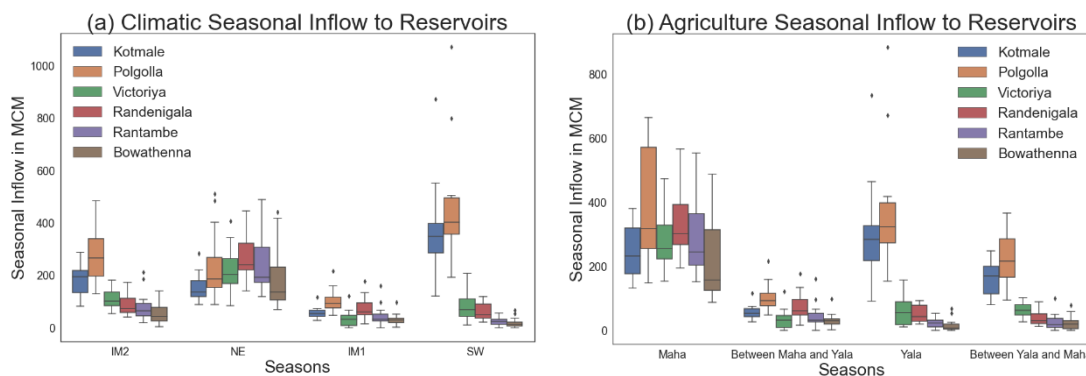


Figure 4.6. Seasonal inflow to reservoirs and diversions (a) Climatic seasonal inflow, and (b) Agriculture seasonal inflow

The seasonal inflow to the reservoir and the diversion weirs are plotted in Figure 4.6 (a) and (b) based on past observed data (2000 to 2015). According to the figure, the

Kotmale reservoir receives more inflow during the SW Monsoon, mainly during the Yala season and during the IM-2 period (the beginning of the Maha season). Also, the IM-1 season (Off-season between the Maha and Yala seasons) seems very dry, and low inflow is received at the Kotmale dam. Except for the Kotmale dam, other dams receive more inflow during the NE monsoon (during the Maha season), while very low inflow can be observed during the other seasons. Further, in some years, the Maha season is water-rich, and the Yala season is dry. Also, the off-season between Maha and Yala seems dry though the whole year seemed water-rich. Therefore, this imbalanced behaviour of local weather affects the process of cultivation decision making. Particularly, in 2014, WMS decided to cultivate less paddy and increase OFC cultivation due to a shortage of water during the Yala season, according to the storage available on the 1st of April. But in the middle stage of the Yala season, the reservoirs received a large inflow, and the water managers were unable to use this inflow effectively.

4.6.1.4 Observed reservoir storage and spillage

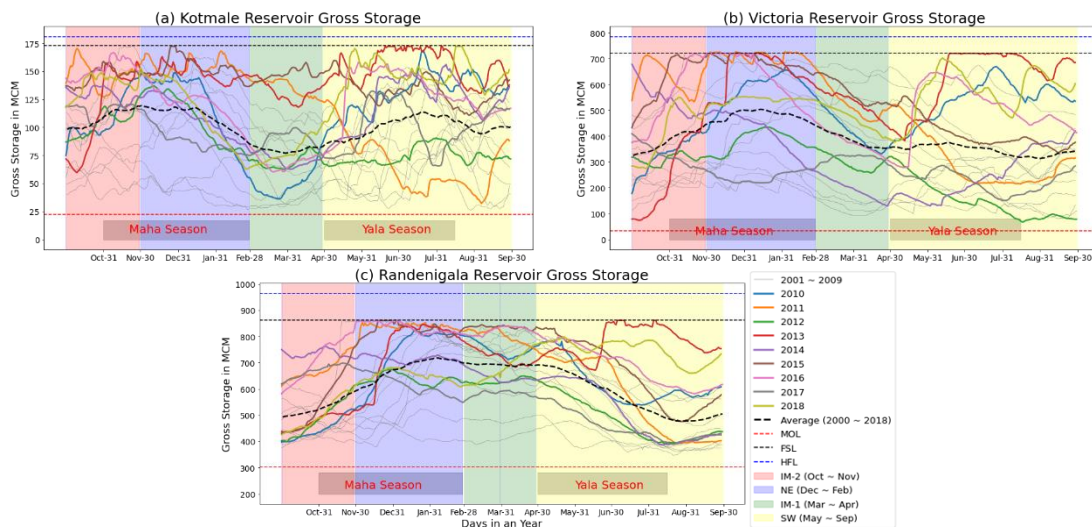


Figure 4.7. Annual reservoir gross storage variation starting from October

Reservoir storage data obtained from MASL was analyzed and plotted annually, starting from October, as shown in Figure 4.7. The Kotmale reservoir receives more

inflow during the SW monsoon, mainly in the latter part of the Yala season and during the IM-2 period (the beginning of the Maha season). Also, it is evident that, in some years, Maha seasons are water-rich while Yala seasons are dry and vice versa. Further, the off-season between Maha and Yala seems dry though the whole year seemed water-rich. Also, it can be noted that the off-season between Yala and Maha seems water-rich in some years, when the water was left unutilized for power generation and ultimately caused several spilling events and flood disasters during NE monsoons (i.e., Maha season).

Further, according to the observed spillage information, as shown in Figure 4.8 (a) and (b), all the reservoirs have experienced spilling events in IM-2, NE, and SW monsoon periods. There was no spilling event recorded during the IM-1 season. In the case of the Kotmale reservoir, spillage was more frequent during the SW monsoon period than the other climatic seasons, i.e., during the Yala agricultural season. The downstream reservoirs, as well as the Kotmale reservoir, experienced larger spilling events during the NE monsoon period (i.e., Maha season), compared to the other seasons.

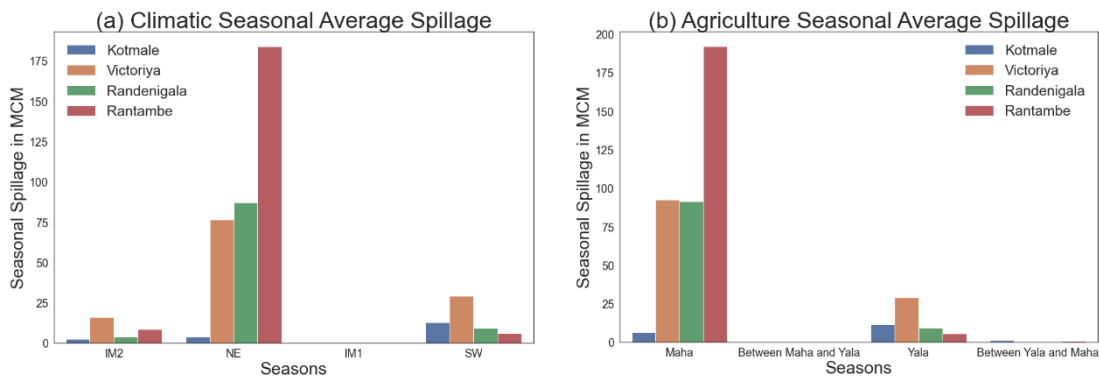


Figure 4.8. Seasonal average spillage of Kotmale, Victoria, Randenigala, and Rantambe reservoirs; (a) Climatic seasons, and (b) Agricultural seasons

4.6.1.5 Observed water diversion to irrigation schemes

According to the records, Kotmale’s water is mainly diverted to systems H and E (see Figure 2.8). Water from the Victoria and Randenigala reservoirs is used for downstream systems along the Mahaweli River.

4.6.1.6 Agriculture

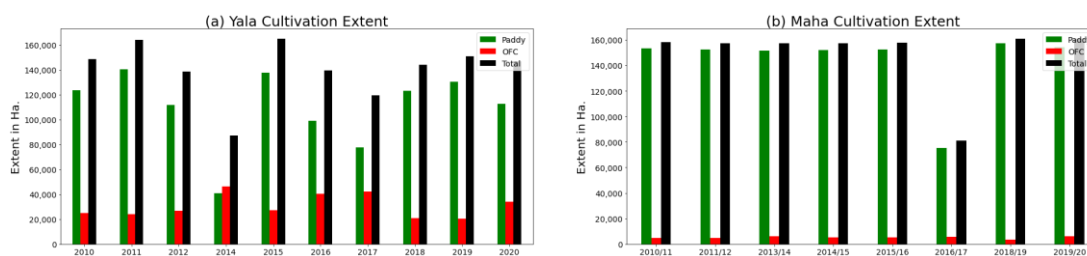


Figure 4.9. Cultivation extents from 2000 to 2020 during Yala and Maha seasons

As explained earlier, the cultivation extent is decided based on the reservoir storage capacity at the beginning of the cultivation season. The cultivation extent decided for each season starting from 2010 was obtained from SOP and plotted, as shown in Figure 4.9. The cultivation of other field crops is gradually increasing in recent years during the Yala season, though the paddy cultivation is dominant during the Maha season.

4.6.1.7 Power generation

According to MASL, power is generated while releasing water for irrigation. In the recent past, Mahaweli river basin hydropower plants are utilized mainly for meeting peak municipal and domestic demands in the morning and evening, with the baseload generated by thermal stations that cannot react quickly to demand peaks. The design specifications of the hydropower reservoirs are given in Table 4-2. Kotmale, Victoria, and Randenigala are the largest hydropower reservoirs in the system. These three dams are located in series, along the river in the upper stream and account for 90% of the storage capacity and 80% of the total power generation capacity of the dams under MASL. Also,

these three dams are designed in a way that the discharge capacity of the downstream dam through either power turbines or lower outlets is greater than the upstream dams' power release. Further, all the power release from these three dams will reach the level of the Rantambe dam, which has the largest spillway capacity, as shown in Table 4-2. After the Rantambe dam, there is no dam along the Mahaweli River except the Minipe diversion.

Table 4-2. Design specifications of hydropower reservoirs

No	Power Station	Year	Lat.(N)	Lon.(E)	Height(m)	Storage(MCM)			Design Discharge (m3/s)			Turbine capacity (MW)
						FSL	MOL	Live	Spill	Lower outlet	Power Turbine	
1	Kotmale	1986	7.064	80.598	87	172.9	22.2	150.7	5560	133	113	201
2	Polgolla	1976	7.322	80.646	14.6	4.1	2	2.1	1268		56.6	38
3	Victoria	1984	7.241	80.788	122	721.2	34	687.2	7900	760	140	210
4	Randenigala	1986	7.199	80.924	94	861.4	303.4	558	7900	200	180	126
5	Rantambe	1990	7.202	80.945	43.5	22	4.4	17.6	10235	400	180	49
6	Bowatenna	1976	7.667	80.666	30	52	17	35	3500			40
7	Moragahakanda	2017	7.698	80.77	65	521		521				25

The daily variation of power generation in each year from 2000 to 2018 is plotted in Figure 4.10 for the Kotmale, Victoria and Randenigala reservoirs. According to the figures, none of the reservoirs has reached their potential power generation capacity in most of the days.

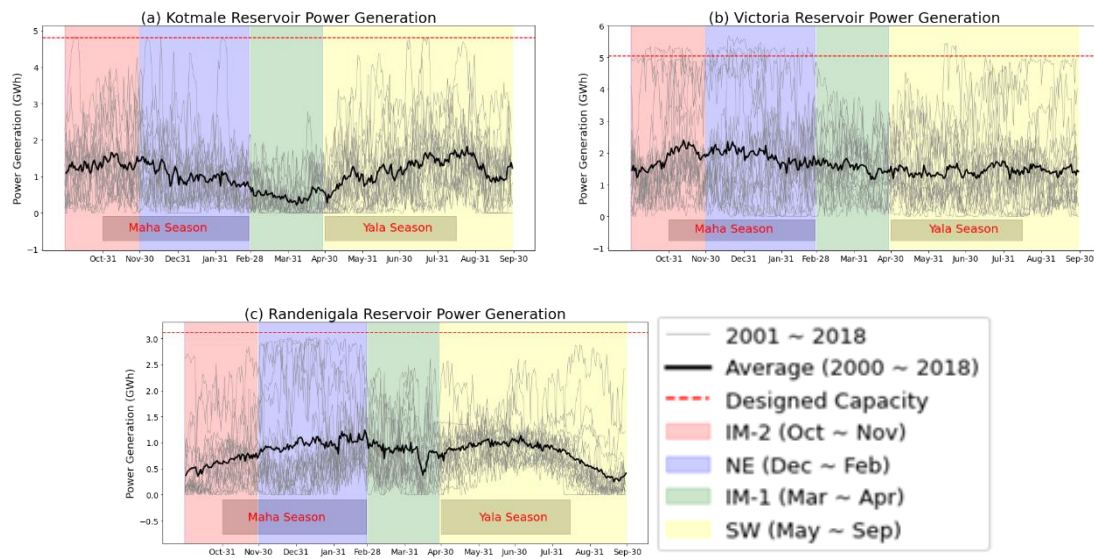


Figure 4.10. Annual power generation starting from October

4.6.1.8 Flood disaster management assessment

Based on the meteorological and climatological variations, observed inflow, and agricultural and drinking water demand, reservoir operation rules have been developed to minimize downstream floods in a previous study by Indika et al. (2018). This study showed that, with the developed operation rules, a reduction of 1.5m flood level at the Mannampitiya Discharge location in the observed 2015 January flood. By considering the above understanding of past observed meteorology, climatology, hydrology, reservoir operations and the previous study, it is decided to adopt the reservoir operation rules shown in Table 4-3 to maintain the monthly maximum reservoir storages in the reservoirs to minimize flood and drought disasters, as well as to maximize the agriculture production and hydropower generation.

Table 4-3. Reservoir operation rule for Kotmale, Victoria, and Randenigala reservoirs

Month	Kotmale		Victoria		Randenigala	
	Flood storage percentage	Capacity after allowing Flood Storage in m ³	Flood storage percentage	Capacity after allowing Flood Storage in m ³	Flood storage percentage	Capacity after allowing Flood Storage in m ³
January	6%	170234000	15%	675750000	15%	820250000
February	6%	170234000	10%	715500000	10%	868500000
March	6%	170234000	6%	747300000	6%	907100000
April	10%	162990000	6%	747300000	6%	907100000
May	15%	153935000	6%	747300000	6%	907100000
June	20%	144880000	6%	747300000	6%	907100000
July	20%	144880000	6%	747300000	6%	907100000
August	15%	153935000	10%	715500000	10%	868500000
September	10%	162990000	15%	675750000	15%	820250000
October	6%	170234000	20%	636000000	20%	772000000
November	6%	170234000	20%	636000000	20%	772000000
December	6%	170234000	20%	636000000	20%	772000000

4.6.2 Seasonal operation optimization

This section provides one of the adaptation strategies which MASL can utilize to seasonal reservoir operation which adopt to the climate change by utilizing seasonal forecast information.

Seasonal forecast data of 2nd, 7th, 12th, 17th, 22nd, and 27th March 2020 (6 days) were considered as forecasting data for April, May and June 2020, as the time series of all these forecast data ends on 29th June 2020 irrespective of their starting dates. Every prediction day consists of 13 ensembles, and in combination, a total of 78 (6 days X 13 ensembles) ensembles were produced for this period. Ensemble forecasted rainfall and HMIS rainfall were compared spatially and temporally.

4.6.2.1 Basin average rainfall

Cumulative basin average rainfall starting from 1st of April 2020 is plotted in Figure 4.11. The figure shows that the observed basin average rainfall falls within the ensemble range of the rainfall forecasted for the selected months.

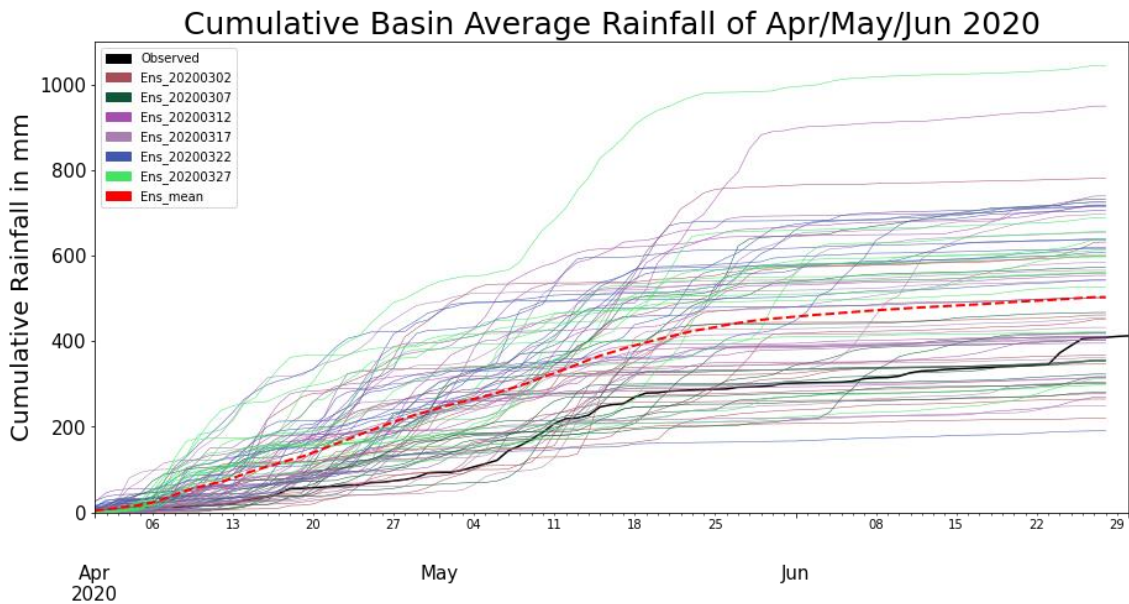


Figure 4.11. Cumulative basin average rainfall of April/May/June 2020

To further understand forecasting efficiency on a basin scale, the basin was divided into three sub-basins based on the agro climatic zones, and the temporal variation of rainfall is plotted in Figure 4.12. Similar to the basin average rainfall, all three sub-basins have shown that the observed sub-basin average rainfall falls within the ensemble range of the rainfall forecasted for the selected months.

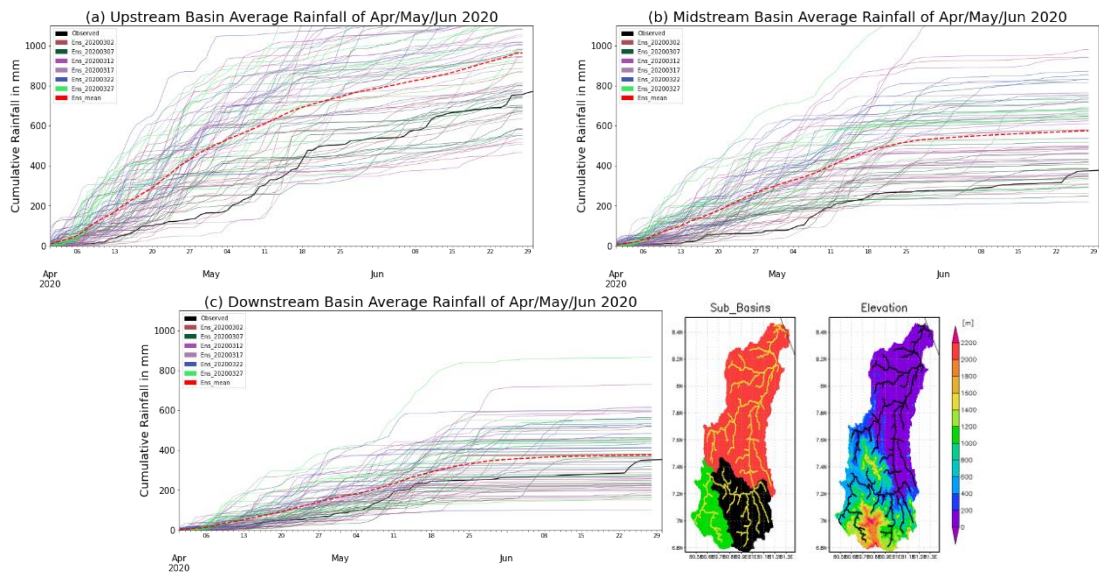


Figure 4.12. Cumulative sub basin average rainfall of April/May/June 2020 and the basin demarcation

To understand the spatial variation of the monthly rainfall, the spatial distribution of the monthly total rainfall of observed HMIS, monthly climatological average, and the ensemble mean of forecasted rainfall for April, May, and June were plotted in Figure 4.13. According to the figure, the rainfall forecast stimulates a similar pattern to the actual observation, where the hilly upstream region receives more rainfall while the lower regions receive less rainfall due to the latitude dependencies.

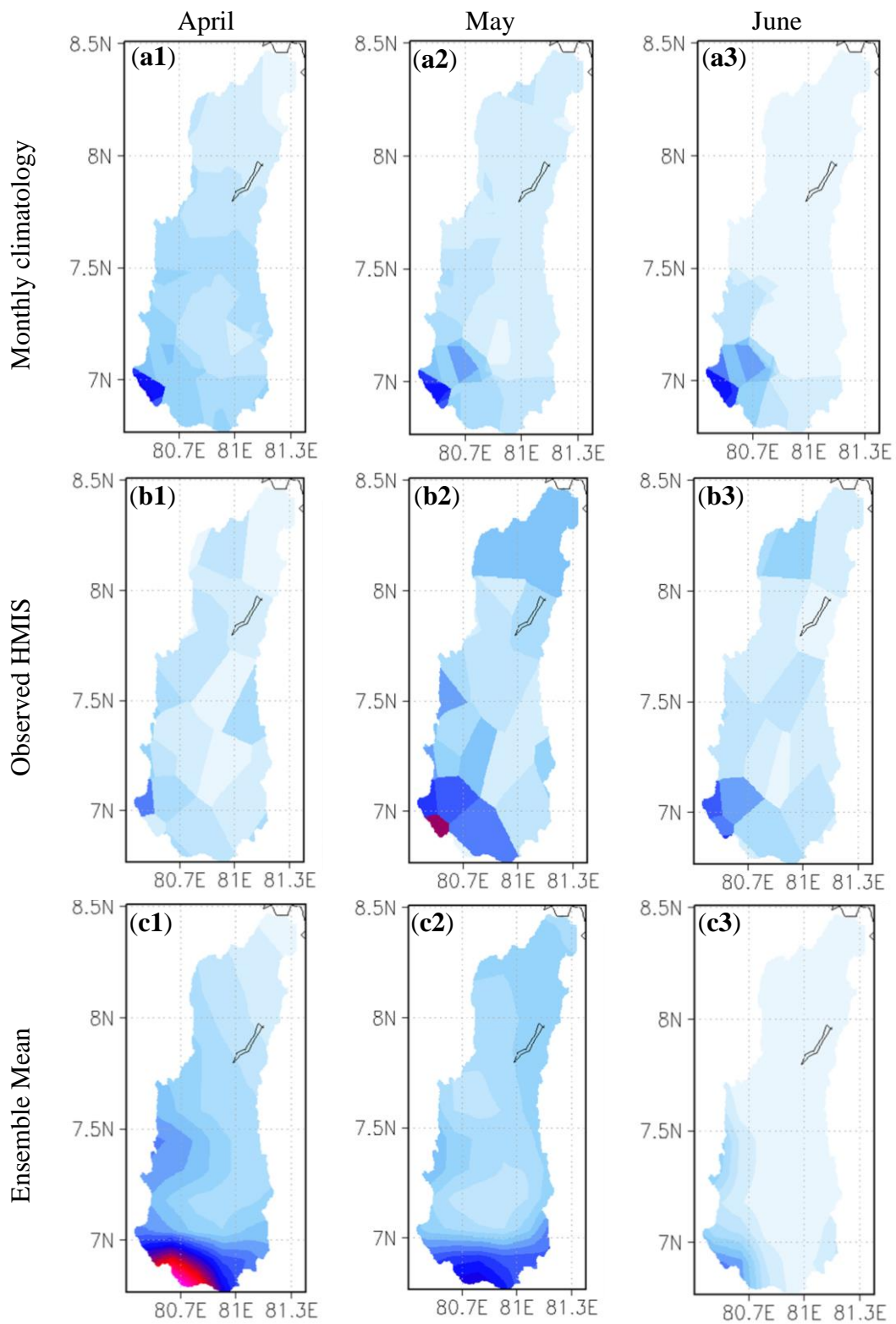


Figure 4.13. Spatial distribution of monthly rainfall

4.6.2.2 Reservoir optimization for seasonal forecasted data

The target was set to utilize the seasonal forecast information of the beginning of March 2020 to optimize the reservoir operation to a) fill the reservoir for the purpose of maximizing water use for the “Yala” cultivation and b) minimize the downstream damage by keeping the reservoir 15% (1st May 2020) empty at the beginning of the “Yala” cultivation according to the reservoir operation rules. This analysis is conducted under two scenarios, as given below, to show the benefits of utilizing seasonal forecasts, optimization tools and reservoir operation rules. The monitoring indexes of Reliability, Resilience, Vulnerability, and Sustainability are checked for both the scenarios for comparing the benefits of maintaining the flood storage.

Scenario 1: Allowing 15% flood storage at the beginning of Yala

- The reservoir will be kept at 153 MCM at the beginning of Yala (1st of May)
- The forecasted inflow will only be released through the power tunnel to generate power during the months of March and April.
- The released water during this period can be utilized to fill the reservoirs downstream if those are empty (but this case is not analyzed in this step)

Scenario 2: Allowing 0% flood storage at the beginning of Yala

- The reservoir will be kept at 172 MCM (Reservoir at FSL) at the beginning of Yala (1st of May)
- The forecasted inflow will only be released through the power tunnel to generate power during the months of March and April.

- The released water during this period can be utilized to fill the reservoirs downstream if those are empty (but this case is not analyzed in this step)

The reservoir storage and discharge variation for the selected scenarios are given in Figure 4.14 and Figure 4.15. The performance criterion indexes for each ensemble and the ensemble mean of each scenario are given in Table 4-4 and Table 4-5.

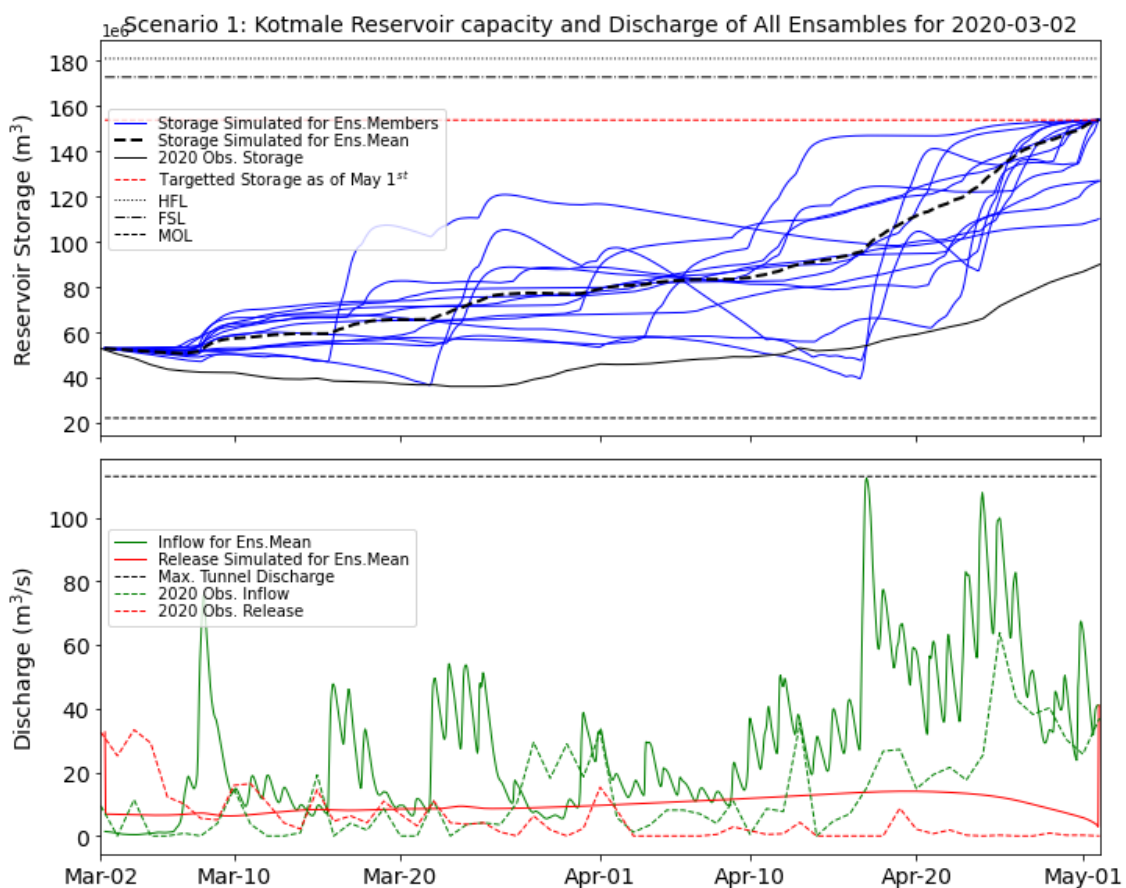


Figure 4.14. Reservoir operation under Scenario 1

Table 4-4. PCIs for ensembles and ensemble mean of scenario 1

PCI	Values for ensembles in %													
	E1	E2	E3	E4	E5	E6	E7	E8	E9	E10	E11	E12	E13	Mean
Reliability (time)	93	82	79	89	26	26	84	41	26	79	43	57	39	79
Reliability (volume)	352	204	411	968	1	1	246	23	1	281	33	61	14	174
Vulnerability	5	4	3	4	2	2	3	2	2	3	2	2	2	3
Resilience	25	36	46	29	16	16	30	22	16	46	23	31	22	46
Sustainability Index	94	87	110	123	0	0	88	38	0	99	41	56	33	88

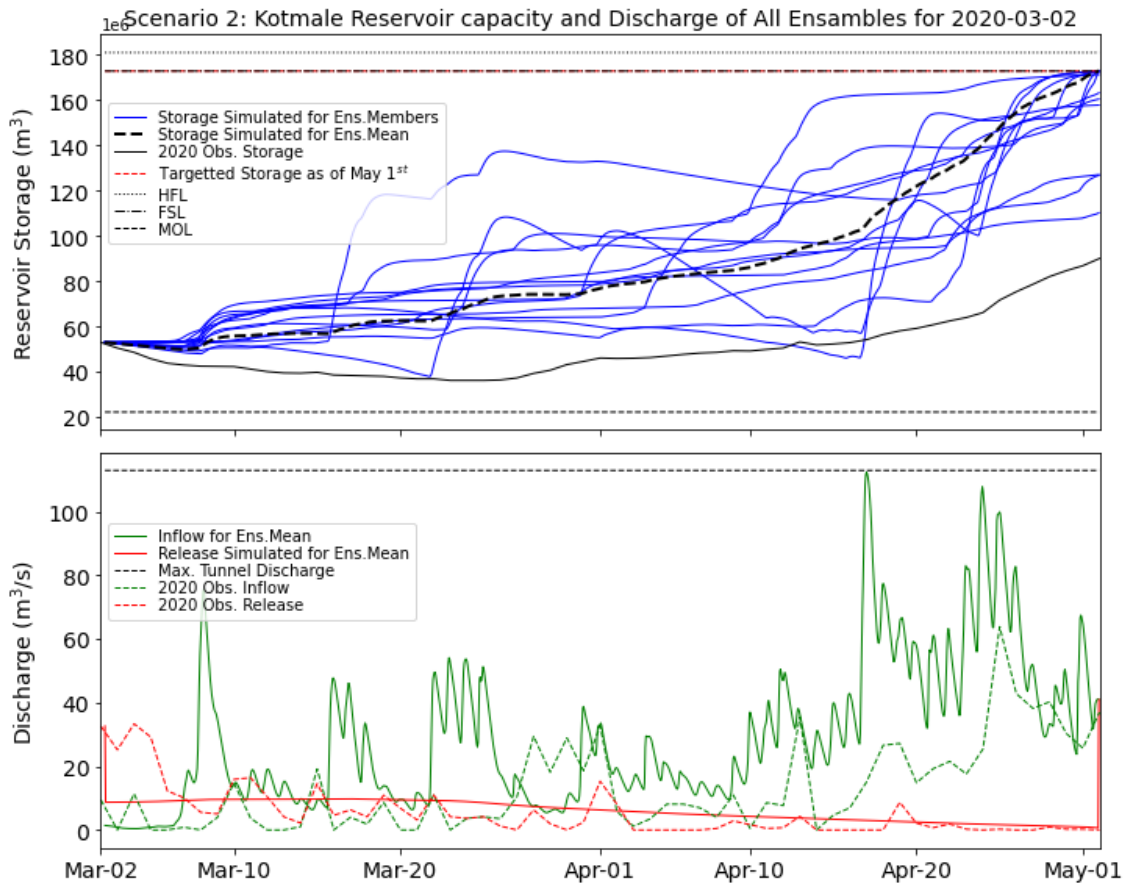


Figure 4.15. Reservoir operation under Scenario 2

Table 4-5. PCIs for ensembles and ensemble mean of scenario 2

PCI	Values for ensembles in %													
	E1	E2	E3	E4	E5	E6	E7	E8	E9	E10	E11	E12	E13	Mean
Reliability (time)	90	67	79	87	26	26	80	26	26	77	26	26	26	74
Reliability (volume)	281	139	346	903	1	1	181	1	1	216	1	1	1	109
Vulnerability	4	3	3	4	2	2	3	2	2	3	2	2	2	2
Resilience	33	20	46	25	16	16	42	16	16	43	16	16	16	50
Sustainability Index	95	65	105	117	0	0	87	0	0	91	0	0	0	79

According to Figure 4.14, scenario 1 was started to fill the reservoir by utilizing 13 forecasted ensembles and the ensemble mean with the initial storage of the reservoir at 53 MCM. The reservoir was allowed to fill up to 153.93 MCM as defined by the operation rules (15% of storage reserved for flood storage) to keep the reservoir ready to receive upcoming floodwaters. Similarly, the scenario-2 operation started with the initial storage of 53 MCM. Still, the reservoir was allowed to fill up to the Full Supply Level

(172.9 MCM), i.e., there was no flood storage to accommodate future floods. Under the scenario-2 conditions, if a sudden flood occurs in the future, the reservoir will start to spill, which may result in downstream damage. The performance matrices were estimated based on the water demand (observed discharge) and water supply (simulated discharge). To understand the benefits of introducing seasonal forecasts, reservoir optimization tools and reservoir operation rules with flood management and without flood management (scenario1 and scenario 2), PCIs corresponding to the ensemble mean of each scenario are plotted in a radar chart shown in Figure 4.16. According to the figure, it is realized that the reservoir operation under scenario 1 (allowing flood storage) increases reliability and sustainability while keeping resilience and vulnerability more or less the same as scenario 2. Therefore, by utilizing seasonal forecasts, optimization tools and reservoir operation rules, we can achieve flood risk reduction and drought risk reduction by saving enough water for the upcoming agriculture season and enhance energy generation by pre-releasing dam water through a power turbine for a future flood.

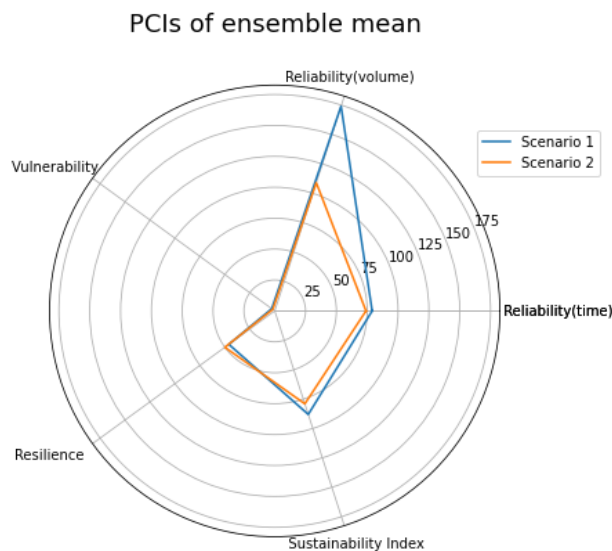


Figure 4.16. Performance criterion indexes of ensemble mean under selected scenarios.

4.6.3 Accumulating short-term operation by using short-term numerical weather prediction

This section provides one of the adaptation strategies that MASL can utilize for short-term reservoir operation to adapt to climate change by utilizing short-term numerical weather prediction information. This adaptation methodology will handle flood risk reduction and release the water as much as possible to adapt to the change.

As explained earlier, a spilling event observed in 2018 was taken into consideration in this chapter. This spilling event started on 16th August 2018 and lasted for 7 days.

4.6.3.1 Basin average rainfall

Basin average rainfall from ensemble forecasting and observation is plotted in Figure 4.17.

The start date of the spilling event is given as Day (0), and the previous and following dates are denoted in negative and positive numbers, respectively, in Figure 4.17. As depicted in the figure, the observed basin average rainfall mostly falls within the ensemble range of the rainfall forecasted for the selected days with some considerable discrepancies. Therefore, it is decided to simulate the discharge by using these ensemble forecasted data for reservoir optimization study.

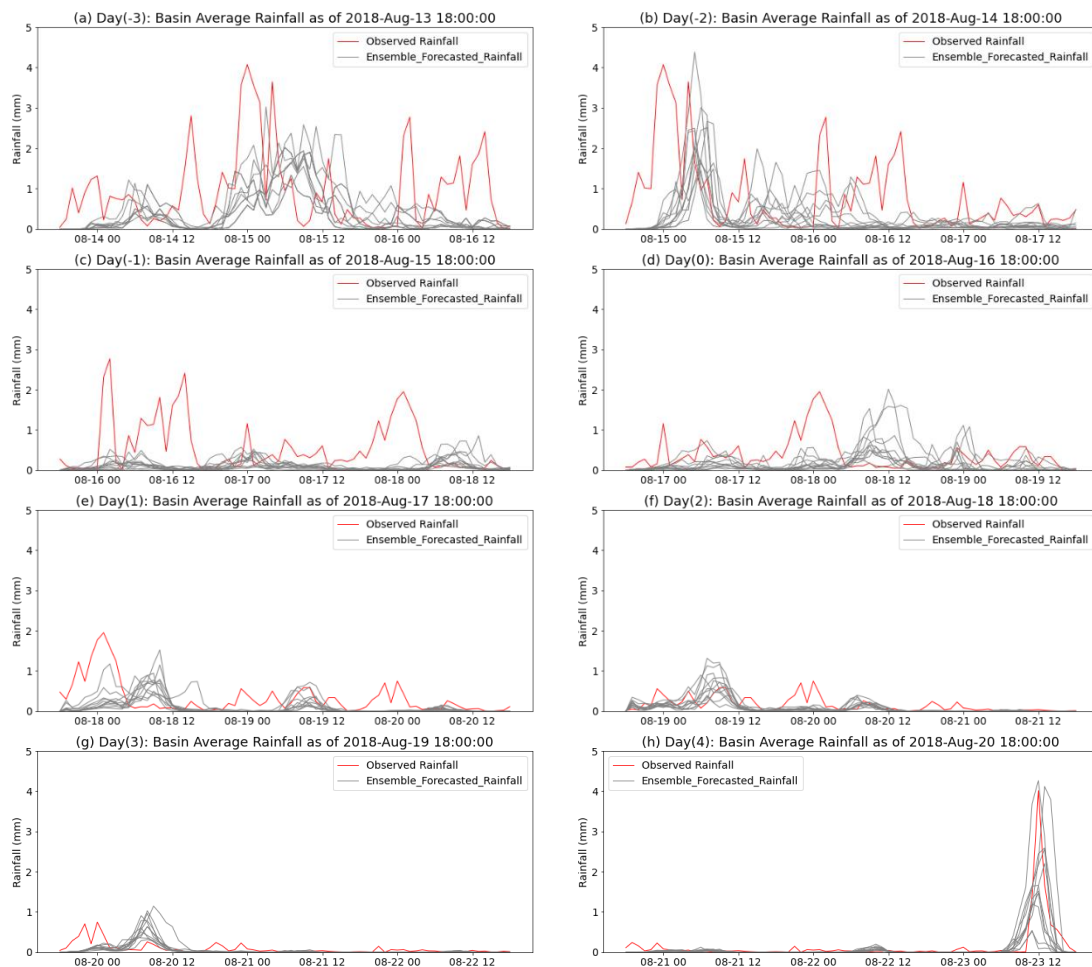


Figure 4.17. Basin average ensemble weather forecasted and observed rainfall

4.6.3.2 Reservoir optimization for short-term weather prediction data

As explained earlier, short-term weather prediction data are available on a daily basis, generated at the 18th hour of a day for the next 72 hours (next 3 days). As the spilling date was 16th August 2018, the forecasted data three days before the spilling date (13th August 2018) were used in this analysis.

The forecasted rainfall of 11 ensembles was coupled with the WEB-RRI to simulate forecasted inflow by initiating the hydrological model with a monitoring model run performed with observed rainfall data.

The target was set to utilize the ensemble weather prediction information on 13th August 2018 to optimize the reservoir operation and to check the status of the operation with the following strategy and operation rules:

Adaptation Strategies:

Due to the uncertainty of the forecasted inflow, decisions on the selection of ensembles should be carefully made. According to the reservoir storage capacity on the day of forecasting, the selection of ensembles has to be decided. If the reservoir is full, it is acceptable to use an ensemble with a higher total sum of inflow and prerelease water through the tunnel for power generation; i.e., even if the prediction fails and if less discharge is received at the reservoir since the reservoir is at full capacity, we may lose only a small quantity of capacity. Meanwhile, we will receive ensemble forecasts for the next day, the actual updated ground conditions about the inflow, and the storage of the reservoir on the next day. Therefore, it would be effective to adjust the operation according to the updated information to avoid additional mistakes due to forecasting uncertainties. Similarly, if the reservoir is at a low stage, it is desirable to use an ensemble with a low accumulated sum of inflow value. At this stage, more priority should be given to filling the reservoir rather than pre-releasing for energy generation. Therefore, as stated above, even with forecasting uncertainty, the decisions can be taken with fewer failures.

An arithmetic sum of forecasted discharge of all the ensembles is calculated, and the ensembles are rank-ordered according to the sum by assigning the first rank to the highest discharge sum ensemble and the 11th rank to the lowest discharge sum ensemble. The reservoir storage has been divided into five regions, as shown in Figure 4.18, to

decide the operation rules for short-term operation. The past 20-year reservoir operation data were analyzed to obtain the day in a year statistics, as shown in the figure.

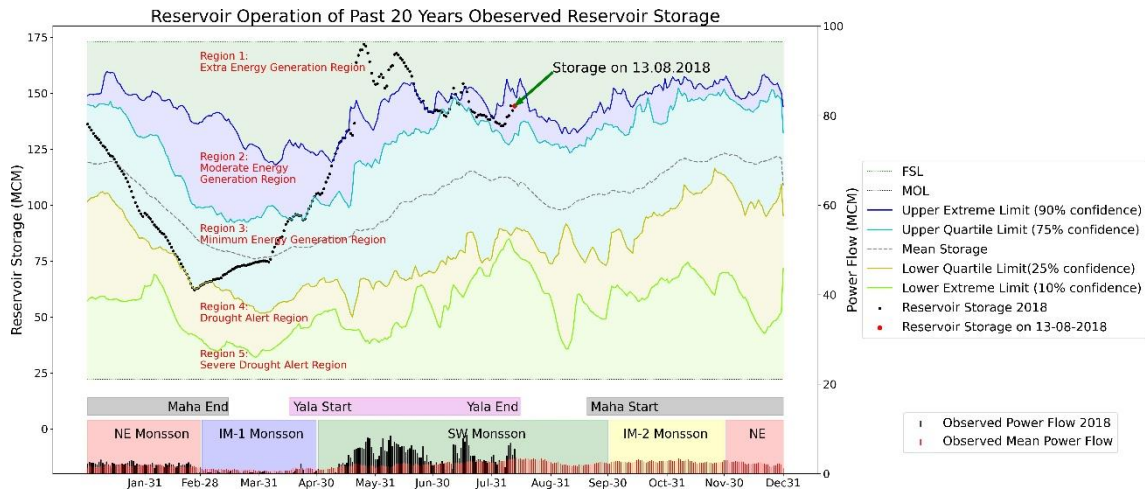


Figure 4.18. Kotmale reservoir operation

Region 1: Extra Energy Generation Region

If the current storage enters this region, the optimizer will reduce the storage towards the lower limit of this region and use the ensemble with rank 2 (20%).

- In this region, all (100%) of the forecasted inflow will be discharged as power flow, and some portion of the reservoir capacity will be released if possible.

Region 2: Moderate Energy Generation Region

If the current storage enters this region, the optimizer will increase the storage in the direction of the upper limit of this region and then use the ensemble with rank 4 (35%).

- In this region, 75% of the forecasted inflow will be released within the time period (73 hours), and 25% of the forecasted inflow will be used to increase the capacity up to the upper limit of this region.

Region 3: Minimum Energy Generation Region

If the current storage enters this region, the optimizer will increase the storage to reach up to the upper limit of this region and then use the ensemble with rank 6 (50%).

- In this region, 50% of the forecasted inflow will be released within the time period (73 hours), and 50% of the forecasted inflow will be used to increase the capacity up to the upper limit of this region.

Region 4: Drought Alert Region

If the current storage enters this region, the optimizer will increase the storage to reach up to the upper limit of this region and then use the ensemble with rank 8 (70%).

- In this region, 25% of the forecasted inflow will be released within the time period (73 hours), and 75% of the forecasted inflow will be used to increase the capacity up to the upper limit of this region.

Region 5: Severe Drought Alert Region

If the current storage enters this region, the optimizer will increase the storage to reach up to the upper limit of this region and then use the ensemble with rank 10 (90%).

- In this region, none (0%) of the forecasted inflow will be released within the time period (73 hours), and 100% of the forecasted inflow will be used to increase the capacity up to the upper limit of this region.

As shown in Figure 4.18, the reservoir storage on 13th August 2018 was observed well within Region 2. Therefore, the optimizer will increase the storage in the direction of the upper limit of this region by using the ensemble with rank 4 (35%). Therefore, 75%

of the forecasted inflow will be released within the time period (73 hours), and 25% of the forecasted inflow will be used to increase the capacity up to the upper limit of this region. The reservoir operation under this condition is given in Figure 4.19. According to the figure, the optimized reservoir operation is performed in order to bring down the reservoir elevation by the end of the time horizon (73 hours) by pre-releasing the forecasted inflow and keeping the reservoir elevation at a low level to receive a future flood, thus preventing the reservoir from spilling. By doing this, the reservoir is ready to receive expected flood inflows to be utilized for power generation.

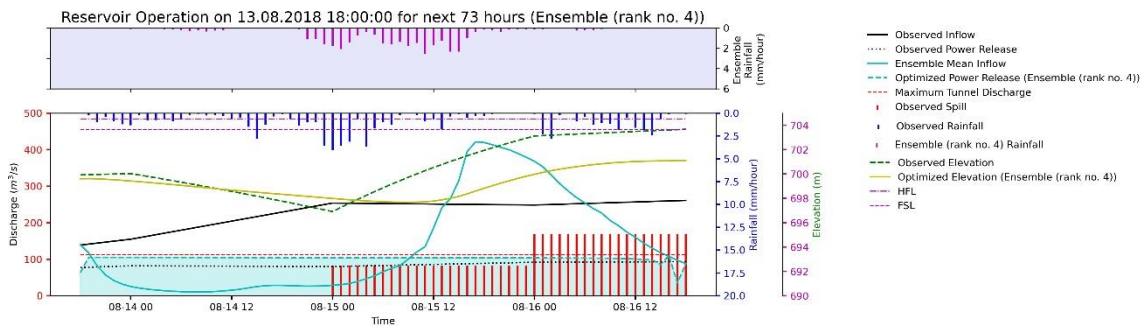


Figure 4.19. Optimized reservoir operation under selected operation rule

Further, Figure 4.20 shows the reservoir storage reduction at the end of the time horizon, and this will allow the reservoir to maintain a flood storage to receive future flood inflows.

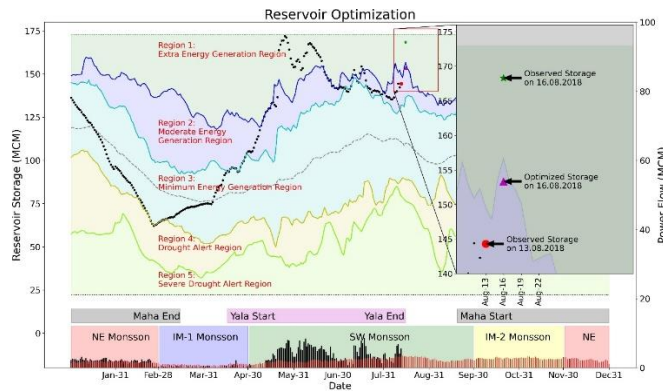


Figure 4.20. Reservoir optimization for selected operation rule

5 Policy proposals

The qualitative level of confidence of hydro-meteorological characteristics and their ranges (at levels of confidence) provided in chapter 3 can be utilized to make future disaster risk reduction decisions by introducing operational changes as adaptations, such as the example operations shown in chapter 4, to DRR and WRM. Information on an increasing level of confidence of hydro-meteorological characteristics indicates future positive changes in terms of water resources and negative changes in terms of disasters (floods and droughts). Policymakers could grasp this information to react to these future changes. Reactions could be in two directions by implementing countermeasures mentioned above: one is to mitigate disasters. The other is to utilize water resources or opportunities brought in by disasters to better society and the environment. Further, decision-makers can decide to either implement new countermeasures or continue the current disaster management practices under an uncertain level of confidence.

Making decisions based on the range at the level of confidence is another crucial factor in the decision-making process. The range provides a spectrum of GCM outputs under uncertainty; thus, decisions must be made under this uncertainty. Furthermore, the gap between the low end and the high end in the range varies according to selected hydro-meteorological characteristics, and the selection of appropriate model output corresponding to the value in the range depends on what kind of countermeasures to be implemented for disaster risk reduction. For example, low-end models could be selected for future infrastructure designs, i.e., hard countermeasures, while high-end models could be selected for managing disasters through soft countermeasures. Further, it is to be noted that the statistical bias correction does not represent the spatial and temporal connectivity;

however, it is beneficial to identify the range of target parameters from the selected GCMs with less computational effort. To overcome the limitations of the statistical approach, the dynamical downscaling method can be used to obtain quantitative outputs, representing the spatial and temporal connectivity for designing infrastructure development (i.e. hard countermeasures) at the local scale. Therefore, future research is needed on quantitative analysis to represent the spatial and temporal connectivity based on the dynamical downscaling approach for supporting local-scale future infrastructure development and identifying the hazard.

In terms of decision making in the MRB, the Mahaweli Authority of Sri Lanka (MASL) is the governing body for coordinating all the stakeholders coming under each water, food, energy and disaster management sectors. They have already established a common platform called Water Management Secretariat (WMS) for coordination among the stakeholders seasonally and by-weekly. WMS is the most advanced decision-making platform within the water sector, which operates in Sri Lanka. It is the ideal place for policymaking according to the future changes in this river basin. There are several stakeholders involved in this basin management in each of the sectors. The water sector is under the purview of Mahaweli Authority of Sri Lanka (MASL), Irrigation Department (ID), and National Water Supply and Drainage Board (NWSDB). The Food sector is under the purview of MASL, ID, and Department of Agriculture (DOA), The Energy sector is under the purview of MASL and the Ceylon Electricity Board (CEB). Finally, the disaster management sector is under the purview of MASL, ID, and Disaster Management Centre (DMC).

According to the study, we could observe several future changes in the Mahaweli river basin under changing climate. This study identifies the future water resources, flood events, the severity of drought, and socio-economic damages due to future flood inundation are increasing with seasonal changes. According to the impact assessment findings and proposed operational changes, this chapter suggests some cost-effective policy changes to the relevant sectors for implementing soft countermeasures.

First, according to the future changes such as upstream receiving more rainfall, SW and IM-2 rainfall and discharge increase, by utilizing the seasonal forecast informed operation, water sectors can plan for diversion of water to the downstream reservoirs to utilize the water for agriculture (for example, during NE monsoon, meteorological drought in downstream is increasing). Further, food sectors can plan seasonally to increase the cropping intensity by the expansion of irrigated land, the decision to supply irrigation water to possible rain-fed lands, and introducing an intermediate cultivation season between main Yala and Maha seasons, for example (a third cultivation season correspond to IM-2 climate season). Also, energy sectors can utilize the pre-releases from hydropower dams for power generation.

Second, according to the finding that the increase of future meteorological drought, especially during the NE monsoon period, and by utilizing the seasonal forecast informed operation, water sectors can plan to release water from upstream reservoirs to cater to the deficits in the downstream reservoirs. On the other hand, the food sectors can take decisions based on seasonal planning to alter crop calendars and crop varieties. Also, they can decide to abandon a season if an extreme drought is predicted as rained cultivation is popular during NE Monsoon (Maha season).

Third, the future hydrological flood is increasing. Using short-term weather forecast informed operation, water sectors can pre-release the water to downstream reservoirs for irrigation usage and minimize the downstream flood damages. Similarly, the energy sectors can utilize this pre-releases for hydropower generation.

Finally, the future damage to population, cropland, and urban area by the flood will increase. Therefore, food sectors can introduce flood-resistant crop varieties and enforce regulations for avoiding cultivation within flood-prone areas. Also, the disaster management sectors could issue flood early warnings for evacuation by utilizing short-term weather forecast, and they could prepare hazard maps and evacuation guidelines. Further, they could enforce land-use regulations and building codes to construct waterproof buildings within the flood plain.

6 Conclusions

6.1 Climate change impact assessments

Chapter 3 presented an integrated approach for assessing climate change impacts on the hydro-meteorological characteristics of river basins. The assessment is accomplished by selecting reliable GCMs based on their regional performance, identifying climate change signals, clarifying uncertainties from the selected GCMs, developing a WEB-RRI model to simulate the basin hydrological responses to floods and droughts seamlessly under climate change, and then facilitating decision-making procedures.

The proposed approach was applied to MRB in Sri Lanka to assess the impacts of climate change on water resources. The GCM selection procedure found that four GCMs (CanESM2, CNRM-CM5, GFDL-ESM2G, and MPI-ESM-LR) out of 44 were capable of satisfactorily simulating the past regional climate. As a result, these models' precipitation and temperature data were obtained and statistically bias-corrected. The bias-corrected results showed that the basin average annual temperature is very likely to increase in the future on average with a future temperature increase of 1.1 °C over the future 20 years. Under this warming future climate, the future annual rainfall over the basin is very likely to increase, and the range will vary from 204 to 476 mm/year. The extreme event analysis showed that future heavy rainfall and meteorological droughts are likely to increase at the basin scale annually, as three out of the four models showed an increase in future anomalies of CWD in terms of heavy rainfall and an increase in future anomalies of CDD concerning to meteorological droughts. On the other hand, the future annual average discharge at the Mannampitiya gauging station is very likely to increase, and the range of

increase will vary from 11 m³/s to 57 m³/s. The extreme flood event analysis showed that the hydrological floods are very likely to increase according to the first 20 peak flows in the future climate. Meanwhile, the last 20 low flow rates indicated that the trend of future hydrological droughts is uncertain. Moreover, the mapping of the all-time maximum inundation depth of more than 1 m showed that the future inundated population, cropland, and urban land area will likely increase. Therefore, there will be more economic damage due to floods in the future under the changing climate. Further, in terms of droughts during the NE and IM-1 monsoon periods, especially the downstream zone of MRB was found to be more vulnerable, which calls for special attention for drought risk reduction by adopting suitable policies.

It is to be noted that statistical bias-correction does not represent the spatial and temporal connectivity; however, it is useful to identify the range of target parameters from the selected GCMs with less computational effort. To overcome the limitations of the statistical approach, the dynamical downscaling method can be used to obtain quantitative outputs, representing the spatial and temporal connectivity for designing infrastructure development at the local scale. Therefore, future research should focus on quantitative analysis to represent the spatial and temporal connectivity based on the dynamical downscaling approach for supporting local-scale future infrastructure development as well as the development of flood and drought forecasting and monitoring for disaster risk assessment, adaptation and mitigation.

6.2 Climate change adaptation and resilience strategies

According to the climate change impact assessment in Chapter 3, MRB will yield sufficient water for future usage. Still, MRB was severely affected by droughts in the

recent past, according to MASL. Further, a seasonally and spatially varied future water availability and shortage that can influence the MRB system operation can be observed. Therefore, Chapter 4 discussed how to strategically plan and utilize future increased water resources by tackling flood and drought disasters in an integrated manner to optimize benefits by incorporating the merits of cutting edge science and technology, i.e., ensemble seasonal weather prediction and ensemble numerical weather forecasting. Chapter 4 introduced an ensemble forecasting system for the optimization of dam operations for reducing flood peaks and making the maximum use of water to support a decision support system for short-time dam operations during heavy rainfall and seasonal planning.

This study is accomplished by utilizing forecast information (both seasonal and short-term) and coupling it with the WEB-RRI model to simulate forecasted discharge at a selected location (Kotmale reservoir). The simulated discharge was then used to perform reservoir operations by RTC-tool 2, a real-time reservoir optimization tool.

The past operation of the Kormale reservoir was fully understood by reviewing the past seasonal operation plan, analyzing various types of data such as dam operation data, diversion data, cultivation and yield data, power generation data, and a previous study which developed reservoir operation rules to minimize flood damage. By understanding the past operation, we developed optimum operation strategies by including future climate change and ensuring water, energy and food security and flood disaster risk reduction. We used short-term weather prediction-informed reservoir operations to utilize forecasted flood storage for power generation and ultimately keep the flood storage in the reservoir ready to receive future floods. On the other hand, we used seasonal forecast information to show the benefits of the reservoir operation conducted by coupling the

information with a hydrological model and an optimization scheme to prepare seasonal plans while reducing flood damage, increasing confidence in agricultural planning, and increasing power generation.

The Japan Meteorological Agency (JMA) provides 13 ensemble members at five-day intervals to generate 65 ensemble integrations for a three-month seasonal ensemble prediction system. The 3-month forecasted data on 2nd March 2020 were utilized to plan reservoir operation for the next 2 months until the beginning of the next Yala season on 1st May 2020 and to evaluate the operation of the Kotmale reservoir. The forecasted rainfall distribution was compared with HMIS observed rainfall data. Using the forecasted rainfall, the river was simulated with the WEB-RRI model, which was coupled with a reservoir optimization model. The performance of the reservoir was evaluated under two scenarios: 1) filling the reservoir by allowing flood storage and 2) filling the reservoir without allowing flood storage, i.e., filling up to the full supply level. The performance matrices were estimated based on water demand (observed discharge) and water supply (simulated discharge). The results found that the reservoir operation under scenario 1 (allowing flood storage) increased reliability and sustainability while keeping resilience and vulnerability more or less the same as scenario 2 (not allowing flood storage). Therefore, by utilizing seasonal forecasts, optimization tools and reservoir operation rules, we can achieve flood and drought risk reduction by saving enough water for an upcoming agriculture season and enhance energy generation by pre-releasing the water through a power turbine in advance to reserve space for a future flood.

A spilling event that was observed from 16th March 2018 to 22nd March 2018 at the Kotmale reservoir was examined by utilizing lagged short-term ensemble rainfall

predictions, which used NCEP-GFS deterministic forecasts and their downscaled versions by WRF. A total of 13 ensemble predictions are available daily generated at the 18th hour of a day for the next 72 hours (3 days). The rainfall distribution was compared with HMIS observed rainfall data. Using the forecasted rainfall, the river was simulated with the WEB-RRI model, which was coupled with a reservoir optimization model. The performance of the reservoir was evaluated with a random adaptation strategy. According to the results, the optimized reservoir operation brought down the reservoir elevation by the end of the time horizon (73 hours) by pre-releasing the forecasted inflow and keeping the reservoir elevation at a low level to receive the future flood, thus preventing the reservoir from spilling. By doing this, the reservoir was ready to receive expected flood inflows to be utilized for power generation.

It is to be noted that these operations were performed either selecting a season or an event due to the data limitation on either observed data or forecasted data. Based on these two types of operations, this study confirmed the following: a) benefits of seasonal planning based on the integration of seasonal forecast information, a hydrological model, an optimization scheme with a defined reservoir operation rules; and b) benefits of the reservoir operation under flood emergency, when conducted by coupling short-term weather prediction, a hydrological model and an optimization scheme with reservoir operation strategies.

References

- Adler, R. F., Huffman, G. J., Chang, A., Ferraro, R., Xie, P. P., Janowiak, J., ... Nelkin, E. (2003). The version-2 global precipitation climatology project (GPCP) monthly precipitation analysis (1979-present). *Journal of Hydrometeorology*, 4(6), 1147–1167. [https://doi.org/10.1175/1525-7541\(2003\)004<1147:TVGPCP>2.0.CO;2](https://doi.org/10.1175/1525-7541(2003)004<1147:TVGPCP>2.0.CO;2)
- Afifi, Z., Chu, H. J., Kuo, Y. L., Hsu, Y. C., Wong, H. K., & Ali, M. Z. (2019). Residential flood loss assessment and risk mapping from high-resolution simulation. *Water (Switzerland)*, 11(4), 1–15. <https://doi.org/10.3390/w11040751>
- Alagiyawanna, A. M. A. H. D., & Jayawardana, I. M. S. P. (2015). Identification of Suitable predictors to Develop a Seasonal Forecasting Model for District Rainfall for the onset of Maha Agricultural Season using Climate Predictability Tool (CPT). *Sri Lanka Journal of Meterology*, 1, 12–19.
- Amarasinghe, U. A. (2010). Spatial Variation of Water Supply and Demand in Sri Lanka. In *National Conference on Water, Food Security and Climate Change* (Vol. 3, pp. 65–71).
- Bender, F. A. M. (2008). A note on the effect of GCM tuning on climate sensitivity. *Environmental Research Letters*, 3(1). <https://doi.org/10.1088/1748-9326/3/1/014001>
- Brunner, P., Simmons, C. T., Cook, P. G., & Therrien, R. (2010). Modeling surface water-groundwater interaction with MODFLOW: Some considerations. *Ground Water*, 48(2), 174–180. <https://doi.org/10.1111/j.1745-6584.2009.00644.x>
- Cai, X., McKinney, D. C., & Lasdon, L. S. (2003). Integrated Hydrologic-Agronomic-

- Economic Model for River Basin Management. *Journal of Water Resources Planning and Management*, 129(1), 4–17. [https://doi.org/10.1061/\(asce\)0733-9496\(2003\)129:1\(4\)](https://doi.org/10.1061/(asce)0733-9496(2003)129:1(4))
- CEB-SL. (2017). *Annual Report 2015*. Retrieved from <https://www.ceb.lk/publication-media/annual-reports/27/en>
- CEB. (2018). *Annual Report*. Retrieved from <https://ceb.lk/>
- Chaturvedi, R. K., Joshi, J., Jayaraman, M., Bala, G., & Ravindranath, N. H. (2012). Multi-model climate change projections for India under representative concentration pathways. *Current Science*, 103(7), 791–802.
- Christensen, J. H., Kanikicharla, K. K., Aldrian, E., An, S. II, Albuquerque Cavalcanti, I. F., de Castro, M., ... Zou, L. (2013). Climate phenomena and their relevance for future regional climate change. *Climate Change 2013 the Physical Science Basis: Working Group I Contribution to the Fifth Assessment Report of the Intergovernmental Panel on Climate Change*, 9781107057, 1217–1308. <https://doi.org/10.1017/CBO9781107415324.028>
- Cloke, H. L., & Pappenberger, F. (2009). Ensemble flood forecasting: A review. *Journal of Hydrology*, 375(3–4), 613–626. <https://doi.org/10.1016/j.jhydrol.2009.06.005>
- CREED. (2015). The Human Cost of Water Related Disasters. In *UNISDR*. <https://doi.org/10.1377/hlthaff.2013.0625>
- Crochemore, L., Ramos, M. H., & Pappenberger, F. (2016). Bias correcting precipitation forecasts to improve the skill of seasonal streamflow forecasts. *Hydrology and Earth System Sciences*, 20(9), 3601–3618. <https://doi.org/10.5194/hess-20-3601-2016>

- Cuo, L., Pagano, T. C., & Wang, Q. J. (2011). A review of quantitative precipitation forecasts and their use in short- to medium-range streamflow forecasting. *Journal of Hydrometeorology*, 12(5), 713–728. <https://doi.org/10.1175/2011JHM1347.1>
- David Eckstein, M.-L. H. and M. W. (2019). Global climate risk index 2019: Who suffers most from Extreme weather events? Weather-related loss events in 2017 and 1998 to 2017. In *Greenwatch*. <https://doi.org/978-3-943704-04-4>
- DCS-SL. (2020a). : *Cultivated extent by crops, 2012 – 2019*. 2019, 45–47. Retrieved from <http://www.statistics.gov.lk/abstract2020/CHAP5/5.1>
- DCS-SL. (2020b). *Production of main crops and food crops, 2010 – 2019*. 4–5. Retrieved from <http://www.statistics.gov.lk/abstract2020/CHAP5/5.19>
- Deltares. (2021). RTC-Tools documentation. Retrieved October 1, 2020, from <https://rtc-tools.readthedocs.io/en/stable/>
- Department of Census and Statistics. (2021). Area of Sri Lanka by Province and District. Retrieved from <http://www.statistics.gov.lk/abstract2020/CHAP1/1.1>
- DOA-SL. (2020). Agro climatic zones. Retrieved May 4, 2020, from <https://www.doa.gov.lk/index.php/en/weather-climate>
- DOM-SL. (2020). Climate of Sri Lanka. Retrieved April 4, 2020, from http://www.meteo.gov.lk/index.php?option=com_content&view=article&id=94&Itemid=310&lang=en#4-northeast-monsoon-season-december-february
- European-Commission. (2015). GHS population grid, derived from GPW4, multitemporal (1975, 1990, 2000, 2015). Retrieved November 25, 2020, from <https://developers.google.com/earth->

engine/datasets/catalog/JRC_GHSL_P2016_POP_GPW_GLOBE_V1#bands

FAO. (2011). *Sri Lanka Country Profile 2011*. Retrieved from <http://www.fao.org/3/ca0407en/CA0407EN.pdf>

Freer, J., Beven, K. J., Neal, J., Schumann, G., Hall, J., & Bates, P. (2013). Flood risk and uncertainty. In *Risk and Uncertainty Assessment for Natural Hazards* (Vol. 9781107006). <https://doi.org/10.1017/CBO9781139047562.008>

Friedl, M., & Sulla-Menashe, D. (2019). MCD12Q1 MODIS/Terra+Aqua Land Cover Type Yearly L3 Global 500m SIN Grid V006 [Data set]. Retrieved November 25, 2020, from NASA EOSDIS Land Processes DAAC website: <https://doi.org/10.5067/MODIS/MCD12Q1.006>

Gebrechorkos, S. H., Bernhofer, C., & Hülsmann, S. (2020). Climate change impact assessment on the hydrology of a large river basin in Ethiopia using a local-scale climate modelling approach. *Science of the Total Environment*, 742, 140504. <https://doi.org/10.1016/j.scitotenv.2020.140504>

Gosain, A. K., Rao, S., & Basuray, D. (2006). Climate change impact assessment on hydrology of Indian river basins. *Current Science*, 90(3), 346–353.

Hashimoto, T., Stedinger, J. R., & Loucks, D. P. (1982). Reliability, Resiliency, and Vulnerability Criteria. *Water Resources Research*, 18(1), 14–20.

Hettiarachchi, P. (2017). Experience during the Floods in May 2017 in the Wet Zone of Sri Lanka. In P. Hettiarachchi, M. Alawathugoda, A. Piyasena, K. Weligapolage, A. Amarasekara, & D. . Somawickrama (Eds.), *Hydrological annual 2016/2017*. Retrieved from

https://www.irrigation.gov.lk/images/pdf/downloads/Hydro_Annual/2016-17n.pdf

Hoegh-Guldberg, O., Jacob, D., Taylor, M., Bindi, M., Brown, S., Camilloni, I., ... Zhou, G. (2018). Impacts of 1.5°C global warming on natural and human systems. In: Global Warming of 1.5 °C. An IPCC special report on the impacts of global warming of 1.5 °C above preindustrial levels and related global greenhouse gas emission pathways [...]. In *Special Report, Intergovernmental Panel on Climate Change*.

Indika, J. R., Rasmy, M., & Koike, T. (2018). *Development of an Integrated Research Method for Effective Water Resource Management in a Complex Watershed System : the Case of Mahaweli River Basin*.

IPCC. (2013a). *Summary for Policymakers. In: Climate Change 2013: The Physical Science Basis. Contribution of Working Group I to the Fifth Assessment Report of the Intergovernmental Panel on Climate Change [Stocker, T.F., D. Qin, G.-K. Plattner, M. Tignor, S.K. Allen, J.* <https://doi.org/10.1260/095830507781076194>

IPCC. (2013b). What is a GCM? Retrieved from https://www.ipcc-data.org/guidelines/pages/gcm_guide.html

Jaranilla-Sanchez, P. A., Wang, L., & Koike, T. (2011). Modeling the hydrologic responses of the Pampanga River basin, Philippines: A quantitative approach for identifying droughts. *Water Resources Research*, 47(3). <https://doi.org/10.1029/2010WR009702>

Jiménez Cisneros, B. E., Oki, T., Arnell, N. W., Benito, G., Cogley, J. G., Döll, P., ... Mwakalila, S. S. (2014). Freshwater resources. In: *Climate Change 2014: Impacts, Adaptation, and Vulnerability. Part A: Global and Sectoral Aspects*.

Contribution of Working Group II to the Fifth Assessment Report of the Intergovernmental Panel on Climate Change. In *Climate Change 2014: Impacts, Adaptation, and Vulnerability. Part A: Global and Sectoral Aspects. Contribution of Working Group II to the Fifth Assessment Report of the Intergovernmental Panel on Climate Change*. Retrieved from [papers2://publication/uuid/B8BF5043-C873-4AFD-97F9-A630782E590D](https://www.ipcc.ch/publications_and_materials/publications_and_materials/publication/uuid/B8BF5043-C873-4AFD-97F9-A630782E590D)

JMA. (2002). Tokyo Climate Centre - WMO Regional Climate Centre in RA II (Asia). Retrieved October 12, 2020, from https://ds.data.jma.go.jp/tcc/tcc/products/model/outline/cps2_description.html

Kangrang, A., Prasanchum, H., & Hormwichian, R. (2018). Development of Future Rule Curves for Multipurpose Reservoir Operation Using Conditional Genetic and Tabu Search Algorithms. *Advances in Civil Engineering*, 2018, 1–10. <https://doi.org/10.1155/2018/6474870>

Kawasaki, A., Yamamoto, A., Koudelova, P., Acierto, R., Nemoto, T., Kitsuregawa, M., & Koike, T. (2017). Data integration and analysis system (DIAS) contributing to climate change analysis and disaster risk reduction. *Data Science Journal*, 16, Art 41:1-17. <https://doi.org/10.5334/dsj-2017-041>

Kellett, J., & Caravani, A. (2013). Financing Disaster Risk Reduction. *Global Facility for Disaster Reduction and Recovery (GFDRR)*, 1–60. Retrieved from [FinancingDisasterRiskReduction](https://www.gfdrr.org/en/publications/financing-disaster-risk-reduction)

Kiczko, A., & Mirosław-Świątek, D. (2018). Impact of uncertainty of floodplain Digital Terrain Model on 1D hydrodynamic flow calculation. *Water (Switzerland)*, 10(10).

<https://doi.org/10.3390/W10101308>

Kobayashi, S., Ota, Y., Harada, Y., Ebata, A., Moriya, M., Onoda, H., ... Kiyotoshi, T. (2015). The JRA-55 reanalysis: General specifications and basic characteristics. *Journal of the Meteorological Society of Japan*, 93(1), 5–48. <https://doi.org/10.2151/jmsj.2015-001>

Koike, T., Koudelova, P., Jaranilla-sanchez, P. A., Bhatti, A. M., Nyunt, C. T., & Tamagawa, K. (2014). *Earth Sciences River management system development in Asia based on Data Integration and Analysis System (DIAS) under GEOSS*. 58(1), 76–95. <https://doi.org/10.1007/s11430-014-5004-3>

Komporn, W., Yoshikawa, S., & Kanae, S. (2020). Use of seasonal streamflow forecasts for flood mitigation with adaptive reservoir operation: A case study of the Chao Phraya river basin, Thailand, in 2011. *Water (Switzerland)*, 12(11), 1–19. <https://doi.org/10.3390/w12113210>

Lehner, B., Verdin, K., & Jarvis, A. (2008). New global hydrography derived from spaceborne elevation data. *Eos*, 89(10), 93–94. <https://doi.org/10.1029/2008EO100001>

Liebmann, B., & Smith, C. A. (1996). Description of a complete (interpolated) outgoing longwave radiation dataset. *Bull. Amer. Meteor. Soc.*, Vol. 77, pp. 1275–1277.

Lucatero, D., Madsen, H., Refsgaard, J. C., Kidmose, J., & Jensen, K. H. (2018). Seasonal streamflow forecasts in the Ahlergaard catchment, Denmark: The effect of preprocessing and post-processing on skill and statistical consistency. *Hydrology and Earth System Sciences*, 22(7), 3601–3617. <https://doi.org/10.5194/hess-22->

3601-2018

MASL-SL. (2018). Mahaweli Authority of Sri Lanka. In S. C. Vithana (Ed.), *GEOS Asia Pacific Symposium*. Retrieved from https://www.restec.or.jp/geoss_ap11/program_tg1.html#day2

MASL. (2015a). *Seasonal Operating Plan Yala 2015*.

MASL. (2015b). *Seasonal Operation Plan of Maha 2015/2016*.

MASL. (2020). MASL-Master Plan. Retrieved from <http://mahaweli.gov.lk/masterplan.html>

Masson-Delmotte, V., Zhai, P., Pörtner, H. O., Roberts, D., Skea, J., Shukla, P. R., ... Waterfield, T. (2018). Summary for Policymakers. In: Global Warming of 1.5°C. An IPCC Special Report on the impacts of global warming of 1.5°C above pre-industrial levels and related global greenhouse gas emission pathways, in the context of strengthening the global response to. In *Ipcc - Sr15*. Retrieved from https://report.ipcc.ch/sr15/pdf/sr15_spm_final.pdf%0Ahttp://www.ipcc.ch/report/sr15/

Mateo, C. M., Hanasaki, N., Komori, D., Tanaka, K., Kiguchi, M., Champathong, A., ... Oki, T. (2014). *Water Resources Research*. 50, 7245–7266. <https://doi.org/10.1002/2013WR014979>.Reply

Maurer, E. P., & Hidalgo, H. G. (2008). Utility of daily vs. monthly large-scale climate data: An intercomparison of two statistical downscaling methods. *Hydrology and Earth System Sciences*, 12(2), 551–563. <https://doi.org/10.5194/hess-12-551-2008>

Mendez, M., Maathuis, B., Hein-Griggs, D., & Alvarado-Gamboa, L. F. (2020).

Performance evaluation of bias correction methods for climate change monthly precipitation projections over Costa Rica. *Water (Switzerland)*, 12(2). <https://doi.org/10.3390/w12020482>

Nakano, M., Kanada, S., Kato, T., & Kurihara, K. (2011). Monthly maximum number of consecutive dry days in Japan and its reproducibility by a 5-km-mesh cloud-system resolving regional climate model. *Japan Society of Hydrology and Water Resources: Hydrological Research Letters*, 5, 11–15. <https://doi.org/10.3178/hrl.5.11>

Nash, J. E., & Sutcliffe, J. V. (1970). River flow forecasting through conceptual models: Part I - A discussion of principles. *Journal of Hydrology*, 10(2), 282–290. [https://doi.org/10.1016/0022-1694\(70\)90255-6](https://doi.org/10.1016/0022-1694(70)90255-6)

Nyunt, C. T., Koike, T., & Yamamoto, A. (2016). Statistical bias correction for climate change impact on the basin scale precipitation in Sri Lanka, Philippines, Japan and Tunisia. *Hydrology and Earth System Sciences Discussions*, (January), 1–32. <https://doi.org/10.5194/hess-2016-14>

OpenModelica. (2021). OpenModelica. Retrieved from <https://www.openmodelica.org/>

Palmer, T. ., & Anderson, D. L. . (1994). The prospects for seasonal forecasting - A review paper. *Quarterly Journal of the Royal Meteorological Society*, 120(518), 755–793. <https://doi.org/10.1256/smsqj.51801>

Pandey, B. K., Gosain, A. K., Paul, G., & Khare, D. (2017). Climate change impact assessment on hydrology of a small watershed using semi-distributed model. *Applied Water Science*, 7(4), 2029–2041. [https://doi.org/10.1007/s13201-016-0383-](https://doi.org/10.1007/s13201-016-0383-6)

- Papaioannou, G., Varlas, G., Terti, G., Papadopoulos, A., Loukas, A., Panagopoulos, Y., & Dimitriou, E. (2019). Flood inundation mapping at ungauged basins using coupled hydrometeorological-hydraulic modelling: The catastrophic case of the 2006 Flash Flood in Volos City, Greece. *Water (Switzerland)*, *11*(11), 1–28. <https://doi.org/10.3390/w11112328>
- Payet-Burin, R., Kromann, M., Pereira-Cardenal, S., Strzepek, K., & Bauer-Gottwein, P. (2019). WHAT-IF: an open-source decision support tool for water infrastructure investment planning within the Water-Energy-Food-Climate Nexus. *Hydrology and Earth System Sciences Discussions*, (April), 1–49. <https://doi.org/10.5194/hess-2019-167>
- PEC. (2019). *Sustainable Sri Lanka 2030 Vision and Strategic Path*. (January), 315.
- Perrone, D., & Hornberger, G. (2016). Frontiers of the food-energy-water trilemma: Sri Lanka as a microcosm of tradeoffs. *Environmental Research Letters*, *11*(1), 14005. <https://doi.org/10.1088/1748-9326/11/1/014005>
- Prasanchum, H., & Kangrang, A. (2018). Optimal reservoir rule curves under climatic and land use changes for Lampao Dam using Genetic Algorithm. *KSCE Journal of Civil Engineering*, *22*(1), 351–364. <https://doi.org/10.1007/s12205-017-0676-9>
- Rasmy, M., Koike, T., Lawford, P., & Hara, M. (2015). *Assessment of future water resources in the tone river basin using a combined dynamical-stastical downscaling approach*. *71*(4), 73–78. https://doi.org/doi.org/10.2208/jscejhe.71.I_73
- Rasmy, M., Sayama, T., & Koike, T. (2019). Development of water and energy Budget-based Rainfall-Runoff-Inundation model (WEB-RRI) and its verification in the

- Kalu and Mundeni River Basins , Sri Lanka. *Journal of Hydrology*, 579(March), 124163. <https://doi.org/10.1016/j.jhydrol.2019.124163>
- Rayner, N. A., Parker, D. E., Horton, E. B., Folland, C. K., Alexander, L. V., Rowell, D. P., ... Kaplan, A. (2003). Global analyses of sea surface temperature, sea ice, and night marine air temperature since the late nineteenth century. *Journal of Geophysical Research: Atmospheres*, 108(14), 4407. <https://doi.org/10.1029/2002jd002670>
- Sahu, N., Yamashika, Y., & Takara, K. (2010). Impact Assessment of IOD / ENSO in the Asian Region Netrananda SAHU *, Yosuke YAMASHIKI and Kaoru TAKARA. In *Annals of Disas. Prev. Res. Inst., Kyoto Univ.*
- Sandoval-Solis, S., McKinney, D. C., & Loucks, D. P. (2011). Sustainability Index for Water Resources Planning and Management. *Journal of Water Resources Planning and Management*, 137(5), 381–390. [https://doi.org/10.1061/\(asce\)wr.1943-5452.0000134](https://doi.org/10.1061/(asce)wr.1943-5452.0000134)
- Sayama, T., Ozawa, G., Kawakami, T., Nabesaka, S., & Fukami, K. (2012). Rainfall–runoff–inundation analysis of the 2010 Pakistan flood in the Kabul River basin. *Hydrological Sciences Journal*, 57(2), 298–312. <https://doi.org/10.1080/02626667.2011.644245>
- Seko, H., Kunii, M., Yokota, S., Tsuyuki, T., & Miyoshi, T. (2015). Ensemble experiments using a nested LETKF system to reproduce intense vortices associated with tornadoes of 6 May 2012 in Japan. *Progress in Earth and Planetary Science*, 2(1). <https://doi.org/10.1186/s40645-015-0072-3>

- Sellers, P. J., Los, S. O., Tucker, C. J., Justice, C. O., Dazlich, D. A., Collatz, G. J., & Randall, D. A. (1996). A Revised Land Surface Parameterization (SiB2) for Atmospheric GCMs. Part II: The Generation of Global Fields of Terrestrial Biophysical Parameters from Satellite Data. *Journal of Climate*, *9*, 706–737.
- Sellers, P. J., Randall, D. A., Collatz, G. J., Berry, J. ., Field, C. ., Dazlich, D. A., ... Bounoua, L. (1996). A Revised Land Surface Parameterization (SiB2) for Atmospheric GCMs. Part I: Model Formulation. *Journal of Climate*, *9*, 676–705.
- Stefanidis, K., Panagopoulos, Y., & Mimikou, M. (2018). Response of a multi-stressed Mediterranean river to future climate and socio-economic scenarios. *Science of the Total Environment*, *627*, 756–769. <https://doi.org/10.1016/j.scitotenv.2018.01.282>
- Suzuki-Parker, A., Kusaka, H., Takayabu, I., Dairaku, K., Ishizaki, N. N., & Ham, S. (2018). Contributions of GCM/RCM uncertainty in ensemble dynamical downscaling for precipitation in East Asian summer monsoon season. *Scientific Online Letters on the Atmosphere*, *14*(Ipc 2013), 97–104. <https://doi.org/10.2151/SOLA.2018-017>
- Tang, J., Niu, X., Wang, S., Gao, H., Wang, X., & Wu, J. (2016). Statistical downscaling and dynamical downscaling of regional climate in China: Present climate evaluations and future climate projections. *Journal of Geophysical Research: Atmospheres*, *121*, 2110–2129. <https://doi.org/10.1038/175238c0>
- Taylor, K. E., Stouffer, R. J., & Meehl, G. A. (2012). An overview of CMIP5 and the experiment design. In *Bulletin of the American Meteorological Society*. <https://doi.org/10.1175/BAMS-D-11-00094.1>

- Teng, J., Vaze, J., Chiew, F. H. S., Wang, B., & Perraud, J. M. (2012). Estimating the relative uncertainties sourced from GCMs and hydrological models in modeling climate change impact on runoff. *Journal of Hydrometeorology*, 13(1), 122–139. <https://doi.org/10.1175/JHM-D-11-058.1>
- The World Bank. (2021). Population Sri Lanka. Retrieved from <https://data.worldbank.org/indicator/SP.POP.TOTL?locations=LK>
- Toby, R., Ellis, K., Jhonson, J. A., Baldos, U. L., Hertel, T., Nootenboom, C., & Polasky, S. (2020). Global Futures: Assessing the global economic impacts of environmental change to support policy-making. Summary report. In *Histories of the Future*. <https://doi.org/10.1215/9780822386810-005>
- UN-Secretary-General. (2019). ECOSOC – Economic And Social Council: Special edition: progress towards the Sustainable Development Goals. In *A Concise Encyclopedia of the United Nations* (Vol. 07404). <https://doi.org/10.1163/ej.9789004180048.i-962.115>
- UN. (2015a). *ADOPTION OF THE PARIS AGREEMENT Proposal by the President* (Vol. 21932).
- UN. (2015b). Sendai Framework for Disaster Risk Reduction: 2015-2030. In *The United Nations Office for Disaster Risk Reduction*.
- UN. (2019). Report of the Secretary-General on SDG Progress 2019: Special Edition. *United Nations Publications*, 1–64. Retrieved from https://sustainabledevelopment.un.org/content/documents/24978Report_of_the_SG_on_SDG_Progress_2019.pdf

- UN Water. (2019). *Policy Brief Climate Change and Water*. 1–8.
- UNDP. (2016). UNDP Support to the Implementation of Sustainable Development Goal 1. In *United Nations Development Programme*. Retrieved from https://www.undp.org/content/dam/undp/library/SustainableDevelopment/1_Poverty_Jan15_digital.pdf
- USGS. (2020). HydroSHEDS. Retrieved May 4, 2020, from <https://www.hydrosheds.org/>
- Ushiyama, T., Sayama, T., & Iwmi, Y. (2017). Development of a Flood Forecasting System Using Regional Ensemble Prediction – Application To Kinugawa Flood in 2015領域アンサンブル予報を用いた洪水予測手法の開発 – 平成27年鬼怒川洪水への適用. *Journal of Japan Society of Civil Engineers, Ser. B1 (Hydraulic Engineering)*, 73(4), I_193-I_198. https://doi.org/10.2208/jscejhe.73.i_193
- Ushiyama, T., Sayama, T., Tatebe, Y., Fujiokacc, S., & Fukami, K. (2014). Numerical simulation of 2010 Pakistan flood in the Kabul river basin by using lagged ensemble rainfall forecasting. *Journal of Hydrometeorology*, 15(1), 193–211. <https://doi.org/10.1175/JHM-D-13-011.1>
- van Vuuren, D. P., Edmonds, J., Kainuma, M., Riahi, K., Thomson, A., Hibbard, K., ... Rose, S. K. (2011). The representative concentration pathways: An overview. *Climatic Change*, 109(1), 5–31. <https://doi.org/10.1007/s10584-011-0148-z>
- Vautard, R., Plaut, G., Wang, R., & Brunet, G. (1999). Seasonal prediction of North American surface air temperatures using space-time principal components. *Journal of Climate*, 12(2), 380–394. <https://doi.org/10.1175/1520->

0442(1999)012<0380:SPONAS>2.0.CO;2

- Viel, C., Beulant, A.-L., Soubeyroux, J.-M., & Céron, J.-P. (2016). How seasonal forecast could help a decision maker: an example of climate service for water resource management. *Advances in Science and Research*, 13, 51–55. <https://doi.org/10.5194/asr-13-51-2016>
- Wächter, A. (2009). Short Tutorial: Getting Started With Ipopt in 90 Minutes. *Dagstuhl Seminar Proceedings*, 1–17. Retrieved from <https://drops.dagstuhl.de/opus/volltexte/2009/2089/>
- Wang, L., Koike, T., Yang, K., Jackson, T. J., Bindlish, R., & Yang, D. (2009a). Development of a distributed biosphere hydrological model and its evaluation with the Southern Great Plains experiments (SGP97 and SGP99). *Journal of Geophysical Research Atmospheres*, 114(8), 1–15. <https://doi.org/10.1029/2008JD010800>
- Wang, L., Koike, T., Yang, K., Jackson, T. J., Bindlish, R., & Yang, D. (2009b). Development of a distributed biosphere hydrological model and its evaluation with the Southern Great Plains experiments (SGP97 and SGP99). *Journal of Geophysical Research Atmospheres*, 114(8), 1–15. <https://doi.org/10.1029/2008JD010800>
- Woldemeskel, F. M., Sharma, A., Sivakumar, B., & Mehrotra, R. (2014). A framework to quantify GCM uncertainties for use in impact assessment studies. *Journal of Hydrology*, 519(PB), 1453–1465. <https://doi.org/10.1016/j.jhydrol.2014.09.025>
- Wood, A. W., Leung, L. R., Sridhar, V., & Lettenmaier, D. P. (2004). Hydrologic implications of dynamical and statistical approaches to downscaling climate model outputs. *Climatic Change*, 62, 189–216.

- World-Grain. (2019). IRRI to help Sri Lanka boost rice sector. Retrieved from <https://www.world-grain.com/articles/11510-irri-to-help-sri-lanka-boost-rice-sector>
- Yamagata, K., Butts, M. B., Grooss, J., Clausen, T. H., Clausnitzer V Clausnitzer, V., Rainer Gründler R Gruendler, D., & Bertram Monninkhoff, D. (2012). Investigating an OpenMI coupling of FEFLOW and MIKE SHE. *Hydrology and Water Resources Symposium*. Retrieved from www.openmi.org
- Zarghaami, M. (2006). Integrated water resources management in Polrud irrigation system. *Water Resources Management*, 20(2), 215–225. <https://doi.org/10.1007/s11269-006-8048-0>
- Zhang, L. E. I., Xu, Y., Meng, C., Li, X., Liu, H., & Wang, C. (2020). Comparison of statistical and dynamic downscaling techniques in generating high-resolution temperatures in China from CMIP5 GCMs. *Journal of Applied Meteorology and Climatology*, 59(2), 207–235. <https://doi.org/10.1175/JAMC-D-19-0048.1>
- Zhang, Y., Jiang, F., Wei, W., Liu, M., Wang, W., Bai, L., ... Wang, S. (2012). Changes in annual maximum number of consecutive dry and wet days during 1961-2008 in Xinjiang, China. *Natural Hazards and Earth System Science*, 12(5), 1353–1365. <https://doi.org/10.5194/nhess-12-1353-2012>
- Zhu, X., Dai, Q., Han, D., Zhuo, L., Zhu, S., & Zhang, S. (2019). Modeling the high-resolution dynamic exposure to flooding in a city region. *Hydrology and Earth System Sciences*, 23(8), 3353–3372. <https://doi.org/10.5194/hess-23-3353-2019>